UNIVERSIDAD COMPLUTENSE DE MADRID
FACULTAD DE CIENCIAS FÍSICAS

TESIS DOCTORAL

Contribuciones a la verificación y mejora de la compatibilidad electromagnética de los telescopios de gran tamaño del observatorio Cherenkov Telescope Array Norte

MEMORIA PARA OPTAR AL GRADO DE DOCTOR

PRESENTADA POR

Oibar Martínez Vílchez

Director

José Miguel Miranda Pantoja

Madrid

UNIVERSIDAD COMPLUTENSE DE MADRID

FACULTAD DE CIENCIAS FÍSICAS

TESIS DOCTORAL

CONTRIBUCIONES A LA VERIFICACIÓN Y MEJORA DE LA COMPATIBILIDAD ELECTROMAGNÉTICA DE LOS TELESCOPIOS DE GRAN TAMAÑO DEL OBSERVATORIO CHERENKOV TELESCOPE ARRAY NORTE

MEMORIA PARA OPTAR AL GRADO DE DOCTORA

PRESENTADA POR

Oibar Martínez Vílchez

DIRECTOR

José Miguel Miranda Pantoja

A mi madre y mi hermana.

Por que sigamos construyendo proyectos,

porque formáis parte de los míos.

Agradecimientos

Quiero agradecer a José Miguel Miranda su dirección y todo el apoyo y las oportunidades que me ha brindado; y a Clara Oliver, Silvia Ronda y Patricia Márquez por ser las mejores compañeras de viaje que se pueden tener. Sin vosotros esto no estaría ocurriendo.

Índice

0. Resumen / Abstract

En esta tesis se presentan distintas aportaciones realizadas con el objetivo de analizar y mejorar la compatibilidad electromagnética de los Telescopios Cherenkov Large Size Telescopes (LST) del Observatorio Cherenkov Telescope Array Norte (CTA-N), situado en el Observatorio del Roque de Los Muchachos (ORM) en la isla de La Palma en España. Este observatorio cuenta en la actualidad con un LST ya construido, el LST1.

A esta labor, se ha contribuido elaborando protocolos de compatibilidad electromagnética y realizando diversas tareas y estudios experimentales en coordinación con el resto de los grupos de la Colaboración CTA. Se han realizado simulaciones por el método de elementos finitos y verificaciones experimentales de las mejoras al sistema de tierras del LST1, propuestas por empresas locales en base a la norma UNE 21186, como fue la instalación de una estructura de pata de ganso que pretendía disminuir la resistencia de puesta a tierra.

Además, se ha participado en dos de las tres campañas de medida de la resistividad eléctrica del emplazamiento del LST1, así como de los emplazamientos de otros telescopios que están por construir. Como resultado de estas medidas se descubrió una capa de resistividad eléctrica muy elevada en la localización del futuro telescopio LST3, de más de 10kΩ·m. Mediante el método de elementos finitos, se ha podido predecir que la instalación de este telescopio con un sistema de tierra equivalente al construido para el LST1 daría lugar a resistencias de tierra que comprometerían seriamente el funcionamiento del telescopio y la seguridad de sus componentes. Se ha detectado asimismo una capa profunda en este mismo emplazamiento de una resistividad considerablemente más baja. Estos hallazgos ayudarán a diseñar los sistemas de tierra de esos futuros telescopios.

Se ha desarrollado un plan de control de carga estática. Este plan abarca no sólo el observatorio, sino también los laboratorios de diseño que se han implicado en la construcción del telescopio LST1. Como parte de la implementación de este plan se han realizado visitas de supervisión a los laboratorios de diseño más relevantes, incluyendo los laboratorios de los grupos pertenecientes al Instituto de Investigación de Rayos Cósmicos de Tokio (ICRR), la Universidad de Kioto, la Universidad de Zúrich y la Universidad de Ginebra. Asimismo, se han llevado a cabo medidas en tiempo real de la carga estática acumulada en los contenedores que alojan los ordenadores y la instrumentación de control del telescopio LST1, en conjunto con el seguimiento de los niveles de humedad relativa. También se ha aportado al proyecto la documentación interna pertinente relativa a este plan.

Por otra parte, se ha contribuido a diversas mejoras que han permitido optimizar el sistema de protección contra descargas atmosféricas. Este sistema fue desarrollado por una empresa alemana a partir del método de la esfera rodante y en base a los requerimientos de máximo nivel de protección fijados por el estándar EN 62305-3. Las puntas captadoras fueron integradas en la estructura del telescopio, implementándose un sistema de doble camino de conductores de bajada a tierra. Se han realizado verificaciones de equipotencialidad eléctrica de las distintas partes conductoras que conforman el LST1, a partir de las cuales se han ofrecido soluciones para mejorar las debilidades detectadas. Por último, se ha participado en los ensayos de algunos de los subsistemas críticos realizando medidas de carga estática y emisiones conducidas sobre el actuador responsable del movimiento de los espejos. Además, se han hecho medidas in situ de las emisiones radiadas del LST1 procedentes de los módulos Xbee que se encargan de la comunicación entre los distintos actuadores y los sistemas de control del telescopio y se ha valorado su impacto en el entorno electromagnético.

This thesis presents different contributions to the analysis and improvement of the electromagnetic compatibility of the Large Size Telescopes (LST) of the Cherenkov Telescope Array North (CTA-N), located in El Roque de Los Muchachos Observatory (ORM) of La Palma island in Spain. The first LST, the LST1, is currently in commissioning phase.

In this task, electromagnetic compatibility protocols have been developed along with various activities and experimental studies agreed in coordination with the rest of the CTA Collaboration groups. In this work, Finite Element Method (FEM) has been used as well as experimental verifications of the upgrades of the LST1 earthing system proposed and implemented by local companies, based on the standard UNE 21186, as it was the installation of a goose leg structure which intended to reduce the earth resistance.

Furthermore, measurement campaigns of the soil electrical resistivity have been carried out in different sites, including all the sites of the LST subarray and other sites of telescopes of the array yet to construct. As a result of those campaigns a layer of very high electrical resistivity was found at the future LST3 site, of more than 10kΩ·m. Using FEM, it was predicted that the construction of this telescope with an earthing system similar to LST1's would lead to earth resistances that would seriously compromise the operation of the telescope and the safety of its components. In addition, a deeper layer of considerably lower electrical resistivity was found

in the LST3 site. These findings will help in the design of the earth systems of those future telescopes.

A static charge control plan has been developed. This plan is applicable not only to the observatory but to the design laboratories of the groups that had participated in the construction of the LST1. As a part of the implementation of this plan, reviews at relevant design laboratories were made, including the Institute for Cosmic Ray Research of Tokyo (ICRR), the University of Kyoto, the University of Zurich and the University of Geneve. In addition, onsite measurements of the electrostatic charge accumulated in the containers that host the control computers and the instrumentation have been carried out, simultaneously monitoring relative humidity levels. Furthermore, the corresponding internal reports have been provided to the CTA Collaboration.

Moreover, contributions have also been made to the lightning protection system by conducting verifications of the equipotentiality of the structure of the telescope and offering solutions to improve it. This system was developed by a German company which used the rolling sphere method and took into consideration the requirements of maximum protection level set by the EN 62305-3 standard. The lightning rods were integrated in the very same structure of the LST1 and a double down conductor system was implemented to derive the excess lightning current to earth. Verifications of the electrical equipotentiality were also made over the different conductive parts that compose the LST1 structure and, based on them, recommendations were provided in order to improve the observed weaknesses.

Finally, contributions to the testing of critical subsystems have also been made by carrying out measurements of static charge and conducted emissions of the actuators that control the mirrors. In addition, onsite radiated emissions of the LST1, coming from the Xbee modules of the actuators, have also been measured.

1. Revisión del estado actual

1.1. Introducción al proyecto Cherenkov Telescope Array (CTA)

Los Telescopios Cherenkov o Imaging Atmospheric Cherenkov Telescopes (IACT) son detectores terrestres para rayos gamma de alta energía. Las características de este tipo de instrumento son:

- Los detectores tienen un espejo para captar la luz y enfocarla en una cámara, por lo que se asemejan a telescopios ópticos.

- Estos telescopios detectan la luz producida por el efecto Cherenkov en el rango de azul a UV del espectro electromagnético.
- Los IACT registran múltiples fotones Cherenkov para un solo rayo gamma incidente en la parte superior de la atmósfera. Son detectados por la cámara como una imagen característica que permite identificar la partícula incidente como un rayo gamma, y especificar su dirección y energía.

Para entender qué es y de dónde surge CTA debemos mencionar a sus antecesores, los telescopios MAGIC (Major Atmospheric Gamma-Ray Imaging Cherenkov).

Los telescopios MAGIC son una continuación del trabajo que se inició con el detector HEGRA (High Energy Gamma Ray Astronomy), construido en 1987 y que dejó de dar servicio en 2002. Ambos experimentos tienen como objetivo la observación de fotones de alta energía de fuentes dentro y fuera de nuestra galaxia. La detección de estos rayos gamma de muy alta energía se puede realizar desde satélites, lo cual conlleva unos elevados costes, o desde un observatorio terrestre. La atmósfera tiene ventanas estrechas que sólo permiten el paso de algunas longitudes de onda, es esencialmente transparente sólo para la luz visible e infrarroja y para las ondas de radio largas, pero no para los rayos gamma. La forma más eficiente que se conoce en la actualidad para detectar esta radiación desde la Tierra e identificar su procedencia está basada en medir la radiación Cherenkov.

El proyecto MAGIC tiene actualmente una demanda de tiempo de observación muy elevada. Los miembros de la colaboración que desean realizar propuestas para investigar una determinada fuente deben contar con la aprobación de un comité específicamente organizado para este propósito. La aceptación de solicitudes es altamente competitiva, haciendo que sea crítico garantizar una alta fiabilidad de todos los subsistemas, optimizando el número de horas de observación cuando las condiciones meteorológicas lo permiten.

La colaboración MAGIC lleva varios años produciendo un número significativo de publicaciones de calidad, tal y como se muestra en la Ilustración 1.

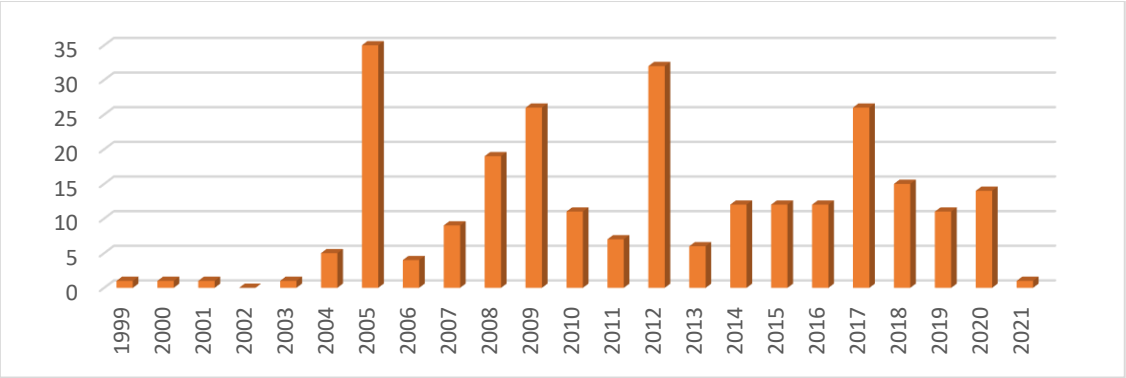

Ilustración 1 Publicaciones MAGIC registradas en Web of Science.

Puede considerarse que el proyecto CTA arrancó con la celebración de una reunión general de las colaboraciones HESS y MAGIC celebrada los días 4 y 5 de mayo de 2006. La primera reunión general oficial de la colaboración tuvo lugar los días 1 y 2 de marzo de 2007.

Igual que MAGIC, CTA es un observatorio para la astronomía de rayos gamma de muy alta energía, pero, a diferencia de MAGIC, CTA estará abierto a las solicitudes que desee realizar cualquier investigador, pertenezca o no a la colaboración, más allá de los institutos que actualmente participan en el diseño del instrumento y en la preparación de su construcción (el Consorcio CTA).

Además, CTA se ha concebido como una agrupación de telescopios capaz de acceder a todo el cielo y, por lo tanto, requiere de observatorios en los hemisferios norte y sur. Cada hemisferio tiene un enfoque científico diferente, con el rango de energía completo requerido sólo en el sur, debido a la posibilidad de observar el centro galáctico. Este rango de energías, que cubre aproximadamente cinco órdenes de magnitud, requiere el uso de diferentes tamaños de telescopios para lograr la sensibilidad requerida. Se prevén tres tipos de telescopios: pequeños, medianos y grandes. Recientemente se ha publicado una estimación actualizada del potencial de CTA para investigar materia oscura en el rango de los TeV [1] y otros temas de cosmología y física fundamental [2].

En el hemisferio norte, hoy en día, se prevé construir un grupo compacto de cuatro telescopios de gran tamaño Large Size Telescopes (LST) y cinco telescopios de tamaño mediano Medium Size Telescopes (MST) distribuidos en un área inferior a $1Km^2$. En el hemisferio sur también se construirán cuatro LST. El número de MST y telescopios de tamaño pequeño Small Size Telescopes (SST) se encuentra aún sin definir debido a restricciones en la obtención de los fondos necesarios. Estos telescopios estarán distribuidos a lo largo de varios kilómetros cuadrados.

El proceso de construcción del primer LST del observatorio norte (CTA-N), el LST1, está ya finalizado y se inauguró en 2018. En la Ilustración 2 se muestra una imagen del LST1, que actualmente se encuentra en la fase de puesta en marcha.

Ilustración 2 Telescopio LST1.

Como se puede observar en la Ilustración 3, el LST1 ha aumentado muy considerablemente el tiempo útil de observación durante el año 2021 [3]. Después de la experiencia de MAGIC, se prevé que la demanda de tiempo de observación en CTA sea aún más competitiva.

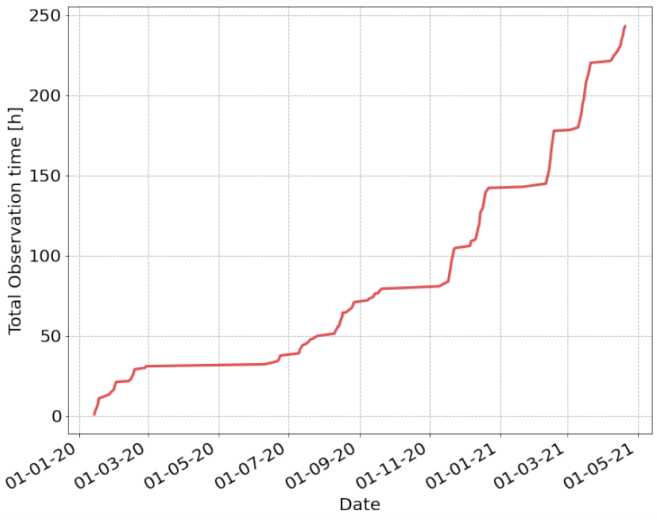

Ilustración 3 Evolución de las horas de observación del LST1.

Actualmente, el calendario estimado para completar la construcción de los tres LST restantes tiene prevista la finalización de los trámites de los permisos de construcción y arranque de los trabajos de Ingeniería Civil en septiembre de 2021, habiendo comenzado en agosto de 2019. La construcción de los telescopios LST2, LST3 y LST4 comenzaría secuencialmente desde los meses de febrero a abril de 2022, finalizando entre septiembre de 2023 y febrero de 2024. El final de la construcción de cada telescopio irá seguido de una fase de puesta a punto y verificación de requerimientos para cada uno de ellos que tendrá una duración de unos siete meses. Así pues, está previsto que el subarray LST estará operativo a partir de septiembre de 2024 [3].

En 2012, el documento de requisitos científicos describe por primera vez los objetivos científicos y las capacidades que ha de tener CTA para el usuario final [4]. El nivel más alto de requerimientos es el Nivel A, en el que se describen los requerimientos generales

- de funcionalidad, para cada subarray de telescopios idénticos [5],
- de usuario, que especifican cómo son los modos de medida en el observatorio y cómo han de implementarse en el software de control de alto nivel [6],
- ambientales, para el funcionamiento y supervivencia de los instrumentos [7]
- y de fiabilidad, disponibilidad, mantenibilidad y seguridad (RAMS)[8],

que se aplican a todos los componentes del Observatorio CTA. En la Ilustración 4 se muestra la primera estructuración de estos requerimientos, los cuales fueron evolucionando en los años posteriores, administrándose mediante la utilidad de gestión de requerimientos Jama.

A partir de estos requerimientos de Nivel A, de alto nivel, se derivan los requerimientos de Nivel B, específicos del producto. Los diferentes productos, que en conjunto forman el Observatorio CTA, incluyen los diferentes tipos de telescopios, la infraestructura del observatorio, el control de los telescopios y la gestión de datos. Los requerimientos de los productos se traducen luego en especificaciones técnicas en el Nivel C. La definición de las especificaciones técnicas es una labor que está asignada a los fabricantes de cada producto, mientras que los requerimientos de Nivel A y Nivel B son definidos por la Oficina de Proyecto de CTA.

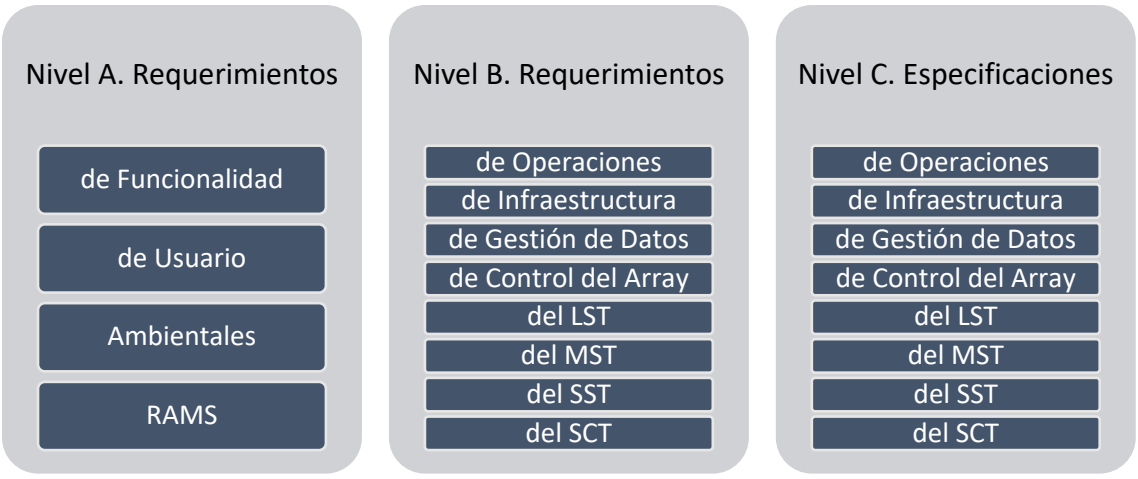

Ilustración 4 Estructura de la documentación de alto nivel de CTA.

A pesar de las múltiples revisiones que sufrieron estos requerimientos desde su primera definición en 2012, los RAMS, entre los cuales se encuentran los relativos a la compatibilidad electromagnética, mantuvieron un papel destacado durante toda la evolución del proyecto.

1.2. Compatibilidad Electromagnética en el LST1

Se dice que un equipo es electromagnéticamente compatible cuando sus emisiones electromagnéticas no comprometen el correcto funcionamiento del resto de equipos eléctricos de su entorno (incluyendo el suyo propio) ni su funcionamiento se ve afectado por su entorno electromagnético. Es decir, que el LST1 sea electromagnéticamente compatible implica que debe haber un control de las emisiones que genera y del grado de susceptibilidad a que posee a las perturbaciones que pueda sufrir durante su operación.

La compatibilidad de los equipos que se comercializan en la Unión Europea está regulada por la directiva CEM 2014/30/UE [9] y la directiva RED 2014/53/UE [10]. La primera de ellas aplica a determinados equipos eléctricos o instalaciones fijas que no sean intrínsecamente inocuos en términos de compatibilidad electromagnética (salvo exclusiones); la segunda aplica a los equipos radioeléctricos (salvo exclusiones). Además, los equipos que estén bajo la aplicación de la Directiva RED quedarán excluidos de que les aplique la Directiva CEM.

Si nos acogemos a las presentes normativas resulta difícil valorar si una instalación científica como CTA se encuentra dentro o fuera del ámbito de aplicación de las mismas. El plan de acción del telescopio vecino más importante, el Gran Telescopio Canarias (GTC), ha sido obtener el marcado de Conformidad Europea (CE) para los distintos subsistemas que conforman la instalación. El marcado CE es el sello que garantiza que un producto cumple con los requisitos que establece la Unión Europea, entre los cuales se encuentran los requisitos de compatibilidad electromagnética.

El Observatorio CTA definió durante la fase preparatoria del proyecto una serie de requerimientos que debían satisfacer los LST, entre ellos, que los LST debían cumplir con las normativas de compatibilidad electromagnética, tal y como se muestra en la Ilustración 5. Además, desde la Oficina de Proyecto de CTA se hizo la recomendación de que el telescopio cumpliera con las regulaciones correspondientes a la implantación del marcado CE. Sin embargo, no se definió ningún estándar aplicable.

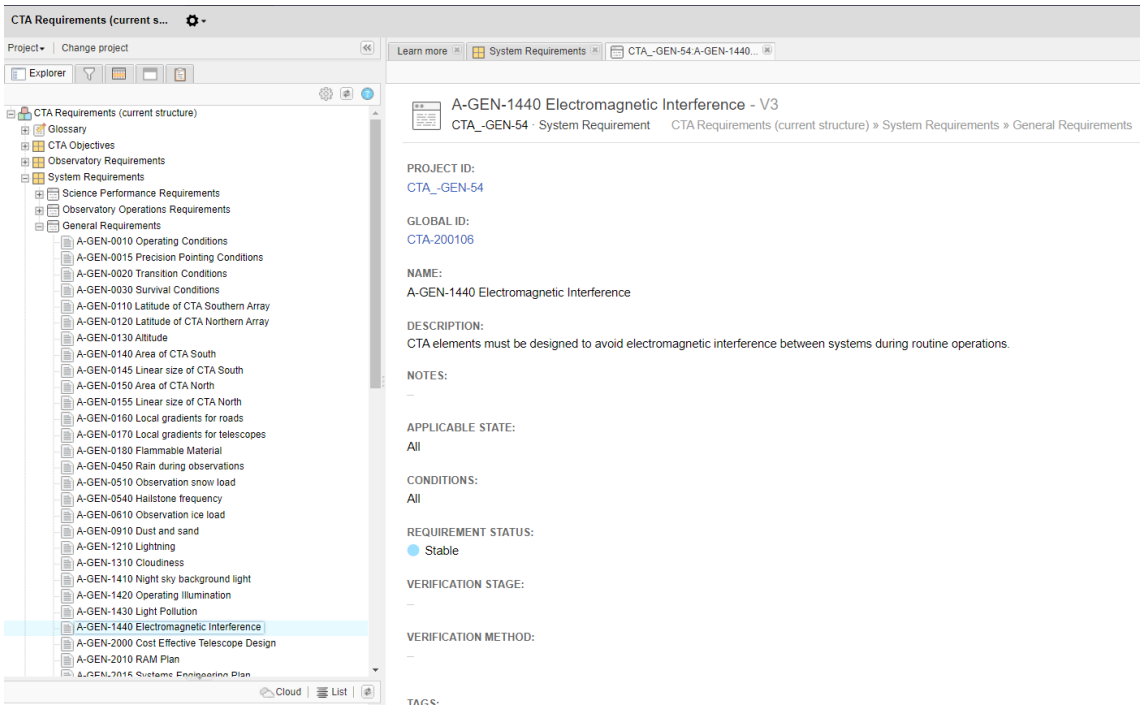

Ilustración 5 Aplicación Jama para gestión de requerimientos.

Para verificar que un producto cumple con la Directiva CEM (o RED) existe una amplia colección de normas europeas que pautan cómo se debe ensayar y evaluar cada producto al que le aplica la directiva. A esas normas las llamamos estándares armonizados.

Los estándares armonizados los desarrolla alguno de los tres organismos europeos de normalización:

- Comité Europeo de Normalización (CEN)
- Comité Europeo de Normalización Electrotécnica (Cenelec)
- Instituto Europeo de Normas de Telecomunicación (ETSI)

A nivel nacional, la normalización está gestionada por los organismos nacionales. El organismo de normalización en España es la Asociación Española de Normalización (UNE).

De forma que, para verificar la compatibilidad electromagnética de un equipo, primero se debe localizar el estándar (o estándares) que le aplica. Dentro del estándar encontraremos definida una colección de ensayos y cómo ejecutarlos. Además, no todos los ensayos del estándar tienen por qué aplicarle al producto.

Esta tarea de definir, en última instancia, a qué ensayos debe someterse un equipo comercial en muchas ocasiones no es algo trivial, y se vuelve una labor de gran dificultad cuando hablamos de un equipo nada convencional como sería nuestro telescopio, ya que no encaja en absoluto en la descripción de equipos a los que aplican ninguno de los estándares. Además, aplicar los estándares de compatibilidad electromagnética, pensados y desarrollados para ensayar equipos comerciales, a subsistemas como los que conforman el LST es en muchas ocasiones absurdo o físicamente irrealizable.

La tarea de garantizar una CEM adecuada para los LST ha sido, durante los últimos diez años, el eje central del trabajo de numerosos ingenieros pertenecientes a grupos de la colaboración; destacando el Instituto Max Planck de Munich (MPI), el Instituto de Física de Altas Energías (IFAE), el Instituto de Investigación de Rayos Cósmicos de Tokio (ICRR), el Laboratorio de Física de Partículas de Annecy (LAPP), el Centro de Investigación de Energías Medioambientales (CIEMAT), el Instituto Nacional de Física Nuclear de Italia (INFN), la Universidad de Zúrich y el Instituto de Astropartículas y Cosmología de París (APC). Es por ello por lo que ha resultado crucial coordinar cuidadosamente todas las tareas llevadas a cabo. Uno de los resultados de estos esfuerzos de coordinación ha sido la definición de los objetivos concretos de esta tesis.

2. Objetivos de esta tesis

El objetivo principal que ha perseguido esta tesis ha sido contribuir a hacer el LST1 electromagnéticamente compatible, realizando las tareas críticas consensuadas en las reuniones de coordinación del proyecto, que se describen a continuación:

1. Definición de protocolos y orientaciones en el proceso de obtención del marcado CE. Desarrollar el requerimiento genérico de alto nivel de compatibilidad electromagnética, especificando los ensayos a realizar e identificando los subsistemas críticos.
2. Estudios sobre la resistividad eléctrica de los emplazamientos. Caracterizar experimentalmente la resistividad eléctrica del terreno a distintas profundidades en los lugares donde se ubicarán los telescopios del subarray LST.

3. Verificación y mejoras a la resistencia de tierra del LST1. Se utilizarán técnicas experimentales avanzadas que se adecúen a las características especiales de los sistemas de tierra de gran extensión que poseen los telescopios y que se encuentran emplazadas en localizaciones de alta resistividad eléctrica. Mediante análisis de campos por el método de los elementos finitos se investigarán cuáles son las configuraciones óptimas del sistema de tierra para cada emplazamiento.
4. Verificación y mejora del sistema de protección contra impactos de rayos atmosféricos. Se verificará la equipotencialidad de todas las partes conductoras que constituyen la estructura del telescopio, buscando las soluciones más adecuadas para asegurar la continuidad eléctrica a lo largo de todos los posibles caminos de bajada a tierra.
5. Desarrollo e implementación de un plan de control de carga estática. Se definirán los procedimientos, supervisiones y ensayos necesarios para garantizar la integridad de la electrónica del observatorio, así como la seguridad de sus trabajadores.

Estos objetivos, a su vez, deben desarrollarse en consonancia con el cronograma global del proyecto, que pretende construir los cuatro LST entre el presente año 2021 y el 2024.

3. Trabajo realizado

3.1. Definición de protocolos

El cuantioso número de subsistemas que componen el LST convierten la verificación de los requerimientos de compatibilidad de la totalidad de los componentes en una tarea inabarcable. Para simplificarla se realizó un análisis de la susceptibilidad de cada dispositivo a generar problemas de compatibilidad electromagnética. En el Anexo I se muestra el desglose de los subsistemas que conforman el LST, el Product Breakdown Structure (PBS), en el que se subrayan estos subsistemas críticos y se resaltan en rojo aquellos que además poseen electrónica no comercializada hecha a medida.

Se identificó la Trigger Interface Board (TIB) como subsistema crítico, por ser una placa electrónica compleja con muchos componentes [11]. Esta placa había sido sometida a ensayos en 2017 en el Instituto Nacional de Técnica Aeroespacial (INTA) [12]. Otro subsistema categorizado como crítico fue el actuador Zürich.

Se acordó que los ensayos que procedían realizarse sobre los subsistemas críticos debían valorar las emisiones conducidas hasta los 10MHz [13], [14]. Además, se debía comprobar la inmunidad a descargas electrostáticas [15], transitorios [16], perturbaciones conducidas inducidas por

campos de radiofrecuencia [17] y caídas, interrupciones breves o cortes de tensión [18]. Asimismo, debían realizarse ensayos de las emisiones radiadas durante la fase de operación del telescopio, en el momento en que estuvieran funcionando los actuadores.

Además, se estableció que debían realizarse pruebas adicionales relacionadas con la operación con niveles muy elevados de resistencia de tierra.

También se estudiaron las diferentes vías que conducen al marcado CE [19], y se mostraron en las reuniones celebradas en Tokio [20] y Kioto [21].

3.2. Resistividad del terreno en los emplazamientos de los LST y MST

En 2019 se realizó un estudio geotécnico en los emplazamientos correspondientes a los 3 LST que faltan por construir y en el emplazamiento del MST3 [22]. Este estudio permitió relacionar las medidas de resistividad del terreno con su composición. La Palma es una isla de origen volcánico. Desde el punto de vista geotécnico, los LST están en una unidad geotécnica tipo III, macizos basálticos alterados [23].

Las columnas estratigráficas de los sondeos llevados a cabo en el estudio geotécnico muestran que los emplazamientos del LST2 y LST4 están compuestos por una mayoría de aglomerado volcánico en los primeros 7-8 metros de superficie, mientras que los emplazamientos del LST3 y MST3 están formados por grandes capas de basalto fracturado, hallándose el aglomerado volcánico a más profundidad.

Las medidas de resistividad del terreno se han hecho siguiendo el método Wenner [24]. En ellas se pudo observar una correlación entre el valor de la resistividad y la composición del terreno.

La Ilustración 6 muestra los resultados obtenidos de las campañas de medida de 2018 y 2019 en los emplazamientos de los LST y sus vecinos, los telescopios MAGIC.

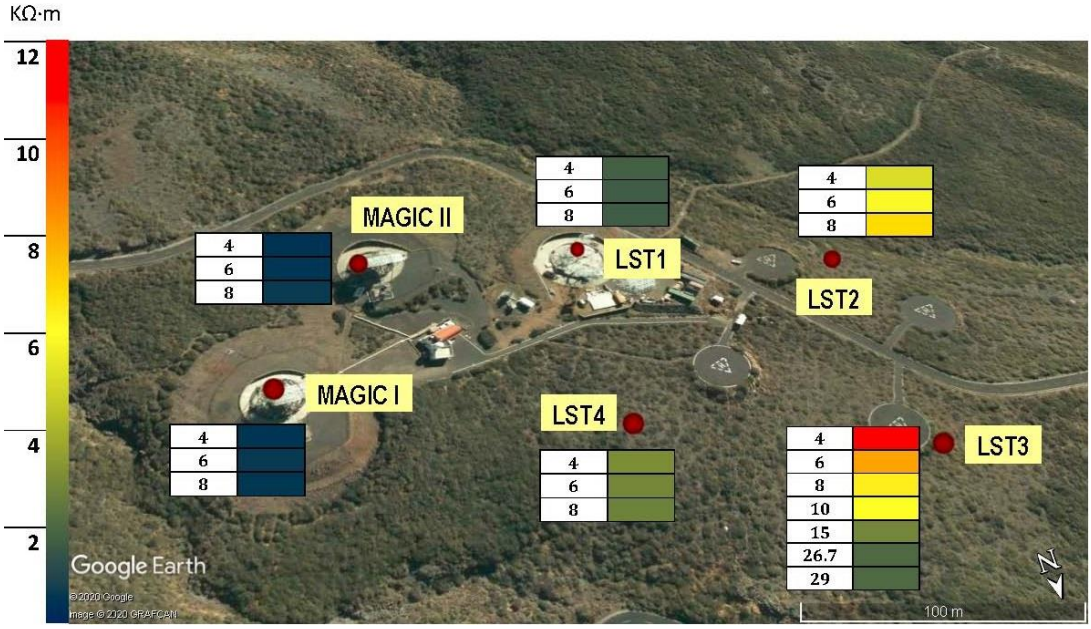

Ilustración 6 Resultados obtenidos de las campañas de resistividad del terreno de 2018 y 2019.

La escala de color indica el valor de la resistividad medida. A cada medida de resistividad le acompaña un número, que se corresponde con la distancia entre picas en metros del método Wenner. La profundidad de la medida se correspondería con ¾ de la distancia entre picas.

Se puede observar en la imagen que algunos emplazamientos se encuentran sobre terreno de resistividad homogénea, mientras que en otros la resistividad disminuye con la profundidad. Este dato es muy relevante a la hora de diseñar los sistemas de tierra de los futuros telescopios, ya que la geometría del contacto será distinta si disponemos de capas de mayor conductividad unos metros más abajo.

En 2020 se realiza otra campaña de medidas en el emplazamiento del futuro MST3. Se obtuvieron medidas de la resistividad superiores a las del emplazamiento del LST3.

d(m)	*5,9*	*9,9*	*13,3*	*17,0*
ρ(KΩ·m)	17,00	9,91	4,66	4,66

Tabla 1 Medidas de resistividad del terreno del emplazamiento del MST3. Se emplean para los valores de resistividad los valores de la escala de color de la Ilustración 6.

La parte más superficial del terreno posee una altísima resistividad, 17KΩ·m medidos a unos 4,5m de profundidad. Sin embargo, nuevamente, la resistividad disminuye con la profundidad. A partir de los 10m de profundidad la capa es mucho más conductiva, en torno a 4,6KΩ·m.

Cabe resaltar de esta tarea que la alta resistividad del terreno, en todo momento, ponía al límite las condiciones de operación del medidor de tierras. Realizar las medidas ha requerido del uso de distintos electrodos: pletinas, picas, conexiones en paralelo de picas auxiliares, etc. así como

de un procedimiento experimental cuidado en el que fue necesario realizar múltiples sondeos para conseguir que todos los electrodos tuvieran contactos fiables. La construcción de algunos de los electrodos diseñados se llevó a cabo en el taller de la facultad. También ha sido necesario usar preparados de bentonita para mejorar el contacto de los electrodos.

La alta resistividad del terreno de los emplazamientos dificulta la realización de una buena conexión de tierra. Estas medidas de resistividad en los emplazamientos de los telescopios que están aún por construir dejaron al descubierto la gran dificultad que va a suponer realizar los sistemas de tierras del LST3 y el MST3.

Mediante el método de elementos finitos se han realizado simulaciones que estiman la resistividad de cada una de las capas a partir de las medidas realizadas y la composición del terreno según los sondeos del estudio geotécnico [25]. Las simulaciones confirman valores de resistividad que oscilan entre 15 y 20 kΩ·m para las capas de basalto fracturado, con valores más bajos para capas más profundas.

3.3. Sistema de tierras de los LST

El sistema de tierra del LST1 está integrado en los cimientos del telescopio y la torre de acceso a la cámara [26]. Paralelamente a la construcción del entramado de acero que da soporte mecánico a la estructura se instaló el sistema de tierras, que está soldado a ese entramado y que consiste en una red de pletinas conectadas a distintos puntos del entramado, tal y como se muestra en la Ilustración 7 [27].

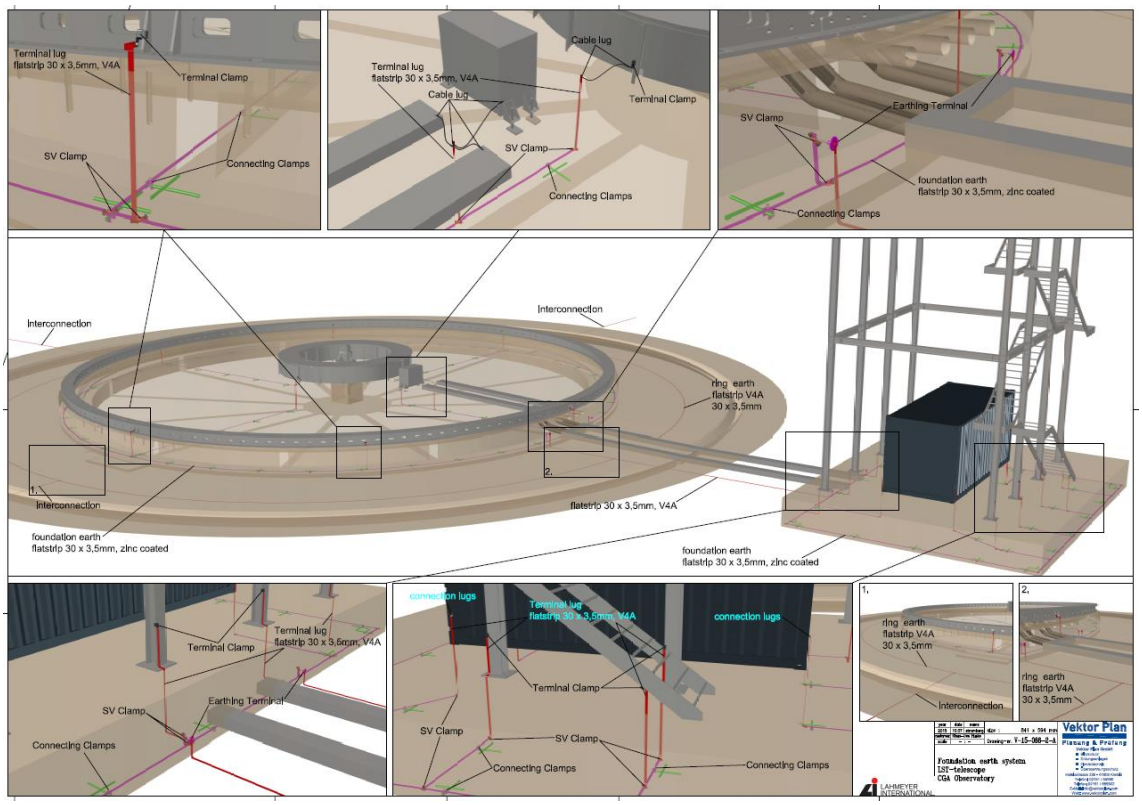

Ilustración 7 Diseño de la conexión a tierra del LST1.

Desde el año 2018 se han realizado distintas campañas de medida de la resistencia de tierra del LST1 con el propósito de valorar el impacto de las mejoras que se han ido implementando.

En mayo de 2019 el Instituto de Astrofísica de Canarias decidió instalar una estructura de pata de ganso que supuestamente mejoraría la resistencia de tierra, siguiendo las recomendaciones de una empresa de instalación eléctrica local que se basó en el estándar UNE [28]. Ya desde 2018 se conocía que la resistividad del emplazamiento del LST1 era homogénea y en 2019, antes de la instalación de la pata de ganso, se desaconsejó su implementación porque se predijo que no supondría una gran mejora.

En el verano de 2019 se midió la resistencia del LST1 por el método de intersección de curvas [29]. Este método fue el mismo que se empleó para hacer las medidas el año previo.

Los resultados de ambos años se muestran en la Ilustración 8.

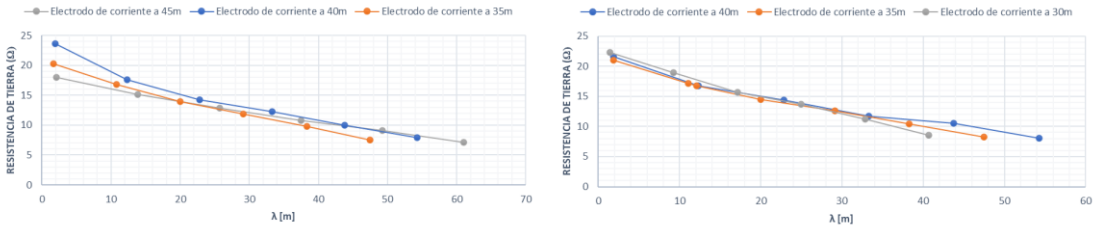

Ilustración 8 Medidas de la resistencia de tierra del LST1 en 2018 (izquierda) y 2019 (derecha) por el método de intersección de curvas.

En 2018 se midió una resistencia de tierra de 10Ω -14Ω y en 2019 de 12Ω-15Ω. Esto puso de manifiesto la poca efectividad de las mejoras realizadas al implementar la pata de ganso, confirmando las predicciones realizadas por nuestro grupo.

Se partió de la hipótesis de que las medidas de la resistencia eran procedimientos ampliamente conocidos y podrían aportar resultados fiables sin grandes dificultades. Sin embargo, pronto se puso de manifiesto que los procedimientos convencionales no eran aplicables para caracterizar la resistencia de tierra del LST. Una de las contribuciones más importantes de esta tesis ha sido poner de manifiesto estas limitaciones, que eran desconocidas por las empresas locales de certificación eléctrica.

Tras investigar sobre distintos métodos para la medida de resistencia de tierra, en 2020, se volvió a medir la resistencia de tierra del LST1, pero esta vez empleando un método de medida distinto, el método de la pendiente [30]. Los resultados se muestran en la Ilustración 9. Se consideraron las medidas realizadas con este método más fiables que las medidas realizadas anteriormente por el método de intersección de curvas por ser más adecuado para la realización de medidas de tierra de sistemas de tierra de grandes dimensiones, como el del LST1.

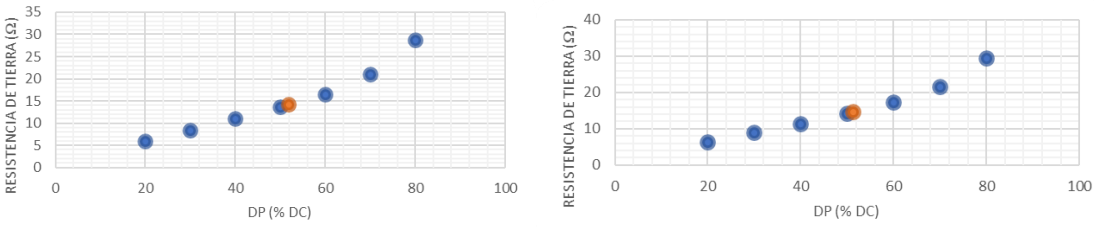

Ilustración 9 Medidas de la resistencia de tierra del LST1 en 2020 por el método de la pendiente con la pata de ganso conectada (izquierda) y con la pata de ganso desconectada (derecha).

Por este método, se midió una resistencia de 14,2Ω para el sistema de tierras completo y de 14,6Ω con la pata de ganso desconectada. Una vez más los resultados indicaron que la implementación de la pata de ganso no suponía una mejora significativa de la resistencia de tierra.

En los emplazamientos del LST3 y el MST3, donde la resistividad disminuye con la profundidad, la estrategia para mejorar el contacto de tierra debe consistir, efectivamente, en insertar electrodos verticales que alcancen esas capas de terreno más conductoras. Sin embargo, en los emplazamientos donde la resistividad es más homogénea, como es el caso del LST1, este procedimiento no supondrá una gran mejoría, y la estrategia debe estar orientada a instalar electrodos de mayor extensión horizontal.

Mediante el método de elementos finitos se han llevado a cabo simulaciones que estiman el grado de mejoría que supondría la implementación de distintos electrodos dependiendo del tipo de emplazamiento [31]. Los resultados de las simulaciones realizadas se muestran en las Ilustraciones Ilustración 10 y Ilustración 11.

Voltage			
Modification	Baseline (original)	Add a radial leg metal plate	Add two vertical rods of 10 m in the radial leg
R_{ES} (Ω)	15.17	13.91	13.27
Improvement	-	**8.3%**	**12.5%**
Voltage			
Modification	Surrounded with an external plate	Surrounded with 3 external plates	Surrounded with 3 external plates (bigger)
R_{ES} (Ω)	11.01	9.82	7.14
Improvement	**27.4%**	**35.3%**	**52.9%**

Ilustración 10 Simulación mediante el método de elementos finitos de distintas conexiones de tierra en un terreno de resistividad homogénea.

Voltage			
Modification	Basic (original)	Surrounded with an external plate	Surrounded with an external plate with 3 vertical rods
R_{ES} (Ω)	69.23	53.46	37.87
Improvement	-	**22.8%**	**45.3%**
Voltage			
Modification	Surrounded with an external plate with 7 vertical rods	Surrounded with an external plate with 7 vertical rods and plates of 60 cm (x20)	Surrounded with an external plate with 22 vertical rods
R_{ES} (Ω)	27.90	25.51	23.58
Improvement	**59.7%**	**63.1%**	**64.2%**

Ilustración 11 Simulación mediante el método de elementos finitos de distintas conexiones de tierra en un terreno de resistividad no-homogénea.

La resistencia de tierra puede variar con los cambios de humedad y temperatura y, como tales cambios pueden ser considerables, las medidas de la resistencia de tierra son medidas difíciles de reproducir y con mucha incertidumbre.

En la Tabla 2, se muestra una tabla con el historial de medidas de resistencia de tierra realizadas al LST1. La disparidad de los resultados es un claro reflejo de la dificultad de esta labor.

Fecha	Resistencia (Ω)	Autor	Método	Estado del sistema de tierra
01/2017	5,25	FERRAZ	Sin notificar	Pata de ganso aún sin instalar
08/2018	17	KAPLAN	Sin notificar	Pata de ganso aún sin instalar
09/2018	11,7	UCM-ELEC	Intersección de curvas	Pata de ganso aún sin instalar
05/2019	13,5	UCM-ELEC	Intersección de curvas	Pata de ganso instalada
08/2020	16,6	UCM-ELEC	Método de la pendiente	Pata de ganso instalada
08/2020	19,4	UCM-ELEC	Método de la pendiente	Pata de ganso desconectada
09/2020	17,81	ABC INSPECCIÓN, S.L.	Sin notificar	Pata de ganso mejorada con electrodos de 10m

Tabla 2 Historial de medidas de resistencia de tierra del LST1.

En noviembre de 2020, tras el informe emitido por la empresa que instaló los electrodos de 10m, se expusieron las limitaciones de la metodología utilizada por las empresas locales para validar las resistencias de tierra de la instalación [32].

Para que las medidas de resistencia de tierra sean fiables es imprescindible que las líneas de medida posean una longitud mínima y tengan la orientación adecuada. La longitud de las líneas de medida deberá ser del orden de 2 a 4 veces el tamaño del electrodo de tierra, que en nuestro caso es superior a 30m [33]. Además, la dirección de la línea de medida deberá atravesar el centro eléctrico del sistema de tierras.

En el informe de ABC Inspección, S.L. se ofrecen los siguientes resultados:

- Resistencia de tierra Kit toma de tierra pararrayos: 17,81Ω
- Resistencia de tierra estructuras metálicas: 1,26Ω
- Resistencia de tierra unión conjunto estructuras y pararrayos 1,22Ω

A los que les acompañan las imágenes de la Ilustración 12.

Ilustración 12 Fotos ilustrativas de las líneas de medida extraídas del informe de ABC Inspección, S.L.

En las fotos que se adjuntaban en el informe, se podía observar cómo la dirección de la línea de medida que emplearon no atravesaba el centro eléctrico de la estructura ni tenía la longitud mínima necesaria para que las medidas fueran fiables (Ilustración 12 izquierda). En otras ocasiones la línea de medida sencillamente no se correspondía con medidas de la resistencia de tierra (Ilustración 12 derecha).

3.4. Sistema de protección contra impactos de rayos del LST1

En el estudio de los riesgos de impacto de rayos en el observatorio se realizó un análisis de los impactos registrados por la base de datos de Vaisala en una superficie de $1km^2$ en torno a los telescopios MAGIC y LST, encontrándose eventos de impactos que alcanzaron los 690kA. Los excesos de carga producidos por estos impactos deben ser disipados en el suelo con rapidez, de lo contrario podría comprometerse la integridad del telescopio y de las personas que lo operan.

Una parte fundamental en la prevención de las acumulaciones de carga en la estructura del telescopio es garantizar una equipotencialidad adecuada entre las distintas partes conductoras de la misma [34].

El diseño del sistema de protección contra impactos de rayos se realizó siguiendo el método de la esfera rodante [35]. El arco de soporte de la cámara contiene parejas de puntas de 0,5 m cada 6 m en ángulo de 45° a ambos lados para ampliar el área de protección y cuenta con un sistema de conductores de bajada que guían la corriente del rayo a la tierra a través de las plataformas de elevación del lado este y oeste. Cada una de las dos torres del sistema de elevación, así como la torre de la cámara, están protegidas por dos pararrayos de cuatro metros. Además, la estructura está construida con materiales conductores y sirve para guiar con seguridad el exceso de corriente del rayo a tierra.

Anualmente se han realizado medidas de continuidad en la estructura del telescopio y en la torre de la cámara. Las campañas de 2018, 2019 y 2020 sirvieron para detectar diferentes problemas de aislamiento de algunas partes de la estructura del telescopio. Las medidas de equipotencialidad se han realizado con el método de cuatro puntas, permitiendo la obtención precisa de resistencias inferiores a 0,1Ω con cables de longitudes superiores a 100m.

Como se puede observar en la Ilustración 13, en 2018 se midieron más de 15Ω de resistencia entre la cubierta del motor de una de las torres laterales y la toma de tierra. Los valores típicos de resistencia entre cualquier punto de la estructura y la toma de tierra no superan los 0,1Ω.

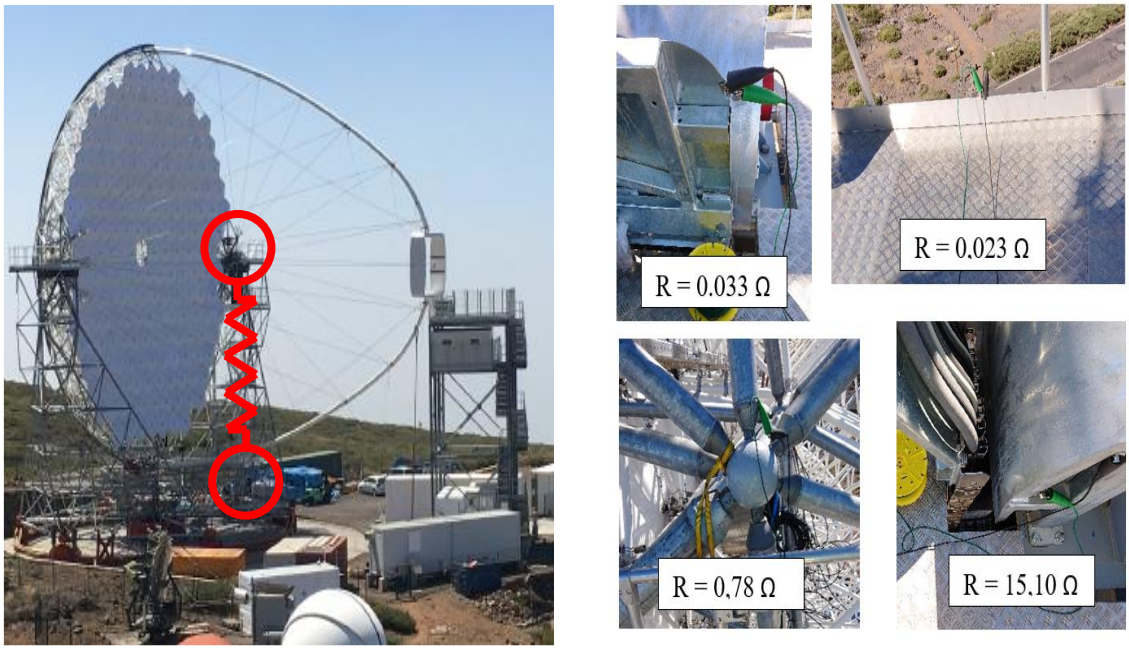

Ilustración 13 Ubicación de la torre y la toma de tierra (izquierda) y medidas de equipotencialidad en 2018 (derecha).

En la campaña del año 2019 se pudo comprobar que el problema de contacto de la cubierta del motor en la torre había sido resuelto. Sin embargo, también sirvió para detectar un nuevo problema. Se habían instalado unas nuevas pasarelas para los operarios en las que se había usado neopreno como antideslizante para las abrazaderas que la fijaban a los tubos de la estructura, dejando las pasarelas eléctricamente aisladas. Se llegaron a medir resistencias superiores a 3Ω entre algunos puntos de las pasarelas y la misma toma de tierra empleada en las medidas de 2018. Se propuso en la reunión general del proyecto LST de septiembre de 2019, celebrada en Rijeka, la implementación de unos cables que conectaran las pasarelas con los tubos de la estructura [36].

En el año 2020 se pudo verificar que seguía existiendo una elevada resistencia entre las pasarelas y el contacto de tierra y se detectó un nuevo problema en unas cubiertas protectoras que se habían instalado para los tensores del arco de la cámara. Estos protectores se instalaron con el objetivo de evitar sobrecalentamientos debidos al enfoque de los espejos. Se muestran algunas medidas de las campañas de 2019 y 2020 en la Ilustración 14.

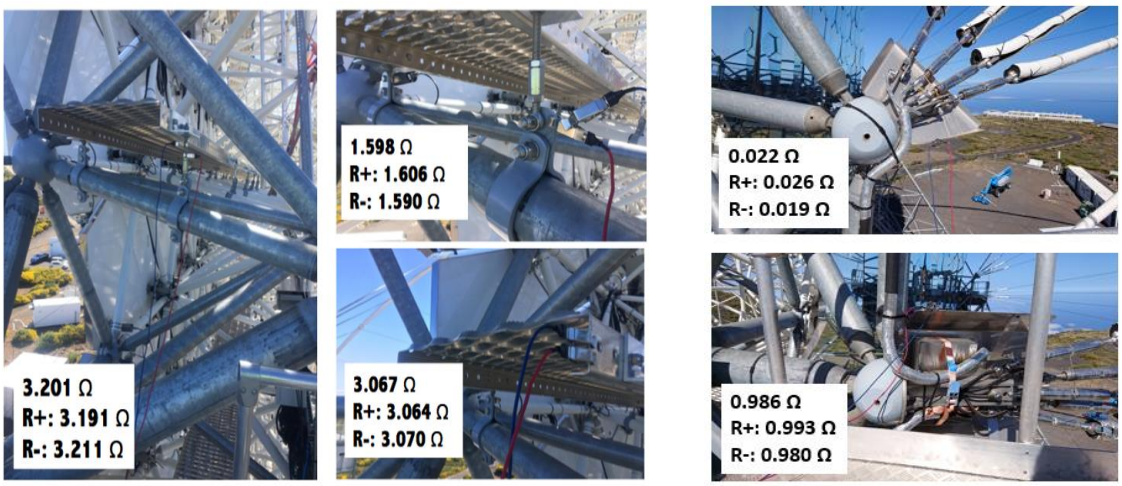

Ilustración 14 Medidas de equipotencialidad en 2019 (izquierda) y 2020 (derecha).

3.5. Control de carga estática

El control de la carga estática es una tarea crucial para garantizar la seguridad del personal de operación y mantenimiento, así como de los subsistemas electrónicos más sensibles. Desde nuestro grupo se ha llevado a cabo un plan de control de carga estática que se ha preocupado de establecer directrices, medir el nivel de carga estática que se generaba por efecto triboeléctrico en todos los contenedores, detectar y prevenir problemas relacionados con la misma y concienciar a los otros grupos sobre la importancia de tener un correcto control de la carga estática en los laboratorios, brindándoles información sobre cómo combatirla [37].

En septiembre de 2019 se hicieron visitas de supervisión en los laboratorios de los grupos de Ginebra y Zúrich [38], [39]. Se pudo comprobar que las recomendaciones de carga estática que se especifican en el plan interno de control de carga estática se cumplían con rigurosidad. En diciembre de ese mismo año se visitaron los laboratorios de los grupos de Tokio y Kioto. Al laboratorio de la Universidad de Kioto se le detectaron deficiencias en el control de la carga estática relacionadas con el tipo de suelo del que disponían los laboratorios. Asimismo, se impulsó la instalación de una zona protegida de descargas electrostáticas para el montaje y la manipulación de subsistemas electrónicos, como las Dragon Boards. En todos los encuentros se impartieron seminarios de formación sobre cómo protegerse de la carga estática.

Se han realizado medidas anuales de carga estática en los contenedores del recinto del LST1. Uno de ellos resultó especialmente problemático, el Commissioning Container, el cual alberga los ordenadores y dispositivos de control del telescopio, y es, por tanto, el contenedor que más circulación de personas soporta de toda la instalación.

Las medidas de carga electroestática se realizaron con un voltímetro electrostático capaz de monitorizar en tiempo real el nivel de carga acumulado en el cuerpo humano.

En 2019 el Commissioning Container presentaba serios problemas de carga estática, que ya habían notificado los operarios. Las medidas realizadas corroboraron el problema, llegándose a medir tensiones, según el Human Body Model (modelo HBM), que superaban los 15kV. Los requerimientos exigían que el máximo nivel de tensión estuviera por debajo del umbral de los 2kV (Clase 1C) [40]. En la Tabla 3 se muestra la clase de los dispositivos según su nivel de inmunidad a descargas electrostáticas.

Class	Voltage range
Class 0	< 250 V
Class 1A	250 V to < 500 V
Class 1B	500 V to < 1000 V
Class 1C	1000 V to < 2000 V
Class 2	2000 V to < 4000 V
Class 3A	4000 V to < 8000 V
Class 3B	≥ 8000 V

Tabla 3 Clasificación de los dispositivos según su inmunidad a descargas electrostáticas según el estándar ANSI/ESDA/JEDEC JS-001 Human Body Model Testing of Integrated Circuits.

El container en aquel momento contaba con un suelo de linóleo construido sobre madera en vuelo sobre el terreno, es decir, aislado. El linóleo, al rozamiento con las sillas de oficina y el calzado al andar, generaba una elevada cantidad de carga que no tenía hacia donde disiparse. Se estudiaron distintas opciones entre las que se contempló, por ejemplo, la instalación de un suelo antiestático, lo cual se descartó por motivos de costes y mantenimiento. Finalmente, se optó por reemplazar el suelo de linóleo por un suelo metálico conectado a tierra e incorporar un humidificador que elevara la humedad relativa.

Ese mismo año se reemplazó el suelo y se instaló un humidificador de acuerdo con los estudios realizados. En la Ilustración 15, se muestran los niveles de tensión que se llegaron a medir en el verano de 2019 (colores cálidos) y las que se midieron en 2020 (colores fríos) tras el reemplazo del suelo. Cada color corresponde a una medición sobre un operador distinto que realiza la misma secuencia de movimientos.

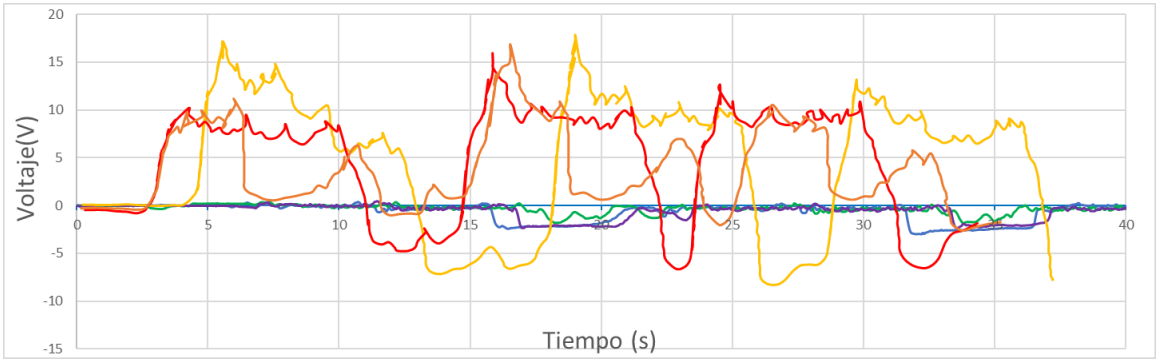

Ilustración 15 Medidas de carga estática en el Commissioning Container en 2019 (amarillo, naranja y rojo) y 2020 (verde, azul y morado) según el modelo HBM.

3.6. Contribuciones a la compatibilidad de subsistemas críticos: El actuador Zürich.

En esta tesis se ha contribuido a los ensayos de acumulación de carga e interferencias conducidas del actuador Zürich, que fue uno de los subsistemas identificados como críticos tanto en acumulación de carga estática como en emisiones conducidas, por tratarse de un elemento electromecánico.

Los actuadores Zürich se encargan del control activo de los espejos del LST y están basados en el diseño de los actuadores MAGIC. La principal diferencia, además de modificaciones que mejoran el rendimiento y la durabilidad del diseño original, es que se pueden controlar de forma inalámbrica gracias al módulo Xbee que incorporan.

Esencialmente los actuadores consisten en un motor paso a paso unido a un eje que mueve una tuerca que está unida a un pistón, transformando la rotación del motor en una traslación. La posición del pistón se lee mediante un conjunto de sensores Hall y un codificador magnético que permite un posicionamiento de una precisión superior a 1mm. La parte frontal del actuador consta de un soporte para fijarlo al espejo [41]. En la Ilustración 16 se muestran el aspecto y el esquema del actuador Zürich.

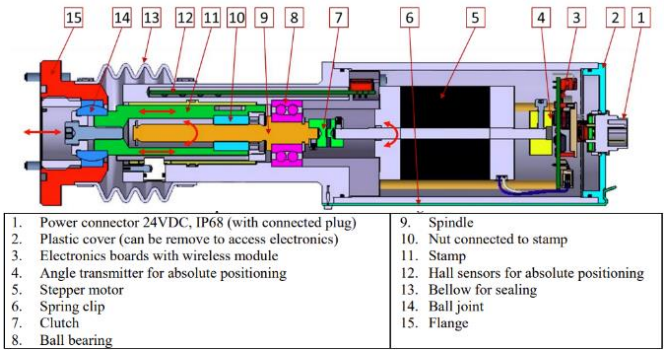

Ilustración 16 Actuador Zürich.

Los actuadores ya habían sido sometidos a pruebas de diseño, realizados sobre unas pocas unidades, y pruebas funcionales, realizadas a todas las unidades. Sin embargo, ninguna de esas pruebas involucraba la compatibilidad electromagnética.

En septiembre de 2019 se produjo una reunión con el grupo de CTA que diseñó los actuadores en el Physik-Institut de la Universidad de Zúrich [39]. El grupo de Zúrich facilitó un actuador que fue sometido a ensayos de compatibilidad electromagnética en el laboratorio de microondas de la Universidad Complutense y al que se le realizaron ensayos de emisiones conducidas y carga estática acumulada en el actuador.

El ensayo de emisiones conducidas se basó en el procedimiento establecido por la norma MIL-STD-461F CE102 [14] y se representa en la Ilustración 17.

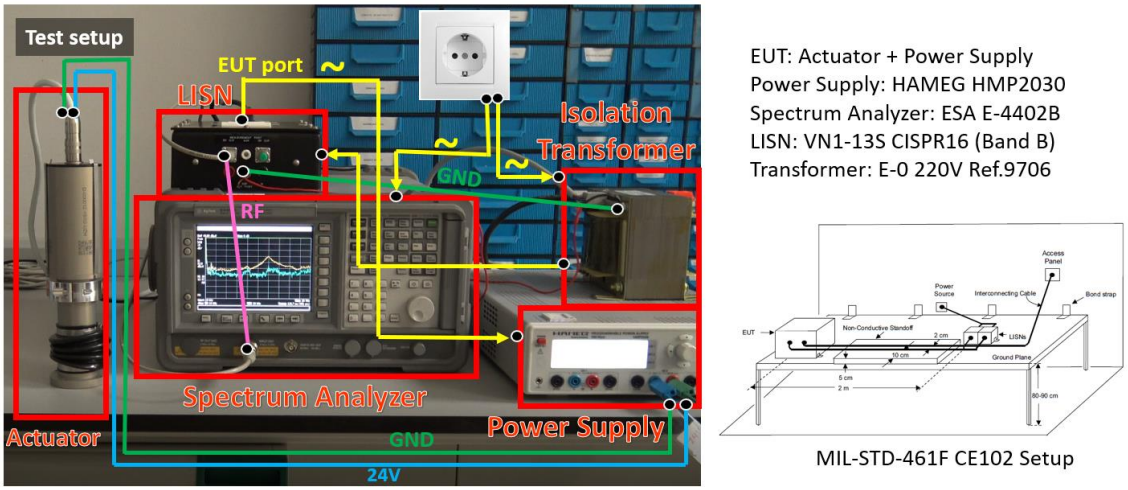

Ilustración 17 Montaje de ensayo de emisiones conducidas del actuador Zürich.

No se detectó ningún pico de emisión a ninguna de las frecuencias que establece el estándar. Además, como se puede observar en la Ilustración 18, las emisiones que producía se hallaban lejos del límite establecido.

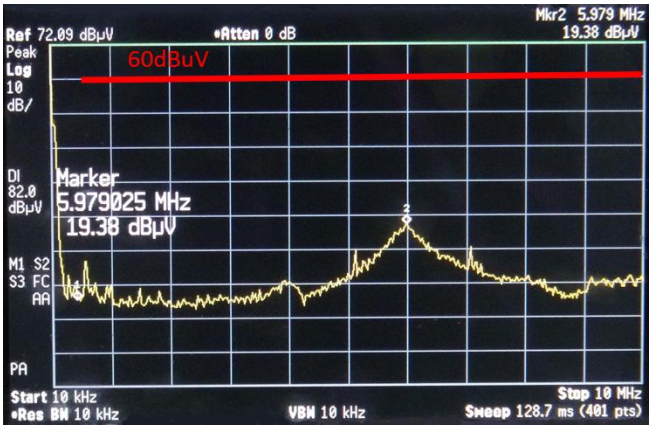

Ilustración 18 Emisiones conducidas del actuador Zürich.

Los ensayos de carga estática se realizaron en distintas configuraciones: con el actuador aislado o en contacto con distintas superficies y realizando distintos movimientos. Se verificó que la carga estática que acumulaba en movimiento era mínima y se disipaba rápidamente en cuanto cesaba el movimiento. En la Ilustración 19 se muestra el ensayo más desfavorable.

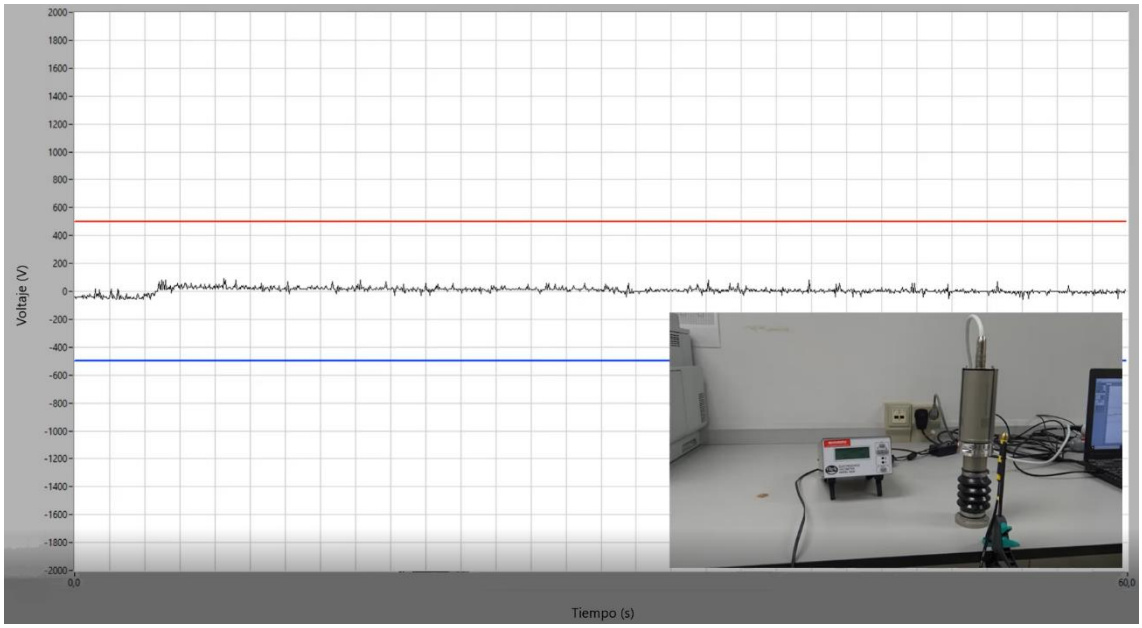

Ilustración 19 Medidas de carga estática en el actuador Zürich.

3.7. Emisiones radiadas del LST1

El LST1 consta de 198 espejos con sus respectivos actuadores. Los módulos Xbee de los actuadores Zürich son módulos comerciales que poseen su propia certificación. Sin embargo, el uso no convencional de los actuadores en el LST1 hace que se requiera la verificación de las emisiones radiadas del sistema en su conjunto durante la operación del telescopio.

Las medidas de emisiones radiadas requieren de un entorno electromagnético limpio, por ello, deben realizarse en cámara anecoica o en campo abierto, lejos de cualquier obstáculo o fuente de interferencias. Este escenario es imposible en el caso del LST1, ya que está emplazado entre otros telescopios y servicios del observatorio que precisan de la comunicación por radio para funcionar. Medir exclusivamente las emisiones del LST1 no es posible, pero se hicieron medidas y se valoró si el telescopio emitía potencias que pudieran poner en riesgo el correcto funcionamiento de las instalaciones adyacentes.

En agosto de 2020 se realizaron las primeras medidas de emisiones radiadas del LST1. En la Ilustración 20 se muestra un ejemplo de las emisiones registradas. Tal y como puede apreciarse, los niveles de potencia son comparables al de su propio entorno electromagnético. Se llegó a la conclusión de que el LST1 no produce emisiones radiadas comprometidas.

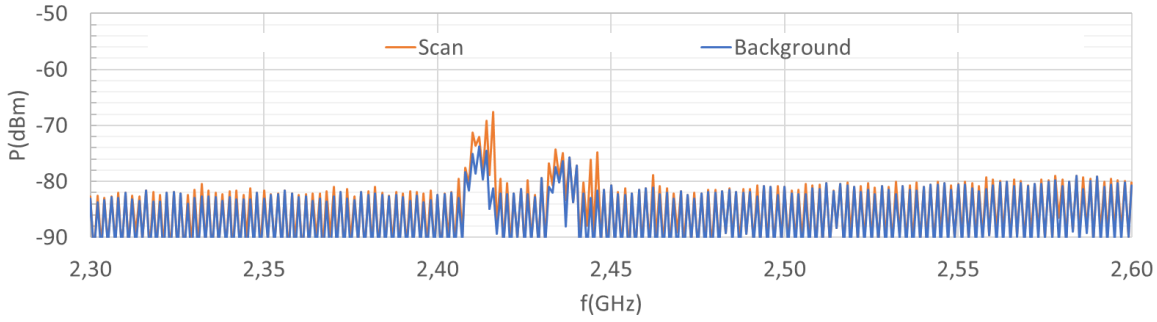

Ilustración 20 Medidas de emisiones radiadas del LST1 tomadas en la parte trasera central a 10 metros de distancia de la valla.

4. Conclusiones

En esta tesis se resumen las contribuciones realizadas para verificar y mejorar la compatibilidad electromagnética de los telescopios de gran tamaño del observatorio CTA-N.

Se considera que una de las contribuciones más importantes de esta tesis es la relativa a las medidas de resistividad del terreno en los emplazamientos de los futuros LST2-4. Mediante un método de cuatro puntas que ha permitido obtener medidas fiables en el límite de operación del medidor disponible, se ha detectado una capa superficial de muy alta resistividad en el emplazamiento del futuro LST3, y se ha podido predecir que la instalación de este telescopio con un sistema de tierra equivalente al construido para el LST1 daría lugar a resistencias de tierra que comprometerían seriamente el funcionamiento del telescopio y la seguridad de sus componentes. Se ha detectado asimismo una capa profunda en este mismo emplazamiento de una resistividad considerablemente más baja, lo cual ayudará a construir un sistema de tierra con una resistencia aceptable para este telescopio.

La campaña de medidas se extendió al emplazamiento de uno de los futuros telescopios del subarray MST. Los valores obtenidos llegaron incluso a superar los del LST3. La difusión de estos resultados a nivel interno del proyecto CTA ofrece a los ingenieros responsables del subarray MST la posibilidad de revisar el diseño de la estructura de tierras de sus telescopios, adaptándola a las recomendaciones que se han emitido en base a las simulaciones realizadas por el método de elementos finitos.

Las medidas de resistividad realizadas también han puesto de manifiesto las limitaciones de las tablas de valores de resistividades presentadas en la bibliografía de referencia, las cuales reflejaban discrepancias altamente significativas en los valores asignados a las posibles composiciones del terreno. En esta tesis se ha presentado un estudio preciso de la correlación

existente entre la composición del suelo del observatorio, obtenida con detalle mediante estudios geotécnicos, y las medidas de resistividad realizadas.

Otro de los resultados más destacados es la utilización de un método de medida de la resistencia de tierra más avanzado que los convencionales, el cual permite obtener medidas más precisas en las instalaciones que utilizan sistemas de tierra de gran extensión. Con este método se ha podido medir de forma fiable la resistencia de tierra del LST1, poniendo de manifiesto las limitaciones de los procedimientos conocidos por las empresas locales de instalaciones eléctricas, tanto para medir la resistencia de tierra utilizando el procedimiento de medida habitual por el método del 62%, como para mejorar el sistema de puesta a tierra de una instalación utilizando el procedimiento habitual basado en el estándar UNE 21186 [28]. La difusión de estos resultados ha brindado a las empresas locales la oportunidad de perfeccionar sus técnicas. Mediante el método de elementos finitos y aprovechando las medidas reales de la resistividad del terreno, se han podido realizar diseños mejorados de los sistemas de tierras de todos los telescopios.

Se han realizado comprobaciones de la equipotencialidad de la estructura que han contribuido a la mejora del sistema de protección contra descargas atmosféricas y se ha elaborado documentación interna sobre el mismo de interés para otros grupos de la Colaboración CTA. Además, se han corregido problemas de acumulación de carga estática en el observatorio y en los laboratorios de diseño de los grupos y se ha elaborado un plan de control de carga estática para los LST con su correspondiente documentación.

Se han realizado ensayos de compatibilidad que han permitido demostrar que los actuadores no inyectan a sus sistemas de alimentación emisiones conducidas que puedan comprometer el funcionamiento de otros subsistemas, ni tampoco son foco de posibles acumulaciones de carga electrostática. Se ha verificado también que las emisiones radiadas del LST1 no comprometen el correcto funcionamiento del resto de elementos de su entorno.

5. Resumen de publicaciones científicas con sistema de revisión por pares

A continuación, se resume el contenido de las publicaciones y mi implicación en las mismas.

5.1. Verification Protocols for the Lightning Protection of a Large Scale Scientific Instrument in Harsh Environments: A Case Study [34]

Este trabajo está dedicado al estudio de los protocolos más adecuados necesarios para verificar la protección contra rayos y la calidad del sistema de tierras en una instalación científica de gran escala ubicada en un sitio con alto riesgo de sufrir impactos de rayos. Ilustramos este trabajo estudiando con detalle el ejemplo de los telescopios más grandes del CTA-N. Describimos cómo se realizó la evaluación de riesgos de impactos y cómo se probaron los voltajes de contacto y el sistema de tierra. Se han utilizado simulaciones por el método de elementos finitos para estimar la corriente que fluye a través de las partes del sistema de puesta a tierra en el caso de un impacto directo. Este trabajo tiene como objetivo brindar asistencia a los científicos y gerentes involucrados en la construcción de instalaciones científicas, particularmente a los encargados de definir requisitos de fiabilidad y seguridad para la protección contra rayos.

He contribuido a este trabajando formando parte del equipo responsable de la toma de medidas de equipotencialidad de la estructura del LST1, realizando el análisis de la clase correspondiente al sistema de protección contra rayos y participando en la redacción y presentación de los datos.

5.2. Applying Electromagnetic Field Analysis to Minimize the Earth Resistance on High Resistivity Soils [31]

En este trabajo se discuten diferentes estrategias de optimización para reducir la resistencia de tierra en un suelo de alta resistividad. Estas estrategias se ilustran con un ejemplo práctico y simulaciones por el método de elementos finitos, que reproducen las condiciones del mundo real. Analizamos un ejemplo de sistema de puesta a tierra de un conjunto de cuatro telescopios idénticos instalados en suelos de alta resistividad (del orden de los (kΩ·m) con dos comportamientos diferentes. En el primero la disipación de corriente ocurre en un suelo uniforme, mientras que el segundo se considera un terreno con cuatro

capas de diferentes resistividades. Estas situaciones corresponden al caso real de los emplazamientos del LST1 y LST3. Se encontró que la mejor estrategia en cada caso difiere: en el caso de suelo homogéneo se deben extender electrodos horizontales lo más lejos posible de la cimentación y en el caso de suelo de múltiples capas se deben combinar estos electrodos con electrodos verticales que conecten con las capas de mayor conductividad.

He contribuido a este trabajo participando en las medidas de resistencia de tierra del LST1 y en la campaña de medidas de resistividad del emplazamiento del LST3, procesando los resultados experimentales y redactando distintas partes del artículo.

5.3. Finite Element Analysis and Experimental Characterization of Soil Electrical Resistivity at El Roque de Los Muchachos Observatory [25]

Este trabajo presenta un estudio de la resistividad eléctrica del suelo del Observatorio del Roque de los muchachos (ORM) y está motivado por los planes actuales de construcción de ATCs, así como otras instalaciones científicas, que demandan baja resistencias de tierra para el funcionamiento de instrumentos sensibles, prevención de daños por descargas electrostáticas y protección contra rayos. El terreno en el observatorio lo forman mayormente materiales de alta resistividad y dureza. Poseer un estudio sobre la composición y las propiedades eléctricas del suelo es esencial para optimizar la resistencia de tierra de las instalaciones futuras. En este trabajo presentamos medidas realizadas en seis ubicaciones diferentes de un área que cubre alrededor de 250m × 275m y donde se han hallado capas de baja resistividad (<2 kΩ·m) a profundidades específicas. La resistividad en los diferentes emplazamientos ha sido simulada, con una discrepancia con las medidas inferior al 10%, con el software COMSOL Multiphysics, usando dos modelos diferentes: un modelo simple, de una sola capa, y un modelo de tres capas. Las principales contribuciones de este trabajo son la presentación de valores fiables de resistividad del suelo en el ORM, junto con la simulación precisa de los perfiles del suelo.

He contribuido a este trabajo participando en la campaña de medidas de resistividad del terreno de 2019 en el ORM, procesando los datos de las campañas, revisando el estudio geotécnico y redactando distintas partes del artículo.

5.4. Sensitivity of the Cherenkov Telescope Array to a dark matter signal from the Galactic centre **[1]**

En este trabajo se evalúa la capacidad de CTA para buscar materia oscura producida térmicamente en la escala de los TeV, a través de las señales de rayos gamma procedentes de la región circundante del centro galáctico.

He contribuido a esta publicación participando en las tareas de puesta a punto del LST1, realizando los trabajos acordados en las reuniones de coordinación.

5.5. Sensitivity of the Cherenkov Telescope Array for probing cosmology and fundamental physics with gamma-ray propagation **[2]**

Este trabajo estudia algunas de las áreas más destacadas de cosmología de rayos gamma que pueden ser exploradas como parte de los Proyectos Científicos Clave de CTA, a través de observaciones simuladas de los Núcleos Galácticos Activos (AGN) y de sus jets relativistas

He contribuido a esta publicación participando en las tareas de puesta a punto del LST1, realizando los trabajos acordados en las reuniones de coordinación.

6. Comunicaciones orales

6.1. Comunicaciones orales en workshops y conferencias internacionales

He sido autora y ponente de las siguientes comunicaciones orales:

- "EMC studies". LST General Meeting (remote). 27/04/2021
- "EMC and Earthing studies". LST General Meeting (remote). 02/11/2020
- "European Directive on Electromagnetic Compatibility and CE Marking: Overview and applicability to Large Scale Installations". Workshop on Earthing and Electromagnetic Compatibility. Proceedings ISSN/ISBN: 978-84-09-22829-4. 24/07/2020
- "Electromagnetic Compatibility Verification for Electronic Boards". Institute for Cosmic Ray Research (ICRR) Universidad de Tokio. 09/12/2019

- "Electromagnetic Compatibility Verification for Electronic Boards". Universidad de Kioto. 02/12/2019
- "Verification of EMC requirements for LST". Universidad de Zúrich. 17/09/2019
- "Verification of Electromagnetic Compatibility Requirements and CE marking". Universidad de Ginebra. 13/09/2019
- "Ground resistance La Palma". LST General Meeting (Rijeka). 09/07/2019

6.2. Comunicaciones orales aceptadas para ser presentadas en Congresos Internacionales

Se han aceptado recientemente tres trabajos relacionados con esta tesis para su presentación en el congreso IEEE-URSI: "International Conference on Electromagnetics in Advanced Applications" que se celebrará en Honolulu (EEUU) del 9 al 13 de agosto de 2021.

- "Finite Element Studies of Large Scale Earth Resistance Measurements" Autores: Silvia Ronda, Clara Oliver, Oibar Martínez, Patricia Márquez y José Miguel Miranda.
- "Applying the European Electromagnetic Compatibility Directive to Large Scientific Plants: A Case Study"
  Autores: Oibar Martínez, Silvia Ronda, Clara Oliver, Patricia Márquez y José Miguel Miranda.
- "A Demonstration Experiment of Charge Accumulation in Human Body" Autores: Clara Oliver, Oibar Martínez, Silvia Ronda, Patricia Márquez y José Miguel Miranda.

7. Otras aportaciones relacionadas con la tesis

7.1. Artículos pendientes de enviar a revista con sistema de revisión por pares

- "Measuring the Earth Resistance in Large Scale Facilities: Practical Improvements to the Slope Method proposed in IEEE Std 81-2012"
  Autores: Oibar Martínez, Silvia Ronda, Clara Oliver, Patricia Márquez y José Miguel Miranda.

7.2. Elaboración de documentos internos de CTA

- Electrostatic Charge Control Plan for LST. Versión 1.2 Febrero 2020
  Autoras: Clara Oliver y Oibar Martínez.

- The Lightning Protection System of LST1. Versión 1.1 Febrero 2020

  Autoras: Oibar Martínez y Clara Oliver.

7.3. Contribuciones al canal de YouTube UCM-ELEC

- Carga y Descarga de un condensador. Parte I: Fundamento teórico

  https://www.youtube.com/watch?v=QwcoqDT5EDU&t=133s

  Autores: Oibar Martínez, Clara Oliver y José Miguel Miranda.

- Carga y Descarga de un condensador. Parte II: Montaje experimental

  https://www.youtube.com/watch?v=y5hH5bRNlpc&t=8s

  Autores: Oibar Martínez, Clara Oliver y José Miguel Miranda.

- Combatiendo la carga estática

  https://www.youtube.com/watch?v=O7pGP0ieLns

  Autores: Clara Oliver, Silvia Ronda, Oibar Martínez y José Miguel Miranda.

Anexo I

LST Product Breakdown Structure - HW parts

- **8.1 Mechanical System**
  - **8.1.0 Common**
    - 8.1.0.1 Licenses
    - 8.1.0.2 Test Reports
  - **8.1.1 Mount**
    - 8.1.1.0 Documentation and Review Reports
    - 8.1.1.1 Lower Structure
    - 8.1.1.2 Elevation Drive
    - 8.1.1.3 Elevation Bearing
    - 8.1.1.4 Platform at Elevation Bearing
    - 8.1.1.5 Stair case up to Elevation Bearing
    - 8.1.1.6 Platform at Elevation Drive
    - 8.1.1.7 Bogie Nodes
    - 8.1.1.8 Bogies
    - 8.1.1.9 Rail
    - 8.1.1.10 Central Pin
    - 8.1.1.11 Azimuth Locking
    - 8.1.1.12 Azimuth Cable Chain
    - 8.1.1.13 Cable Ducts
  - **8.1.2 Optical Support Structure**
    - 8.1.2.1 Dish Structure
    - 8.1.2.2 Elevation Drive Arch and Cables
    - 8.1.2.3 Camera Support Structure (CSS)
    - 8.1.2.4 Tension Cables and Anchoring Devices for CSS
    - 8.1.2.5 Dish Access
    - 8.1.2.6 Counterweight
    - 8.1.2.7 Cable Ducts
  - **8.1.3 Camera Access Tower**
    - 8.1.3.1 Access Tower Structure
    - 8.1.3.2 Arch Locking System
- **8.2 Optical System**
  - **8.2.1 Primary Mirror**
    - 8.2.1.1 Mirror Facets
    - 8.2.1.2 Mirror Supporting Pads
  - **8.2.2 Optics Alignment**
    - 8.2.2.1 Actuators
    - 8.2.2.2 Interface Plates
    - 8.2.2.3 AMC Control and Power Boxes
    - 8.2.2.4 AMC Cameras
    - 8.2.2.5 AMC Cabling
    - 8.2.2.6 AMC Main Cabinet
- **8.3 Camera**
  - **8.3.1 Mechanics Structure**
    - 8.3.1.0 Assembly and Testing
    - 8.3.1.1 Camera Body
    - 8.3.1.2 Camera Fixation
    - 8.3.1.3 Camera Enclosure
    - 8.3.1.4 Camera Front Door
    - 8.3.1.5 Camera Star Imaging Screen
  - **8.3.2 Focal Plane Instrum.**
    - 8.3.2.1 Light Guides
    - 8.3.2.2 Photosensors
    - 8.3.2.3 Preamplifier Board
    - 8.3.2.4 FPI Slow Control Board
  - **8.3.3 Signal Processing**
    - 8.3.3.1 Readout Board
    - 8.3.3.2 L0/L1 Trigger
    - 8.3.3.3 Backplane
    - 8.3.3.4 Trigger Interface Board
  - **8.3.4 Cam Auxiliary Systems**
    - 8.3.4.1 Ethernet Switches
    - 8.3.4.2 Power Distribution System
    - 8.3.4.3 Envirnomental Control
    - 8.3.4.4 Embedded Camera Controller
    - 8.3.4.5 UCTS Auxiliary
    - 8.3.4.6 Camera Cabling
    - 8.3.4.7 External Cooling Unit
    - 8.3.4.8 Camera Server
    - 8.3.4.9 Central CCD Camera Pixel
    - 8.3.4.10 Hydraulic Pump
    - 8.3.4.11 Transportation and Installation Tool
- **8.4 Auxiliary Systems**
  - **8.4.1 Energy Storage**
  - **8.4.2 Lightning Protection**
  - **8.4.3 Calib. and Pointing Ctrl**
    - 8.4.3.1 Camera Displacement Monitoring & SG Hood
    - 8.4.3.2 Camera Displacement Monitoring
    - 8.4.3.3 Starguider
    - 8.4.3.4 Optical Axis Ref. Laser
    - 8.4.3.5 Calibration Light Source
    - 8.4.3.6 Distance Meter
    - 8.4.3.7 PSF Camera
  - **8.4.4 Drive Control System**
    - 8.4.4.1 Main Drive Control System
    - 8.4.4.2 Encoders
    - 8.4.4.3 Azimuth
    - 8.4.4.4 Elevation
    - 8.4.4.5 Precision Inclinometer
    - 8.4.4.6 Drive Cables
    - 8.4.4.7 End Switches & Interlocks
  - **8.4.5 Drive Container**
    - 8.4.5.1 Container
    - 8.4.5.2 Racks
    - 8.4.5.3 UPS
  - **8.4.6 Struct. Condit. Monitor**
    - 8.4.6.1 Accelerometers
    - 8.4.6.2 Strain Gauges
    - 8.4.6.3 Readout of Structure Condition
    - 8.4.6.4 Structure Condition Cabling
    - 8.4.6.5 CSS Load Pins
  - **8.4.7 Cabling Structures**

Bibliografía

[1] A. Acharyya et al. including O. Martinez, «Sensitivity of the Cherenkov Telescope Array to a dark matter signal from the Galactic centre», *J. Cosmol. Astropart. Phys.*, vol. 2021, n.º 1, ene. 2021, doi: 10.1088/1475-7516/2021/01/057.

[2] H. Abdalla et al. including O. Martinez, «Sensitivity of the Cherenkov Telescope Array for probing cosmology and fundamental physics with gamma-ray propagation», *J. Cosmol. Astropart. Phys.*, oct. 2021, doi: 10.1088/1475-7516/2021/02/048.

[3] D. Mazin, «LST Status», *LST Steer. Committe, LST Gen. Meet.*, 2021.

[4] D. F. Torres, U. Barres de Almeida, y C. Boisson, «Science Requirements for CTA», *Doc. Interno CTA*, 2012.

[5] J. A. Hinton, «Performance Requirements for CTA», *Doc. Interno CTA*, 2013.

[6] C. Boisson, «User Requirements for CTA», *Doc. Interno CTA*, 2013.

[7] J. Carr, «Environmental Requirements for CTA», *Doc. Interno CTA*, 2013.

[8] J. M. Miranda, «Reliability , Availability , Maintainability and Safety Requirements for CTA», *Doc. Interno CTA*, 2013.

[9] Parlamento Europeo y Consejo Europeo, «Directiva de Compatibilidad Electromagnética (CEM) 2014/30/UE», *D. Of. la Unión Eur.*, pp. 79-106, 2014, [En línea]. Disponible en: https://eur-lex.europa.eu/legal-content/ES/TXT/PDF/?uri=CELEX:32014L0030&from=ES.

[10] Parlamento Europeo y Consejo Europeo, «Directiva de Equipos Radioelectronicos (RED) 2014/53/UE», *D. Of. la Unión Eur.*, pp. 62-106, 2014, [En línea]. Disponible en: https://eur-lex.europa.eu/legal-content/ES/TXT/PDF/?uri=CELEX:32014L0053&from=ES.

[11] P. Peñil, L. Á. Tejedor, J. A. Barrio, y M. López, «A trigger interface board to manage trigger and timing signals in CTA large-sized telescope and medium-sized telescope cameras», *arXiv*, 2017, doi: 10.22323/1.301.0808.

[12] Instituto Nacional de Técnica Aeroespacial, «Doc. Nº. CC-TRE-7212-022-INTA-17 EMC TEST REPORT OF EQUIPMENT CTA», 2017.

[13] United States Department of Defence, «MIL-STD-461E Requirements for the Control of Electromagnetic Interference Characteristics of Subsystems and Equipment», *Interface Standard*, 1999. .

[14] United States Department of Defence, «MIL-STD-461F Requirements for the Control of Electromagnetic Interference Characteristics of Subsystems and Equipment», *Interface Stand.*, 2007.

[15] International Electrotechnical Commission, «IEC 61000-4-2 Electrostatic discharge immunity test», *Basic EMC Publ.*, 2008.

[16] International Electrotechnical Commission, «IEC 61000-4-4 Electrical fast transient/burst immunity test», *Basic EMC Publ.*, 2012.

[17] International Electrotecnical Commission, «IEC 61000-4-6 Immunity to conducted disturbances, induces by radio frequency fields», *Basic EMC Publ.*, 2014.

[18] International Electrotecnical Commission, «IEC 61000-4-11 Voltage dips, short interruptions and voltage variations immunity tests», *Basic EMC Publ.*, 2004.

[19] Comisión Europea, «"Guía azul" sobre la aplicación de la normativa europea relativa a los productos», *D. Of. la Unión Eur.*, 2016, [En línea]. Disponible en: https://eur-lex.europa.eu/legal-content/ES/TXT/PDF/?uri=CELEX:52016XC0726(02)&from=BG.

[20] O. Martinez, «Electromagnetic Compatibility Verification for Electronic Boards», *Present. en el Inst. Cosm. Ray Res. la Univ. Tokio el 9 diciembre 2019*, 2019.

[21] O. Martinez, «Electromagnetic Compatibility Verification for Electronic Boards», *Present. en la Univ. Kioto el 2 diciembre 2019*, 2019.

[22] J. G. González, «Informe Geotécnico. Cimentación de los telescopios LST-2, LST-3, LST-4 y MST-3», *Col. Of. Ing. Técnicos Obras Públicas e Ing. Civiles Tenerife*, 2019.

[23] Gobierno de Canarias, «Guía para la planificación y realización de estudios geotécnicos para la edificación en la Comunidad Autónoma de Canarias GETCAN-011», *Doc. Reconocidos del Código Técnico la Edif.*, 2010, [En línea]. Disponible en: https://www.gobiernodecanarias.org/optv/doc/labobras/descargas/getcan011.pdf.

[24] F. Wenner, «A Method Of Measuring Earth Resistivity», *Bull. Bur. Stand.*, 1915, doi: https://doi.org/10.6028/bulletin.282.

[25] S. Ronda, O. Martinez, C. Oliver, P. Marquez, y J. M. Miranda, «Finite Element Analysis and Experimental Characterization of Soil Electrical Resistivity at El Roque de los Muchachos Observatory», *J. Electromagn. Anal. Appl.*, vol. 7, n.º 07, pp. 89-102, 2020, doi: 10.4236/jemaa.2020.127008.

[26] I. de F. d'Altes Energies, «Cimentación para Instalación del Telescopio Prototipo LST (Large Size Telescope)», 2015.

[27] J. Wettingfeld y A. Kern, «Study of a Lightning Protection Concept for the CTA Project», *Vektor Plan. Tech. Rep.*, 2016.

[28] Asociación Española de Normalización (UNE), «UNE 21186 Protección española contra el rayo: pararrayos con dispositivos de cebado», *Norma Española*, 2011. https://www.une.org/encuentra-tu-norma/busca-tu-norma/norma/?c=N0048559.

[29] G. F. Tagg, «Measurement of the resistance of an earth-electrode system covering a large area», vol. 116, n.º 3, pp. 475-479, 1969.

[30] G. F. Tagg, «Measurement of the Resistance of Physically Large Earth-Electrode Systems», *IEE Proc.*, vol. 117, n.º 11, pp. 2185-2190, 1970, doi: 10.1049/piee.1970.0399.

[31] S. Ronda, C. Oliver, O. Martinez, P. Marquez, y J. M. Miranda, «Applying Electromagnetic Field Analysis to Minimize the Earth Rresistance on High Resistivity Soils», *Prog. Electromagn. Res. M*, vol. 96, n.º July, pp. 157-167, 2020, [En línea]. Disponible en: https://www.jpier.org/PIERM/pier.php?paper=20072303.

[32] O. Martínez, «EMC and earthing studies», *Present. el 2 noviembre 2020 en el Gen. Meet. LST1 Celebr. en remoto*, 2020.

[33] CENELEC, «EN 50522 Earthing of power installations exceeding 1KV a.c.», *Eur. Stand.*, 2010.

[34] O. Martinez, S. Ronda, C. Oliver, P. Marquez, y J. M. Miranda, «Verification Protocols for the Lightning Protection of a Large Scale Scientific Instrument in Harsh Environments: A Case Study», *Aceptado en la Rev. J. Power Energy Eng.*, 2021.

[35] Asociacion Española de Normalizacion y Certificacion, «Proteccion contra el rayo parte 3: Daño fisico a estructuras y riesgo humano, UNE-EN 62305-3», *Norma Española*, 2011.

[36] O. Martínez, «Verification of ground contacts , ground resistance and soil resistivity», *Present. el 9 julio 2019 en el Gen. Meet. LST1 Celebr. en Rijeka*, 2019.

[37] C. Oliver y O. Martínez, «Electrostatic Charge Control Plan for LST», *Doc. Interno CTA*, 2020.

[38] O. Martinez, «Verification of Electromagnetic Compatibility Requirements and CE marking», *Present. en la Univ. Ginebra el 13 septiembre 2019*.

[39] O. Martinez, «Verification of EMC requirements for LST», *Present. en la Univ. Zúrich el 17 septiembre 2019*.

[40] ESD Association & JEDEC Solid State Technology Association, «ANSI/ESDA/JEDEC JS-001», 2010, [En línea]. Disponible en: http://www.esd-resource.com/userfiles/2011-05-20/201105200647101.pdf.

[41] A. Gadola, «Zurich Actuator Characteristics», *Doc. Interno CTA*, [En línea]. Disponible en: https://cta.physik.uzh.ch/public/amc/Mirror_Actuator_System_Characteristics.pdf.

Tabla de ilustraciones

Journal of Power and Energy Engineering

ISSN Print: 2327-588X ISSN Online: 2327-5901

Acceptance Notification

May 12, 2021

Dear Author(s),

Thanks for your contribution to the ***Journal of Power and Energy Engineering*** (**JPEE**).

We are pleased to inform you that your manuscript:

Paper ID: 1770874

Manuscript Title: Verification Protocols for the Lightning Protection of a Large Scale Scientific Instrument in Harsh Environments: A Case Study

Author(s): O Martinez, S Ronda, C Oliver, P Marquez, JM Miranda

has been accepted. Congratulations!

Your paper will appear online in the upcoming issue in JPEE Vol. 9 No. 6 in June 2021.

Thank you very much for your support to our journal.

Journal of Power and Energy Engineering Editorial Board
SCIENTIFIC RESEARCH PUBLISHING LIMITED
Building 5, Headquarters Space of Optical Valley, Tangxun Lake North Road #38, East Lake High-Tech Development Zone, Wuhan 430223, Hubei Province, China
https://www.scirp.org/journal/jpee
Email: jpee@sciresp.org

Journal, 2020, *, *-*
https://www.scirp.org/journal/***
ISSN Online: **-**
ISSN Print: **-**

Verification Protocols for the Lightning Protection of a Large Scale Scientific Instrument in Harsh Environments: A Case Study

Oibar Martinez, Silvia Ronda, Clara Oliver, Patricia Marquez, Jose Miguel Miranda

Departamento de Estructura de la Materia, Fisica Termica y Electronica,
Facultad de Fisicas, Universidad Complutense de Madrid
28040 Madrid, Spain
Email: miranda@ucm.es

How to cite this paper: O. Martinez, S. Ronda, C. Oliver, P. Marquez and J.M. Miranda, (2020) Verification Protocols for the Lightning Protection of a Large Scale Scientific Instrument in Harsh Environments: A Case Study. ******, *****, *-*.
https://dx.doi.org/10.4236/***.2020.*****

Received: **** **, ***
Accepted: **** **, ***
Published: **** **, ***

Abstract

This paper is devoted to the study of the most suitable protocols needed to verify the lightning protection and ground resistance quality in a large-scale scientific facility located on a site with high risk of lightning strikes. We illustrate this work by reviewing a case study: the largest telescopes of the Northern Hemisphere Cherenkov Telescope Array, CTA-N. This array hosts sensitive and high-speed optoelectronics instrumentation and sits on a clear, free from obstacle terrain at around 2400 m above sea level. The site offers a top-quality sky but also features challenging conditions for a lightning protection system: the terrain is volcanic and has electrical resistivities well above 1 kOhm·m. In addition, the environment often exhibits humidities well below 5%, and strong winds poses challenging conditions. On the other hand, the high complexity of a Cherenkov telescope structure does not allow a straightforward application of lightning protection standards.

We describe here how the risk assessment of direct strike impacts was made and how contact voltages and ground system were both tested. Finite Element Simulation (COMSOL Multiphysics) has been used to estimate the current flowing through the parts of the earthing system designed for the telescopes in the case of a direct strike impact. This work is intended to provide assistance to scientists and managers involved in the construction of scientific installations, particularly those in charge of defining verifiable reliability and safety requirements for lightning protection.

Keywords

Lightning Protection, Earth Resistance, FEM, COMSOL

1. Introduction

Specific standards are available to provide guidelines on lightning protection strategies. While NFPA 780 standard means to regulate the lightning protection systems in USA [1], in european installations the following two international standards are well known: IEC 62305 [2], which establishes the installation commitment of a lightning protection system, and IEC 62561 [3], which focuses on the components of lightning protection. The requirements of the EN 50536 standard [4], which determines the installation commitment of storm detectors, as well as the main characteristics thereof, must also be met. Also in some cases local standards must be considered.

While all these standards provide valuable information, they are mostly focused on the analysis of buildings and industrial installations, and some peculiarities of scientific installations are not always well covered by them. In particular, we focus this work on the Risk and earth quality assessments, and apply this to an example of a large scale scientific installation: the largest telescopes of CTA-N observatory.

CTA-N has been conceived as an array of fourteen Cherenkov Telescopes of two different sizes, which will be constructed in La Palma Island, Spain. Cherenkov Telescopes can provide valuable information on different astrophysical sources from the gamma rays reaching the Earth's atmosphere. The largest telescopes of CTA are called Large Size Telescopes (LST's) and the construction of the first one was finished in October 2018. The design and construction of the LST Lightning Protection System faced a number of technical difficulties that were addressed with the protocols described in this paper.

2. Risk Assessment

Risk assessments for lightning protection must quantify the exposure of structures, their contents, their internal systems and involved individuals to direct and indirect lightning strikes. The assessment described in IEC 62305-2 Ed.2:2010-12 [5] was taken as baseline reference for the definition of the protocols described here. Two main types of loss apply to a large scale facility:

- Loss or injury of human life;
- Economic losses.

The risk calculation was carried out by analyzing two major points:

- Probability of direct strike impact
- Severity of the damage

The calculation of the probability of direct strike impact was made via the models available of international standards. These models typically make use of tabulated values of the average annual lightning flash density per square kilometer in the area, and take into account local parameters like the height of the structure and that of surrounding objects. However, a more convincing alternative for large scale facilities which must not comply with specific, rigid regulations might be the use of worldwide databases of strikes which take data from an array of ground sensors and are updated on real time [6], [7].

A systematic evaluation of the damage severity started with a preparation of a list of most feared events, which was based on:

- A mature Product Breakdown Structure, which enables one to identify the critical parts and their interfaces.
- An accurate cost model which accounts not only for the cost of the damaged item but also for the cost of the replacement. This is particularly relevant when the Installation is located in an area of difficult access.
- A basic knowledge of the foreseeable damage on subassemblies under risk, which should be supported by a reliability model, a failure analysis and lightning strike resilience tests made in a certified laboratory.

The rating of the most feared events must be performed with suitable risks scales. Large scale facilities are typically handled by wider scope risks plans and analyses, and therefore it is advisable to develop risks scales which harmonize with the other type of risks analyzed during the design stage: technical, economical, schedule, managerial, etc [8].

The outcome of the risk assessment was followed by a decision-taking process in which a specific level of protection is approved. The physical implementation of the corresponding lightning strike protection system is then part of an iterative process in which a preliminary design must be reviewed and validated within a framework of requirements in terms of cost, schedule and technical feasibility.

CTA-N site was chosen for its suitability to astronomical observations, being free from terrain obstacles. Located at around 2400 m above sea level, it offers a top-quality sky but also features challenging conditions for a lightning protection system: the terrain is volcanic and features a high resistivity, in the kOhm·m range. The relevant ambient conditions to be considered for design and selection of materials are:

- Ambient temperature -20 to +40°C
- Humidity 2 to 100 % RH

- Extreme ice (snow covered) of <20 mm (see also picture below)
- Wind gusts up to 200 km/h
- Reduced pressure and air density as applicable at 2400 m altitude
- Increased solar radiation and exposure to UV as applicable at 2400 m altitude. Components used for the lightning protection must be resistant to UV radiation, especially plastics.

Due to solar radiation, the temperature of components can become significantly higher than the maximum air temperature. Component temperatures depend very much on their thermo-elastic properties resulting from their color and their surface finish. Component temperatures up to 100°C are possible during hot summer days. On the other hand, due to thermal radiation to cold sky, the temperature of components can also become significantly lower than the minimum air temperature. Depending on their surface finish, component temperatures can be as low as -40°C. During winter ice pile up may become a serious issue, especially for slender component. This happens occasionally.

In CTA, a failure or a damage of one telescope does not significantly influence the availability of the whole CTA system. This means, that an outage of one telescope due to a lightning strike does not have significant consequences, also not economically, for the whole operation process of CTA. In case of such an outage only the damage costs of the telescope being struck are to be considered for the economic losses. No follow-on costs exist.

The probability of direct strike was estimated from the database of Vaisala, where the strikes on a 10 km x 10 km area around the LST site were analyzed. A total of 138 strikes were registered from 2013 to 2017, with peak current densities ranging from 3.1 kA to 693.5 kA. We estimated a probability of one impact on one LST per 88 years by using the IEC-62305-2 standard model and Vaisala data. A probability of one impact per 25 years was obtained when using the same model but with the tabulated lightning flashes per km^2 per year that is assigned by this standard to Canary Islands.

The result of the risk assessment concluded that the following protection measures were needed:

- A lightning protection system class III according to IEC standards, integrated in the LST structure;
- A certain shielding effectiveness of all the cabling and the electrical components (housings) on the telescope;

- Two level surge protection system at all cables entering the telescopes from the outside (equipotential bonding).

3. LST Lightning Protection System

The LSTs are the most complex and highest structures of the CTA Observatories. These instruments measure the Cherenkov light from an Extensive Air Shower generated by the interaction of very high energy gamma rays from the Universe in the upper atmosphere. An LST has a shape which resembles a large parabolic antenna, with a 23-meter reflective surface supported by a tubular structure made of carbon fibers and steel tubes. The reflective surface has 370 square meters and is made of an array of segmented mirrors that can be controlled individually by a subsystem of actuators. This surface collects and focuses the Cherenkov photons into the Camera, where 1855 photo-sensors convert the light in electrical signals that can be processed by dedicated electronics. The total moving weight of the telescope (excluding the rail) is around 100 tons. The dish is the support for all the elements of the LST segmented mirror and is designed to house 207 hexagonal mirror facets. The basic elements of the space frame are tetrahedral structures of Carbon Fiber Reinforced Polymer (CFRP) tubes of 60, 80 and 100 mm diameter.

Using Monte Carlo simulations, the sensitivity of the CTA Observatories were optimized between 20 and 200 GeV with a design of four LSTs of 28 m focal length. Figure 1 shows a picture of the first LST (LST1) constructed in Spain, together with a detail of the implemented Lightning Protection System. The high complexity of a Cherenkov telescope structure does not allow a straightforward application of lightning protection standards for accurate predictions of direct strike probabilities. The LST is an alt-azimuth telescope with a parabolic reflective surface, as can be seen in Figure 1a. It is supported by a tubular structure made of CFRP, aluminum and steel tubes. The Camera Support Structure is stiffened by 26 tension cables produced by filament winding process. The main purpose of the tension cables is to limit the out-of-plane deformations. They have a cross section of 130 mm^2 and their length can vary between 17 m and 28.6 m. The installation of the mechanical structure, optics and camera started in July 2017 and was finished in 15 months.

Preliminary studies of the lightning protection system were performed based on an array of four standalone lightning rods surrounding the telescope structure. The efficiency of this system was studied by the Dynamic Electro-Geometrical Model (DEGM). The studies led to the conclusion that better efficiencies were possible by integrating an array of rods in the own telescope. The final design of the lightning protection system was carried out by the Rolling Sphere Method developed by Ralph H. Lee in 1977 for shielding buildings and industrial plants [9]. This method was extended by J.T. Orrell for use in substation design [10], and it is based on the principles and theories by Whitehead [11]. It is widely used in a number of standards, such as the IEEE Guide for Direct Lightning Stroke Shielding of Substations, the BS-EN/IEC 62305 or the NFPA 780 lightning protection standards, among others. The technique involves rolling an imaginary sphere over the surface to be protected. The sphere

rolls up and over lightning masts, shield wires, fences, and other grounded metal objects intended for lightning shielding. A piece of equipment is protected from a direct stroke if it remains untouched by the sphere. Equipment that touches the sphere or penetrates its surface is not protected. This method meets different protection levels depending on the radius of the sphere.

The arch used for the camera support contains an array of air-termination rods having a length of 0.5 m which are angled with 45° to both sides to enlarge the protection area. The rods are fixed every 6 m from the camera up to the metal rail of the telescope base, passing by the upper arch and the periphery of the telescope dish. The carbon fiber parts of the dish were protected by a conductor around both edges. Half circumference down to the elevation platform were considered sufficient. The conductors are connected on top to the elevation arch and on bottom to the housing of the elevation bearing. The mirrors are sufficiently protected by the dish and the arch conductors. The elevation bearings were bridged by flexible strips at both sides. At each side two strips are connected between the metallic parts of the optical support structure and the tower head across the bearings. In this way the strips allow the elevation movement of the telescope dish. The lightning current from the telescope structure rods is guided to earth via both East and West side elevation platforms. Each of the two towers of the elevation system as well as the camera maintenance tower are protected by two four-meter lightning rods.

The lower structure is built with highly conductive materials and serves well to safely guide the excess lightning current to earth. However, in order to provide a clear electrical continuity, extra down conductors from the elevation bearings were installed and fed down to the azimuth locking system, where they are connected to earth.

The following Surge Protection Devices (SPD) were installed on various systems:

- SPD type 1 consists on a single-phase SPD that can also be used as 3-phase N AC network protection. It is used as primary protection, installed in the main panel power supply systems (it is DIN rail compatible). The installation of this device is compulsory according to EN 62305 and EN 60360 standards, and it can derive to ground currents up to 100 kA.
- SPD type 2 is dedicated to protect the most sensitive equipment. It can be used in common or differential mode, and provides protection against high currents up to 40 kA. It is installed in the diverted panels, close to the vulnerable equipment. It is DIN rail compatible.
- Specific SPDs were installed on telecommunication panels, data lines and low voltage distribution systems.

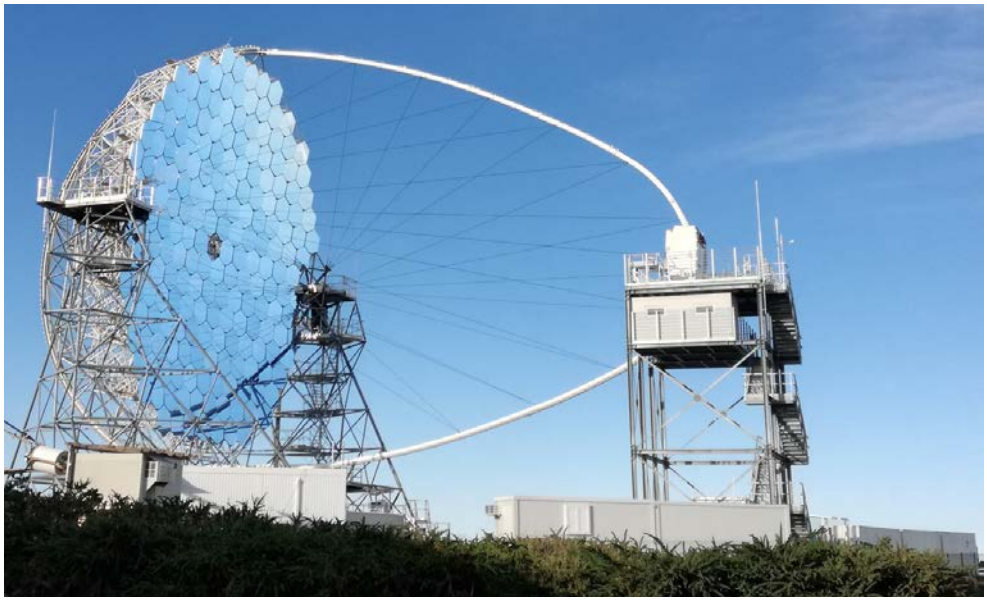

(a)

(b)

Figure 1. The first LST of the CTA-North observatory (a), and detail of the lightning rods installed on the Camera Support Arch Structure (b).

5. Specific Tests on Critical Components

The evaluation of the damage strike severity was made after the Failure Mode and Criticality Analysis of the whole telescope, and specific tests on the following critical elements:

- Mirror actuators, which are sensitive to possible damage by the induction of Electromagnetic Fields generated by the lightning currents.

- CFRP tubes, which might be impacted by a direct strike.

The definition of the most suitable protocol to assess the damage suffered by the actuators was a major issue. High quality studies on the lightning strike current waveforms can be found in [12]. Several standards propose models for lightning strikes current pulses. IEC-62305-1 suggests a 10/350 μs current wave as reference for tests [13]. It simulates the first return stroke of a lightning event with a triangular like pulse where the rise time is 10 μs and the time to drop to 50% of the peak amplitude is 350 μs. Another widely used standards in Aircraft Lightning Tests is the EUROCAE-ED-84 / ARP5412 [14].

The current strike tests were made at the high current facility of the Official Central Laboratory for Electrotechnic Tests (LCOE). Figure 2 shows the result of the impact of a positive 200 kA strike on a sample of a CFRP tube using EUROCAE-ED-84 standard. Verification of Electromagnetic Pulse induction on the actuators was also made. The tests were made without energizing the actuator, which showed no damage after the strike.

The assumption that the actuator is not energized during a true lightning strike is justified by the fact that during storms these actuators are switched off. The resilience of the CFRP to the lightning strike was excellent due to the large conductivity of the material. Given the fact that the structural analysis of the telescope demonstrated that no single failures of a CFRP compromise the mechanical stability, these high current tests were an objective evidence that the risk of strikes on the structure is acceptable.

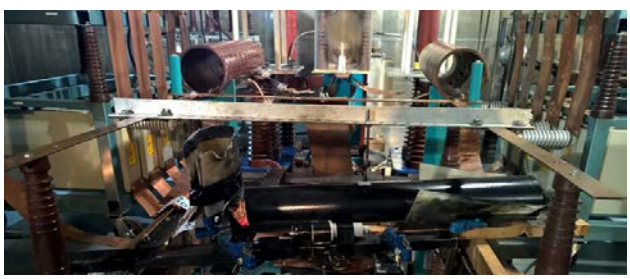

(a)

(b)

Figure 2. Detail of the damage made to a sample of CFRP by a strike with a peak current of 200 kA, by using the protocol described in EUROCAE-ED-84 / ARP5412 standards at LCOE laboratories. Overview of the experimental setup where the yellow arrow indicates the place where the controlled impact of the current strike was applied to the carbon fiber (a), and detail of the damage produced after the strike (b). The actuators were located nearby to assess the robustness of the electronics to the electromagnetic field induced by the current strike.

6. Foundation earth Resistance and Soil Resistivity

Figure 3 shows the base structure and a detail of the LST1 foundation, which is made of reinforced concrete. The foundation of the remaining telescopes will have a very similar design but they will be dimensioned according to the specific conditions of the soil. The Rail is fixed to the foundation by means of a pedestal, a curved I-beam. The I-beam is fixed on top of steel feet, in a way that allows small movements in radial directions that occur due to temperature expansion during the day and night. The steel feet are fixed to the concrete beam with anchor bolts.

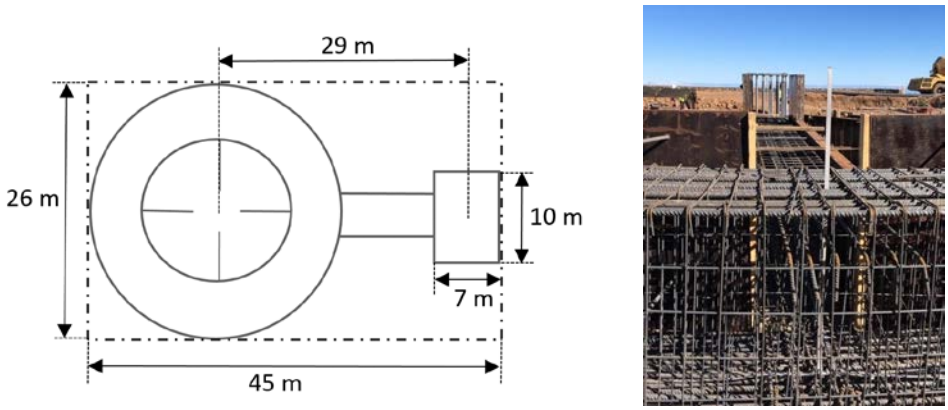

Figure 3. LST1 Foundation: Schematics showing the size of the foundation ground, which was connected to the camera access tower ground (a), and foundation structure (b).

The LST1 site posed special difficulties due to the abundant bushes and stones located on the terrain, which do not allow one to insert the rods in every needed point and to achieve the best electrode line directions. In addition, the high electrical resistivity of the soil limits the maximum electrode line length. In order to obtain a reliable measurement a total of 18, 3-point resistance measurements were made, distributed in three different electrode line orientations.

The LST1 earth resistance measurement gave values ranging between 11.7 and 14.0 Ohm, depending on the measurement method and electrode positions. The intersecting curves method and the slope method were chosen for the tests due to their high accuracy for large distributed grounds [15], [16]. Ground measurements were also made with the standard 62% method, providing a significantly higher values, in the order of 17 Ohm. The first two measurements were made during a day where ambient humidity was 12%, the 62% method measurements was made in a day where ambient humidity was 40%. The 62% method is one of the most popular among workers on electrical installations for ground resistance measurements. However, this method is not accurate when measuring large and complex earth systems, as is the case of the LST earth system. The reason is that the total length of the electrode line needs to be too long, around 6.5 times the characteristic size of the earth system, in order to properly apply the corresponding equations. Overlooking this condition leads to noticeable overestimations of the ground resistances.

The standard improvements which can be made to reduce the earth resistance in difficult terrains are generally based on

a) burying horizontal conductive plates or meshes,
b) burying vertical electrodes connected in parallel or
c) modifying the own terrain, which can be done by either changing the entire terrain material in a large volume or adding earthing enhancing compounds.

A combination of several procedures was also considered, inspired in the Taiwan Photon Source (TPS) storage ring design, which has a 0.2 Ohm earth system with 62 vertical electrodes and a grid of 4 rings. Bentonite was used to lower the resistivity of the terrain [17]. However, the earth resistance scales with the soil resistivity and the TPS ring were installed in a site with a resistivity having almost two orders of magnitude lower than the soil at LST1 site. Some theoretical models of earth resistances as function of conductor geometry and soil resistivity can be found in the standard BS 7430:2011 [18], the recent review of the Electrical Engineering portal [19], and the classical MIL-HDBK-419A for vertical electrodes [20]. Models for the calculation of the resistance of a grid with encased vertical electrodes can be found in the IEEE Std 80-2000 [21]. IEC 62561-7 standard discusses prequalification methods for ground enhancement materials [22].

A number of earth enhancement materials were considered. The most promising ones were materials containing cement, which after installation acquire properties that are very close to concrete [23]. However, they were finally disregarded due to environmental restrictions. Finite Element Simulation software has been used to reproduce real-world conditions in terms of structure designs and soil profiles and have allowed us to evaluate the improvements that should be adopted to reduce the earth resistance of the LSTs [24]. We have considered how the earth resistance value changes as a function of the shape, size and number of horizontal and vertical electrodes depending the soil properties. The possibility of inter-connecting in parallel several telescopes has also been analyzed. The simulation results in [24] revealed that the best strategy in each case differs: when the soil is uniform, it is advisable to extend horizontal electrodes as far as possible from the foundation. However, when layers with different resistivity are present, to bury vertical electrodes that connect with deep high conductive layers is the best strategy.

Ample information can be found on recommended values of maximum earth resistances according to international standards. In line with the previous standard, BS 6651, the new S/EN 62305-3 standard recommends a single integrated earth termination system for a structure, combining lightning protection, power and telecommunication systems. This standard encourages an earth resistance requirement below 10 Ohm. NFPA and IEEE recommend 5 Ohm or less, NEC 250.56 25 Ohm or less, and 5 Ohm or less if sensitive instrumentation is installed.

Local Spanish norm ITC-BT-18 (REBT) [25] describes the regulations that are compulsory for the installation of earth termination systems, but no specific limits on earth resistance are specified. The regulation is focused on the contact voltages, which must be less than 24 V in conductors and 50 V elsewhere. The limit in earth resistance must be established

from the current limit of the differential breakers in service, and taking into account the parasitic resistances of the ground wires. There is an additional regulation from norm BT-26 [26], which states a maximum earth resistance of 37 Ohm for buildings without lightning protection systems and 15 Ohm for those which have one.

Ronda et al. made a detailed study of the soil electrical resistivity of El Roque de los Muchachos Observatory [27]. Measurements were made using Wenner method [28] in six different locations of the telescopes: the four LST sites and two nearby similar instruments, the MAGIC telescopes. In addition, the resistivity at the sites was simulated with COMSOL Multiphysics software considering a simple single layer model and a three-layer model. While five of the studied places showed resistivity values compatible with a single layer structure (homogeneous), the sixth one, contained materials in the shallow layers with significantly higher resistivities, so it corresponds to an in-homogeneous, four-layer model in COMSOL.

On the other hand, it is well known that the electric properties of a ground system subject to high impulse currents is quite different from that at low frequency. It is not only the fact that the inductive behavior of electrodes become relevant with respect to its resistive behavior. In addition, large current pulses ionize the soil around the electrode, and this makes the impulse response typically nonlinear [29]. Numerical electromagnetic models can be used to simulate the lightning response of a grounding electrode, although recent work claims that accurate predictions of electrode behavior under a lightning strike can be made with impulse impedances, which can be obtained from special experimental procedures [30], [31].

7. Structure Equipotentiality

Several test points were chosen to perform a survey of the structure equipotentiality. The results of the measurements can be seen in Figure 4. The only points which exhibited a resistance above 1 Ohm is the plate covering the elevation bearing, which was fixed with an extra bond to the elevation access platform, and the catwalks for dish maintenance work. According to the conceptual design, the wires chosen for the installation of the lightning down conductor cables should be of stainless steel and have a standard diameter of 10 mm. These wires have an ohmic resistance of 0.01 Ohm/m. In other words, a single wire of 10 m is already giving a resistance comparable to several contact resistances measured at the LST structure.

The wires foreseen to connect the lightning rods to the ground system of the LST1 are also in disadvantage against the LST1 structure in terms of high frequency impedances. A wire is, by its own nature, inductive, but the LST structure is not. The equivalent inductance of the LST structure is expected to be significantly lower than the one of a cable. A standard calculator predicts an inductance of 1000 nH/m for the wire proposed in a preliminary conceptual design. Therefore, a cable of 10 m may reach a reactance of around 6 Ohm for

the strike characteristic frequencies (100 kHz), which is comparable to its ohmic resistance.

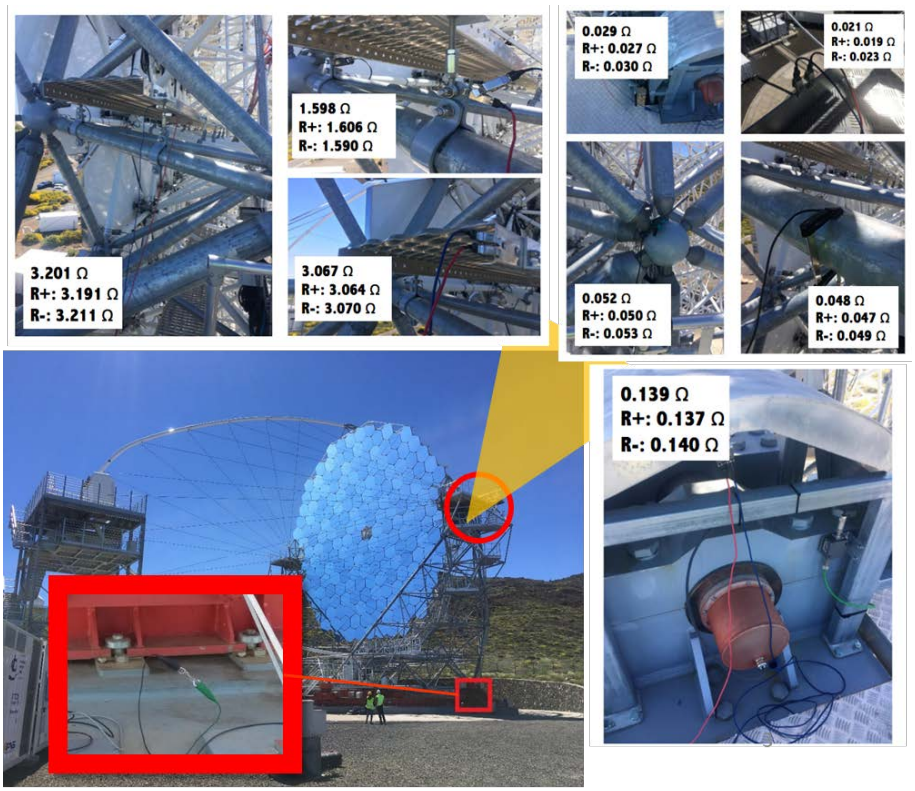

Figure 4. Survey of structure equipotentiality.

Increasing down conductor cable diameter doesn't help: 20 mm diameter only reduces inductance in 10%.

8. Electric Current Dissipation After a Lightning Strike

FEM has been used to estimate the current that will be dissipated during a lightning strike in a LST telescope, as well as to study how a high discharge current pulse is guided through the grounding electrodes to Earth.

The domain under study is depicted in Figure 5. It is a hemisphere that contains a recreation of the complete geometry designed for the earthing system of the LST, which includes:

- The metal grid, which consists of two solid blocks. One of them is located under the telescope camera and the other under the mirror.
- A composition of thin metal plates, which are surrounding and connected to the solid blocks. These metal plates are designed with 3.5 mm height and 30 mm width.

The material has the properties of structural steel (conductivity of 4.03 MS/m). The soil below earth resistance installation is considered with a homogeneous resistivity of 1.5 kOhm·m.

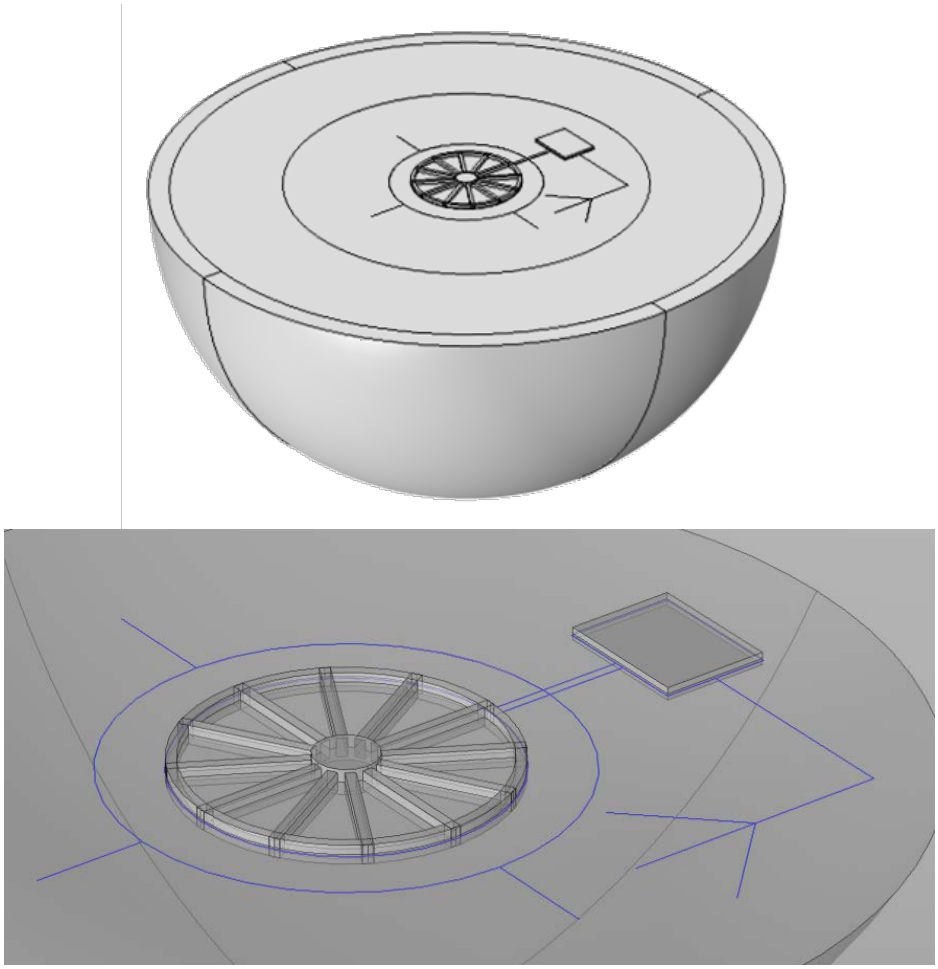

Figure 5. Implemented model geometry. Metal grid of the reinforce is displayed in grey color and metal plates surrounding it are in blue.

We have studied how the current in the case of a lightning strike in the centre of the structure is distributed through the earthing plates, according to the resistances of the different paths. A single injection of a stationary 300 kA current in the centre of the structure is simulated. This is a worst-case scenario, since the current in the structure is dissipated via two different down-conductor paths. Since the simulation is made with stationary currents, it cannot provide information on inductive effects. As the current that flows in the core of one plate can induce voltage in adjacent cables, we calculate the average current density in the surface of each plate. The results for the current flow thru the metal plate structure are shown in Figure 6. There is a reduction of around one order of magnitude between the original incident current and the one in the external parts of the structure. All these data are important for the design of the electric installation since it helps to evaluate critical design parameters, such as the minimum distance between earth plate paths and cabling feeding sensitive equipment.

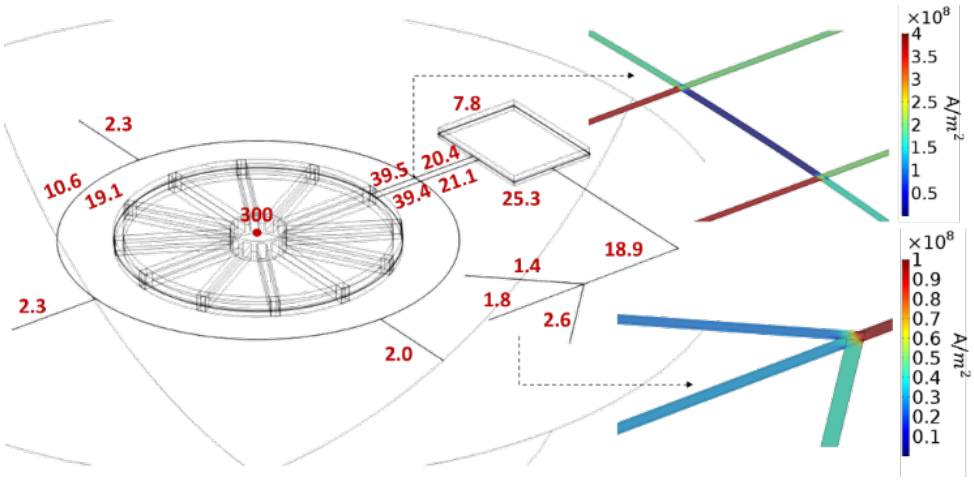

Figure 6 Averaged current in kA within the plates in the case of a 300 kA punctual current threat in the center of the structure.

Concluding Remarks

This paper illustrates that international standards on lightning protection are not always applicable in a straightforward way to Large Scale Scientific Facilities. In this work we are proposing a design and verification protocol for lightning protection systems installed on scientific facilities which addresses critical issues that are common to installations on harsh environments. This protocol was applied to the lightning protection system of the large scales telescopes of CTA-N array, and covered the following items:

- Risk assessment
- Rolling Sphere based Design
- Destructive Tests on Critical Items
- Structure Equipotentiality verification
- Earth Resistance measurement and optimization
- Strike current dissipation assessment via Finite Element Method simulation

The Risk Assessment was based on rating the lightning strike risks in a way that can be harmonized with other risks analysis that are usually encountered in the design study of a large scale facility, like technical, economical, schedule or managerial risks. The likelihood of a lightning strike could accurately be assessed by using a sensor network service able to provide strike statistics with high resolution and sensitivity. The Risk Assessment provided valuable input for the final design, which was based on an array of passive Franklin Rods mounted on the telescope structure and three adjacent buildings: the two elevation tower platforms. The rod system was dimensioned according to the rolling sphere method for a Class I system, well above the minimum requirement of Class III provided by the risk

assessment of conventional lightning protection standards.

The ground resistance assessment is of major concern when soil resistivities are high, and the large and complex sizes of ground foundations encountered in large scale facilities demand the use of special techniques, like the curve intersection method. The case study presented here shows that conventional methods tend to significantly overestimate the ground resistances.

Finally, FEM simulations could provide an insight on the soil resistivity measurements and the earthing system structure functionality. We demonstrate its usefulness to do:

- Correlations between materials found in the geotechnical surveys and the measured resistivities.
- Strike current estimations expected in the plates due the dissipation of a direct lightning strike, leading to a reduction of one order of magnitude in the case of the LSTs earthing system.

Acknowledgements

This paper has been funded by the Spanish National Research Plan via project PID2019-107847RB-C43.

References

[1] National Fire Protection Association (2020), "Standard for the Installation of Lightning Protection Systems", *NFPA780*, https://www.nfpa.org/codes-and-standards/all-codes-and-standards/list-of-codes-and-standards/detail?code=780

[2] International Electrotechnical Commission (2020), "IEC62305:2020 Series", *Ed. 2:2020*, https://webstore.iec.ch/publication/6797

[3] International Electrotechnical Commission (2017), "Lightning protection system components (LPSC) - Part 1: Requirements for connection components", *IEC62561-1:2017*, https://webstore.iec.ch/publication/26401

[4] Spanish standardization body UNE (2013), "Protection against lightning-Thunderstorm warning systems",*UNE-EN50536:2011/A1:2013*, https://www.une.org/encuentra-tu-norma/busca-tu-norma/norma/?Tipo=N&c=N0052167

[5] International Electrotechnical Commission, (2010) "Protection against lightning – Part 2: Risk management", *IEC 62305-2 Ed.2: 2010-12*, https://webstore.iec.ch/publication/6794

[6] Cummins, K.L. and Murphy, M.J. (2009) "An overview of lightning locating systems: History, techniques, and data uses, with an in-depth look at the U.S. NLDN." *IEEE Transaction on Electromagnetic Compatibility*, 51, 499-518, https://ieeexplore.ieee.org/document/5173582

[7] Nag, A., Murphy, M.J., Schulz, W. and Cummins, K.L. (2015) "Lightning locating

systems: Insights on characteristics and validation techniques", Earth and Space Science, 2. https://agupubs.onlinelibrary.wiley.com/doi/full/10.1002/2014EA000051

[8] Bernardino, T. (2014), "Application of international quality standards to scientific research: product assurance in large scientific installations", *Doctoral dissertation, Universidad Complutense de Madrid*, https://eprints.ucm.es/24112/.

[9] Lee, R. H. (1977), "Protection Zone for Buildings Against Lightning Strokes Using Transmission Line Protection Practice", *IEEE Industrial & Commercial Power Systems Conference*, 1977-May. https://ieeexplore.ieee.org/abstract/document/4503576

[10] Orrell, J. T. (1988), "Direct Stroke Lightning Protection", communication presented at *EEI Electrical System and Equipment Committee Meeting, 25 Oct. 1988*. Reproduced in Annex G of "IEEE Guide for Direct Lightning Stroke Shielding of Substations," in IEEE Std 998-2012 (Revision of IEEE Std 998-1996) , vol., no., pp.1-227, 30 April 2013, doi: 10.1109/IEEESTD.2013.6514042. https://ieeexplore.ieee.org/document/6514042

[11] Gilman D. W. and Whitehead, E. R., (1973) "The mechanism of lightning flashover on high voltage and extrahigh voltage transmission lines", *Electra*, no. 27, 65-96, Mar. 1973. https://e-cigre.org/publication/ELT_027_3-the-mechanism-of-lightning-flashover-on-high-voltage-transmission-lines

[12] Rakov, V. A. et al. (Working Group C4.407), (2013) "Lightning Parameters for Engineering Applications", *CIGRE publications*, https://www.researchgate.net/publication/283303928_Lightning_Parameters_for_Engineering_Applications

[13] IEC 62305-1:2010, (2010) "Protection against lightning - Part 1: General principles" https://webstore.iec.ch/publication/6793

[14] IS Society of Automotive Engineers, Aerospace recommended practice – 5412. (1999), "Aircraft lightning environment and related test waveforms", *SAE International edition*. https://www.sae.org/standards/content/arp5412/

[15] Tagg, G. (1969) "Measurement of the Resistance of An Earth-Electrode System Covering a Large Area.", *IEE Proceedings*, Vol. 116, Mar. 1969. http://digital-library.theiet.org/content/journals/10.1049/piee.1969.0097

[16] Tagg, G. (1970) "Measurement of the Resistance of Physically Large Earth-Electrode Systems", *IEE Proceedings*, Vol. 117, Nov. 1970. http://digital-library.theiet.org/content/journals/10.1049/piee.1970.0399

[17] Tzong-Shyan Ueng, Yu-Chih Lin, Jui-Chi Chang, Chien-Kuang Kuan, (2011) "The ground testing of TPS ground system", *Proceedings of IPAC2011*, San Sebastián, Spain, 2011. http://accelconf.web.cern.ch/accelconf/ipac2011/papers/tups062.pdf

[18] "Code of practice for protective earthing of electrical installations", BS 7430:2011 https://global.ihs.com/doc_detail.cfm?document_name=BS%207430&item_s_key=00131083&csf=TIA

[19] "Measurements and calculations of Earth Electrode Systems", Electrical Engineering Portal, (2018) https://electrical-engineering-portal.com/earth-electrode-systems#types-earth-electrodes

[20] US Department of Defense, (1987) "Grounding, Bonding and Shielding for Electronic Equipments and Facilities", MIL-HDBK-419A, 29th December 1987 https://www.wbdg.org/FFC/NAVFAC/DMMHNAV/hdbk419a_vol1.pdf

[21] "IEEE Guide for Safety in AC Substation Grounding", IEEE Standard 80-2000 (Revision of IEEE Standard 80-1986). https://standards.ieee.org/standard/80-2013.html

[22] IEC 62561-7:2018, "Lightning Protection System Components (LPSC), Part 7: Requirements for Earthing Enhancing Compounds", (2018) https://webstore.iec.ch/publication/33885

[23] Lindsay, T. "National Electrical Grounding Research Project, Technical Report" (2007). https://www.nfpa.org/-/media/Files/News-and-Research/Archived-reports/negrp-finalreport.ashx?la=en

[24] Ronda, S., Oliver, C., Martinez, O., Marquez, O. and Miranda, J.M. (2020) "Applying Electromagnetic Field Analysis to Minimize the Earth Resistance on High Resistivity Soils" *Progress In Electromagnetics Research M*, V 96, 157–167. https://www.jpier.org/PIERM/pier.php?paper=20072303

[25] "Reglamento Electrotécnico Para Baja Tensión (REBT)" (in Spanish), ITC-BT-18, BOE-A-2002-18099, 2002, https://www.boe.es/buscar/doc.php?id=BOE-A-2002-18099

[26] "Reglamento Electrotécnico Para Baja Tensión (REBT)" (in Spanish), ITC-BT-26, BOE-A-2002-18099, 2002, https://www.boe.es/buscar/doc.php?id=BOE-A-2002-18099

[27] Ronda, S., Martinez, O., Oliver, C., Marquez, O. and Miranda, J.M. (2020) "Finite Element Analysis and Experimental Characterization of Soil Electrical Resistivity at El Roque de los Muchachos Observatory," *J. Electromagn. Anal. Appl.*, V 7. https://www.scirp.org/journal/paperinforcitation.aspx?paperid=101519

[28] Wenner, F. (1915) "A Method of Measuring Earth Resistivity", *Bull. National Bureau of Standards*, Bull 12(4) 258, p. 478-496; 1915/16. https://nvlpubs.nist.gov/nistpubs/bulletin/12/nbsbulletinv12n4p469_A2b.pdf

[29] Jinliang, H., Gao, Y., Zeng, R., Zou, J., Liang, X., Zang, B., Lee, J. and Chang, S. (2005) "Effective Length of Counterpoise Wire Under Lightning Current", *IEEE Transactions on Power Delivery*, vol 20(2). https://ieeexplore.ieee.org/document/1413429?arnumber=1413429. Also in https://www.researchgate.net/publication/3275110_Effective_Length_of_Counterpoise_Wire_Under_Lightning_Current

[30] Visacro, S., Alipio, R. , Murta Vale, M.H. and Pereira, C. (2011) "The Response of Grounding Electrodes to Lightning Currents: The Effect of Frequency-Dependent Soil Resistivity and Permittivity", *IEEE Trans. on Electromagnetic Compatibility*, V 53(2). https://ieeexplore.ieee.org/stamp/stamp.jsp?arnumber=5723004

[31] Visacro, S. (2018) "The Use of the Impulse Impedance as a Concise Representation

of Grounding Electrodes in Lightning Protection Applications", *IEEE Trans. on Electromagnetic Compatibility*, V 60(5).
https://ieeexplore.ieee.org/stamp/stamp.jsp?arnumber=8259490

Progress In Electromagnetics Research M, Vol. 96, 157–167, 2020

Applying Electromagnetic Field Analysis to Minimize the Earth Resistance on High Resistivity Soils

Silvia Ronda*, Clara Oliver, Oibar Martinez, Patricia Marquez, and Jose M. Miranda

Abstract—Different optimization strategies to reduce the earth resistance in a high resistivity soil are discussed in this work and illustrated with a practical example. Finite Element simulations reproducing real-world conditions in terms of structure design and soil profiles have been made to evaluate the improvements that should be adopted to minimize earth resistance. We analyze an example of an earthing system of an array of four identical telescopes installed on high resistivity (k$\Omega\cdot$ m order) soils with two different behaviors. In the first one, current dissipation occurs in an uniform soil. In the second one, a terrain with four layers of different resistivities is considered. This situation corresponds to a real world case of an observatory constructed in a volcanic terrain. It was found that the best strategy in each case differs: extend horizontal electrodes as far as possible from the foundation in the first case and combine these electrodes with buried vertical electrodes that connect with deep high conductive layers in the second. The results are discussed in terms of the achieved improvements depending on the modifications introduced in the main structure.

1. LOWERING THE EARTH RESISTANCE: MOTIVATION AND OVERVIEW

The earth electrical resistance plays a major role in the safety of both personnel and instrumentation. Grounding is also a fundamental part of any lightning protection system. It is vitally important, as explained in the standards related to lightning protection [1–4] that in the event of a lightning strike, excess charge induced in the lightning rods finds a safe and low resistance path to follow for its correct dissipation in order to prevent any damage. Moreover, a high earth resistance may compromise the proper operation of the surge protection devices. It is therefore understandable that a number of standards that regulate the implementation of grounding are within the framework of protection against atmospheric discharges.

Local regulations not always pose specific limits to a maximum acceptable earth resistance. This is the case of the *Low Voltage Electrotechnical Regulation.* For this standard, the maximum earth resistance will be the one which ensures that, throughout the life of the installation and at any time of the year, touch voltages greater than 24 V cannot be produced in the accessible metal parts of the installation, being 50 V for the rest of the parts [5]. But even in these cases one should note that touch and step voltages are better controlled with low earth resistances.

European standards such as EN-62305-3 [3] recommend specific limits to earth resistance, less than 10 Ω when being measured at low frequency. However, in EN-62305-3 it is also mentioned that the recommended value of the global earth resistance of 10 Ω is quite conservative in the case of structures in which direct equipotential bonding is applied. It also remarks that, although the value of resistance must be as low as possible in all cases, the most important measure is the equipotential bonding.

The standard improvements which can be made to reduce the earth resistance in difficult terrains are generally based on:

Received 23 July 2020

* Corresponding author: Silvia Ronda Peñacoba (silronda@ucm.es).

The authors are with the Department of Matter Structure, Thermal and Electronics Physics, Faculty of Physics, University Complutense of Madrid, Spain.

a) burying horizontal conductive plates or meshes,
b) burying vertical electrodes connected in parallel or
c) modifying the own terrain, which can be done by either changing the entire terrain material in a large volume or adding earthing enhancing compounds.

A combination of several procedures is also possible. For instance, the Taiwan Photon Source (TPS) storage ring has a $0.2\,\Omega$ earth system with 62 vertical electrodes and a grid of 4 rings. Bentonite was used to lower the resistivity of the terrain [6]. Some theoretical models for basic configuration of vertical electrodes and horizontal grids are adopted in the standards BS 7430:2011 [7] MIL-HDBK-319A [8] and summarised in [9].

The use of vertical electrodes connected in parallel poses several practical limitations. In order to prevent loss of effectiveness, it is necessary to keep a minimum distance between electrodes, which is typically around 5 times larger than the electrode length. Otherwise, the overlapping of the local equipotential lines around each electrode reduces the efficiency of the configuration. Typical electrode lengths can be 2–3 m. The amount of resistance that is reduced with each additional electrode decreases as the number of electrodes increases, but the basic parallel resistor formula of circuit theory will always underestimate the final resistance.

It is generally accepted that the electrodes should usually be installed with a backfilling material of high conductivity, which increases the effective diameter. Concrete is hygroscopic and has a resistivity of 30–$90\,\Omega\cdot\mathrm{m}$. This is particularly interesting in medium and highly resistive soils because a wire or metallic rod encased in concrete has lower resistance than a similar electrode buried directly in the earth. Some models of the calculation of the resistance of a grid with encased vertical electrodes can be found in the IEEE Std 80-2000 [10].

One solution could be replacing the soil with a low resistance material [11]. A number of earth enhancement materials are commercially available. Many are composed of carbon-based materials or clays like bentonite (or a mixture of both). These materials can also be used as backfilling materials to improve the resistance of an electrode. Chemical treatment of soil has environmental implications and should not be considered as a long term solution, and there is additionally a risk of corroding the earthing system. Coke breeze has also been used, but it poses serious concerns due to its highly corrosive nature. IEC 62561-7 standard discusses prequalification methods for ground enhancement materials [12].

Bentonite clay is actually a natural earth soil, mostly composed of the mineral montmorillionite, which was formed by volcanic action in the past. It is noncorrosive, stable, and has a resistivity of $2.5\,\Omega\cdot\mathrm{m}$ at 300% moisture. It has almost no environmental concerns and will not corrode the copper like other compounds based on carbon. Bentonite is hygroscopic, but just because of this it needs moisture in the ground to maintain its properties.

Some earthing enhancement materials contain cement, which after installation acquire properties that are very close to concrete. This prevents the material from leaching into the soil or washing away by groundwater. This type of material does not require any maintenance and has been shown to significantly reduce the long-term resistance of grounding electrodes in a study commissioned by the National Fire Protection Research Foundation [13]. However, alternatives should be considered because these solutions could not be feasible in terms of environmental conservation and costs. This could be the case when earthing must be done in areas of difficult access and with soils that are hard to excavate.

2. A CASE STUDY: LST SUBARRAY OF CTA-NORTH PROJECT

In order to illustrate how the electromagnetic field analysis can help to optimize the design of an earthing system, we analyze a practical example with challenging demands: The earthing system of an array of four telescopes built in a soil of volcanic nature and very low humidity content.

Cherenkov Telescope Array (CTA) North Project aims to build a large scale observatory hosting four Large-Sized Telescopes (LST) and another subarray of smaller, Medium-Sized Telescopes (MST). CTA-North subarrays are located in the Roque de los Muchachos Observatory, a protected area with regulations that pose severe limits to land removal operations and uses of earth enhancement compounds.

2.1. Description of the Telescopes

The LST is an instrument with a mechanical structure hosting several sensitive optical and electronics subsystems. Figure 1 shows a picture of the localization of all the LST (1-4) and a photo of the first telescope built in the observatory, the LST1.

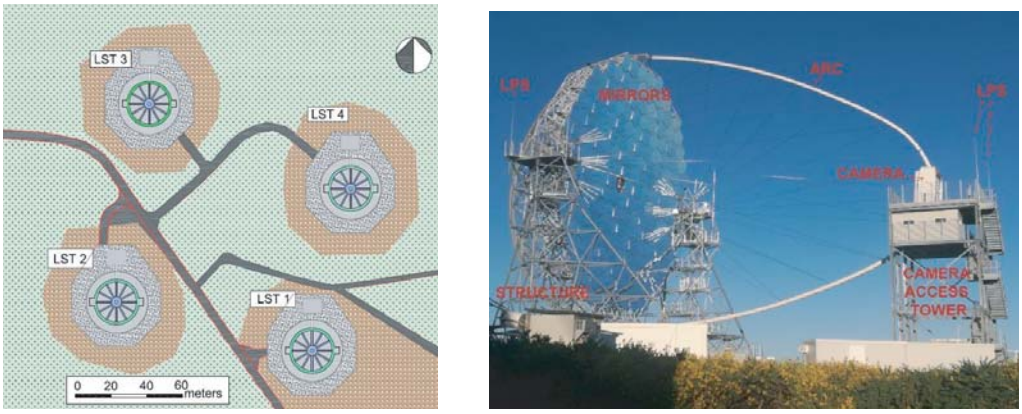

(a) (b)

Figure 1. Current view of the localization of (a) the four LSTs and (b) photo of LST1.

LST supports an array of 198 mirror plates, which conform a parabolic dish of 23 m diameter. The mirror plates are mounted on a structure of tubes. Tubes are composed of galvanized steel, aluminium, and carbon fibre. Each mirror can be moved with two actuators. The mirrors focus the light on a camera composed by an array of fast photomultipliers and associated electronics, and the recorded data are sent via optical fibres to a control room for further processing and storage.

The camera is the most complex system of the telescope and has two input power lines: one phase 230 V UPS and 3 phases AC 400 V. Inside the camera, both lines feed the main power distribution box, which contains surge protection devices. The UPS line feeds those elements that need power for safety reasons in case of a power failure. The other one feeds the rest of the camera subsystems either directly or through 24 V power supplies.

The telescope structure rests on seven points, with the central axis of rotation and six moving bogies equally spaced in a hexagonal arrangement. The bogies run on a circular rail of 23.9 m diameter and 500 mm width, which is fixed to the terrain with a concrete foundation. The total weight of LST telescope is 103 tons [14, 15].

2.2. Soil Conductivity Surveys

During the earthing system design, soil conductivity was one of the elements that received special attention, since it has an important influence on earth resistance value [16, 17]. In practice, earth resistance is roughly inversely proportional to soil conductivity. This parameter was measured for the four telescope sites using Wenner method [18]. A significant diversity of values was found among the sites, and all of them exhibited conductivities below 1 mS/m. All sites except LST3 showed uniform conductivity up to depths of 10 m. However, in LST3 the terrain corresponds to a non-homogeneous soil with extremely low conductivity layers due the presence of fractured basalt rocks. The depth, thickness, and conductivity of each layer were estimated by correlating geotechnical surveys with finite element simulations of the Wenner method. An agreement with measurements was obtained within 10% error margin [19]. Table 1 shows the final values of the soil conductivities for all LST sites.

2.3. Foundation and Baseline Design of the Earthing System

The foundations of the telescopes are made of concrete and a steel bar armature. They have a central part of reinforced concrete under the axis of rotation of the telescope. A circular beam of reinforced

Table 1. Soil resistivity and geometrical parameters of the soil considered in models for LST telescopes.

	Layer depth (m)	σ (S/m)
LST1	0–∞	$6.67\ 10^{-4}$
LST3	0–2.85	$0.54\ 10^{-4}$
	2.85–4.75	$2.86\ 10^{-4}$
	4.75–6.25	$0.65\ 10^{-4}$
	6.25–∞	$6.67\ 10^{-4}$

	Layer depth (m)	σ (S/m)
LST2	0–∞	$1.95\ 10^{-4}$
LST4	0–∞	$4.08\ 10^{-4}$

concrete is under the rail, and it is connected to the central part with radial beams. Another nearby reinforced concrete foundation is under the camera access tower [20], which is a metallic tower specially designed for two purposes: facilitate the camera maintenance and improve the anchorage of the telescope during storms. In terms of safety, the LST structure has to be equipotential [3, 4, 21].

The design of the LST1 earthing system with the sketch of the metal plate structure is illustrated in Figure 2.

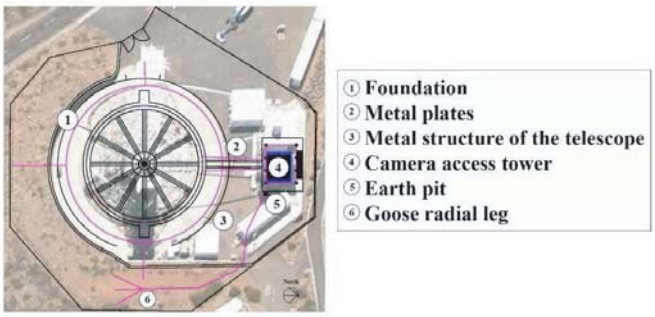

Figure 2. Schematic of the real earthing system designed for LST telescopes. Magenta lines indicate the structure of the horizontal plates used for earthing.

The steel armature of the foundation is connected with metal plates, which are extended outside the reinforced concrete in the four cardinal directions. The metal plates are also connected to the metal structure of the telescope. Lightning rods are integrated in the LST1 structure and the upper level of the camera access tower. They are connected to the earthing system by stainless steel cables which merge in an earth pit with a lightning counter. From this pit, an extension of the earth system was made with a copper plate ended in three additional plates arranged as a goose radial leg and located in the eastern side of the telescope. This installation is done according to UNE standard [22].

3. FINITE ELEMENT SIMULATION

Finite Element Method (FEM) has been used to calculate the earth resistance of the telescopes under test: LST1 and LST3. LST2 and LST4 sites feature a uniform resistivity soil, like LST1. Therefore, as all telescopes are identical the results for LST1 can be rescaled with the resistivities to obtain the expected earth resistances of LST2 and LST4 without additional simulations. FEM simulations were done with COMSOL Multiphysics v5.3a software. For the models presented in this work, Electric Currents Module and a stationary study have been used.

The computational domain is a 3D hemisphere that contains the complete geometry modeled for the earthing system of the telescopes. Soil below earth resistance installation is designed with the characteristics displayed in Table 1. Thus, an homogeneous terrain is considered in LST1 case and a four layer model in LST3, as can be seen in the illustrations of Figure 3.

(a) (b)

Figure 3. Implemented model geometry and conductivity parameters of the soil. (a) LST1 and (b) LST3.

The earthing system modeled, based on the real one, has two main parts:

- The metal grid. This consists of two solid blocks. One of them is located under the telescope camera and the other under the mirror.
- A composition of thin metal plates. They are surrounding and connected to the solid blocks.

As a guide to consider the size of the structure, one can take as a reference that the distance between the centers of the two solid blocks is 28.5 m. An illustration of the complete interconnected electrodes in COMSOL and a representative simulation scenario is shown in Figure 4. To avoid contour artifacts due the finiteness of the simulated volume, an *Infinite Element Domain condition* has been imposed to an external layer. Electrical ground ($V = 0$) is located at the infinite. A hemisphere surrounding the earthing system limits the zone of interest, where a more dense mesh is made.

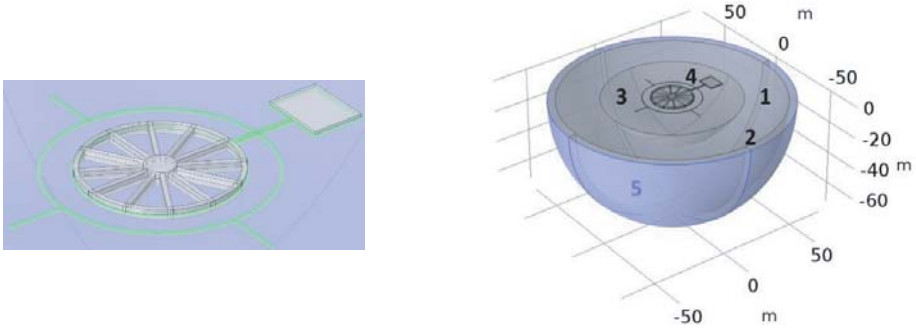

(a) (b)

Figure 4. (a) Basic structure designed in COMSOL for the earthing system of the telescopes. (b) Metal grid of the reinforce is displayed in grey color and metal plates surrounding it are in green. Implemented model geometry. (1) Soil (LST1 case). (2) Infinite Element Domain Layer. (3) *Extra fine* mesh zone surrounding earth resistance structure. (4) Earth resistance structure. (5) Ground.

According to the materials used in the LST1 earthing system, metal plates are designed with 3.5 mm height and 30 mm width. Material for the electrodes (solid blocks and plates) has the properties of structural steel ($\sigma = 4.032\ 10^6$ S/m, according to COMSOL's Materials Library).

For boundary condition, the complete earth resistance structure is considered as current source of 1 A. Then, applying Ohm's equation, COMSOL calculates the resistance of the terminal and voltage distribution.

The main difficulty of these simulations comes from the high difference among the relevant dimensions involved in the geometry of the models (lengths in the order of mm combined with others with several m). To avoid that the mesh is too coarse or contains adjacent elements with large differences in scale, the meshing should be made with a nonuniform density. An *Extremely fine* condition set

by COMSOL was chosen for the thin plates, an *Extra fine* condition for the solid blocks and the surrounding soil (zone 3 in Figure 4). Finally, the other domains are meshed with *Normal* condition. Additionally, the external layer of the hemisphere has a special distribution appropriated for contour domains called *Boundary Layers*. Despite this differentiation, it was necessary to adjust the tetrahedral element minimum size because some domains are too narrow with respect to the rest of the geometry, and very short boundary segments were necessary. On average, a quality factor of 0.5 is achieved in all models.

4. RESULTS AND DISCUSSION

The optimization of the earthing system in each telescope has been studied. We evaluate the impact in the earth resistance value of several structural modifications with respect to the baseline configuration. Tables 2 and 3 show the results for LST1 and LST3, respectively. Normalized voltage distribution in 3D, calculated earthing system resistance R_{ES}, and percentage of R_{ES} reduction with respect to the original (improvement) are all shown in the tables. As a reference to better visualize the dimensions, a dotted line corresponding to 53.5 m length is also included in the images.

Table 2. Comparison among the models to lower the earth resistance in LST1 telescope. Dashed line corresponds to a 53.5 m length. The voltage shown is normalised to the peak one.

Structure	**1.1**	**1.2**	**1.3**
Voltage	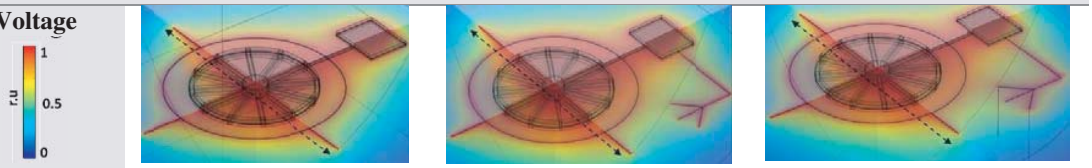		
Modification	Baseline (original)	Add a radial leg metal plate	Add two vertical rods of 10 m in the radial leg
R_{ES} (Ω)	15.17	13.91	13.27
Improvement	**-**	**8.3%**	**12.5%**

Structure	**1.4**	**1.5**	**1.6**
Voltage	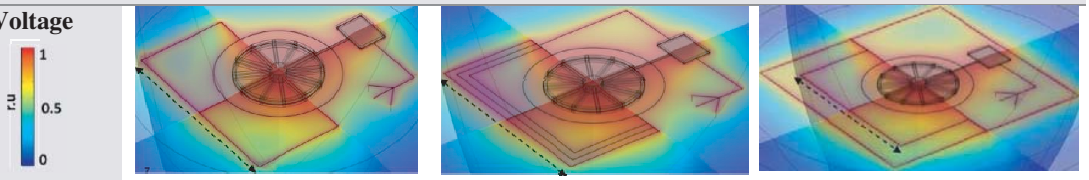		
Modification	Surrounded with an external plate	Surrounded with 3 external plates	Surrounded with 3 external plates (bigger)
R_{ES} (Ω)	11.01	9.82	7.14
Improvement	**27.4%**	**35.3%**	**52.9%**

It can be seen that for some configurations, the observed resistance is very high as compared to the widely accepted 10 Ω limit for structures with a lightning protection system. In the case of LST3 telescope, the soil immediately surrounding the earth electrodes has a high resistivity value. The intent is to reduce the earth electrode resistivity using the possibilities that have been presented in this work (adding metal plates of different shapes). Based on the results obtained, there is a need to discuss the applicability of different modifications depending on the case under study.

Table 3. Comparison among the models to lower the earth resistance in LST3 telescope. Dashed line corresponds to a 53.5 m length. The voltage shown is normalised to the peak one.

Structure	**2.1**	**2.2**	**2.3**
Voltage	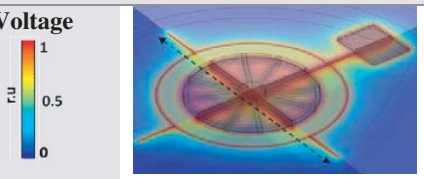		
Modification	Basic (original)	Surrounded with an external plate	Surrounded with an external plate with 3 vertical rods
R_{ES} (Ω)	69.23	53.46	37.87
Improvement	-	**22.8%**	**45.3%**

Structure	**2.4**	**2.5**	**2.6**
Voltage	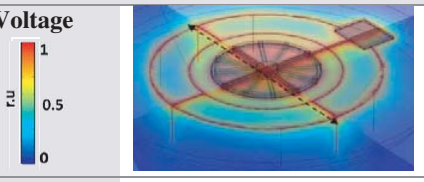		
Modification	Surrounded with an external plate with 7 vertical rods	Surrounded with an external plate with 7 vertical rods and plates of 60 cm (x20)	Surrounded with an external plate with 22 vertical rods
R_{ES} (Ω)	27.90	25.51	23.58
Improvement	**59.7%**	**63.1%**	**64.2%**

4.1. Systems with Horizontal Plates

When the earth resistance is not low enough, lengthening the horizontal earth electrodes in the soil is a popular solution [23]. The comparison of 1.4 with 1.6 indeed reveals the effectivity of extending the plates away from the main structure, to favor the dissipation of the electric current in a larger surface. When all plates are located too close from each other, the decrease of the resistance is marginal. This can be illustrated by comparing 1.5 configuration with 1.4. Despite the addition of two external plates, the improvement is only 7.9%. This result agrees well with previous works which show that resistance in designs with higher density of rods in the center of the grounding grid is often higher than those designs that place the rods at the grid periphery [24]. This is attributed to the shielding effect between electrodes.

The use of radial plates usually improves the resistance of the earthing system, by allowing current to diverge on each conductor, offering lower impedance [25]. This technique seems more effective than a single long conductor. It is also recommended to install at least one vertical electrode per radial conductor when it can connect to a lower resistivity soil layer [26]. In our case, both scenarios 1.2 and 1.3 consider this case. The radial "goose leg" added in 1.2 has a resistance of 54.24 Ω as calculated with COMSOL. Since this value is high as compared to the 15.17 Ω of the main structure, it does not contribute that much to the decrease. For this reason, adding vertical electrodes in this part of the structure is not the optimal solution in terms of improvement (4.2%) and cost.

The discussion for nonuniform soils is more complex. The difference of current distributions in the layers rises when reflective coefficient increases due the resistivity value change in the interfaces. In our case, we have a high resistivity upper layer. It seems that lower earth resistance can be obtained through matching deep low resistivity materials, i.e., with vertical electrodes. If we compare 2.1 and 2.2 cases, a significant improvement is achieved (22.8%), but installing additional and/or wider horizontal plates (case 2.5) does not result into a noticeable effect as compared to previous models. The high

resistivity of the terrain heavily influences the resistance of the structure and imposes a limit to the current dissipation in this first layer. In this case, connecting electrodes with the best conductive layers is the most effective strategy.

4.2. Systems with Horizontal Plates Combined with Vertical Electrodes

The periphery of the earth system is the best place to insert vertical electrodes [27]; therefore, this was the place chosen for the simulation trials. In LST1, structure 1.3 did not show a noticeable improvement with 10 m long metal plates in the end of the radial leg. To evaluate how effective is for this case to bury vertical electrodes in the earthing system, we studied the effect of adding to structure 1.6 plates of 10 m. We added 2, 4, 6 (structure 1.7), 8 10, 12 (structure 1.8) and 16 electrodes. Results and representative illustrations are shown in Figure 5.

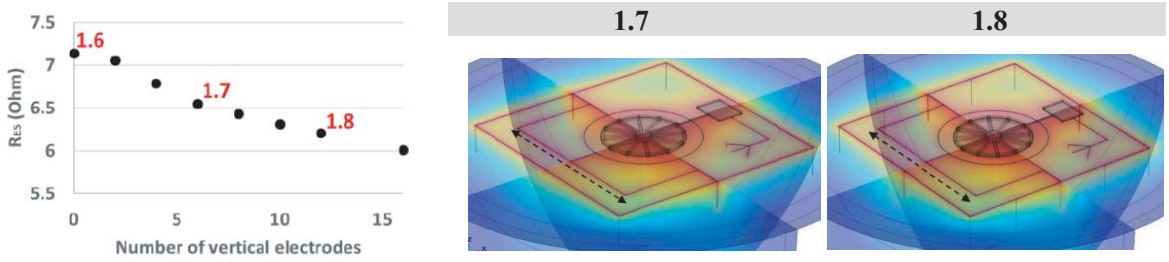

Figure 5. Relationship between the number of vertical electrodes added to structure 1.6 and the calculated earth resistance R_{ES}. Illustration of the cases with 6 vertical electrodes (1.7) and 12 (1.8).

We can confirm that resistance decreases with the increase of the number of vertical electrodes. However, the tendency shows that a saturation is expected when the number of electrodes is very high, because the shielding effect increases [27, 28].

On a multilayered soil, the method of long vertical electrodes does not improve the situation when the soil resistivity of the bottom layer is very high. On the other hand, when a low resistivity soil layer is under a higher one, adding deep electrodes can achieve good results. The comparison of 2.2 with 2.3 and 2.4 shows that long vertical electrodes can always reach better results. However, in 2.6 we have increased the number of vertical electrodes up to 22, and the enhancement is not as noticeable as desired. This could be related with the current reflections produced due to resistivity interfaces. So, the choice of electrode length, location, and number is determined by the soil structure.

4.3. Simulations of Parallel Connection of Earthing Systems

The large resistivity of the LST3 site is the main factor limiting the earth resistance minimization for this telescope. However, the fact that the four LSTs are far enough from each other offers the possibility of efficiently reducing the earth resistance by interconnecting all the earth layouts, which in practice means a connection of four resistors in parallel. According to previous work on the behavior of vertical electrodes connected in parallel, the electrodes must be separated from each other at least five times of their equivalent radius, so the ground potential has decayed to 20% of the potential rise [29]. However, this result cannot be applied in a straightforward way to the connection of the LST earth systems for two main reasons: the optimum layouts for uniform terrains are very shallow, and it is unclear what would be the influence of the non-uniformity of the LST3 soil resistivity.

In order to clarify these points a simulation was done by considering a structure in which LST1 and LST3 earth systems are connected, taking into account the different soil resistivities under them. Figure 6 shows a schematic of the model geometry.

The calculations using FEM are presented in Table 4. In the first column, the case in which both structures are present but not inter-connected is shown. In the second column, we connect them with an horizontal steel plate similar to the one used in the previous designs. The current source for the

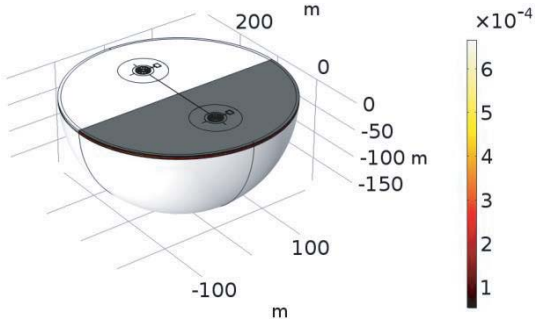

Figure 6. Implemented model geometry and conductivity parameters of the soil for the case in which LST1 ans LST3 are interconnected.

Table 4. Comparison among the results for LST3 earth resistance value (R_{ES}) when LST1 and LST3 structures are present and they are/not interconnected in parallel. The current terminal condition is imposed in LST3 (represented in color blue).

Structure	**Separated**	**Parallel**
Description	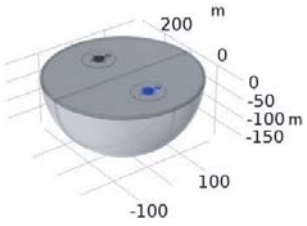	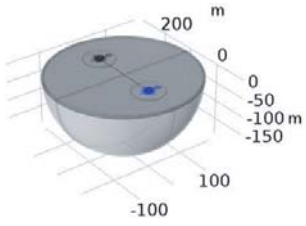
	Ground-structures independent	Ground-structures connected in parallel
Voltage	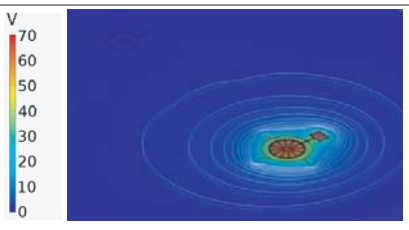	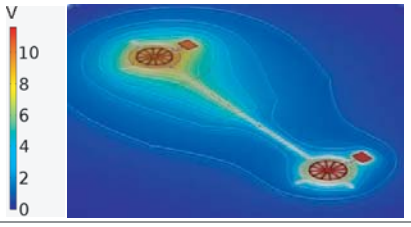
R_{ES} (Ω)	70.74	11.6
Improvement	**-**	**82.7%**

earth resistance calculation is injected at the LST3 earth system. Voltage distribution, equipotential curves, and earth resistances are shown in the table.

Since LST1 resistance is 15.17 Ω (see structure 1.1 in Table 2), the rule for two resistances in parallel predicts a 12.5 Ω resistance value for this configuration. The reduction needed to accomplish the requirements is almost achieved with a reduction of 82.7% of the resistance of LST3 earth. Furthermore, the simulation shows that the inter-telescope distances are long enough, and the non-uniformity of LST3 soil does not make any strong influence on the accuracy of the simple parallel resistor model. Assuming linearity between the soil resistivity and earth resistance for the homogeneous soils and making use of the fact that all telescopes are identical, it is possible to estimate the earth resistances for LST2 and LST4 without further simulations, and calling ρ_i to LST_i soil resistivity we can estimate the earth resistances R_{ES_i} as

$$R_{ES_i} = \rho_i \frac{R_{ES_1}}{\rho_1} \tag{1}$$

Using expression (1) one readily obtains that the total earth resistance for the complete LST subarray would be 7.2 Ω.

5. CONCLUSIONS

Different methods of lowering the earth resistance value modifying the earthing structure design and calculating its value with Finite Element simulation have been discussed in this paper. The results demonstrate how the voltage distribution and earth resistance value are influenced by the earthing system design. To evaluate the optimum modifications that should be made, we have considered the influence of the shape, size, and number of horizontal and vertical electrodes depending on the soil properties. The possibility of inter-connecting in parallel several structures has also been analyzed.

The following conclusions can be drawn from the simulations described below:

- The optimum strategy for a uniform, high resistivity soil is extending the horizontal plates as far as possible from the main structure. Vertical electrodes do not provide significant improvements.
- If the soil contains several layers vertical electrodes connecting with the best conductivity layer are effective in producing significant resistance reduction.
- It is confirmed by simulations that the interconnection of several earth systems located at distances of the order of five times or more the size of the earth system leads to an arrangement of parallel resistors that can produce considerable earth resistance reductions. This approach is particularly powerful when the installation consists of several facilities built on soils of highly different resistivities. In this case, each facility takes benefit of the best one.

ACKNOWLEDGMENT

This work has been funded by the Spanish Ministry of Science and Innovation, thru the research project FPA2017-82729-C6-4-R.

REFERENCES

1. International Electrotechnical Commission (IEC), "Protection against lightning — Part 1: General principles," IEC 62305-1, Ed 2.0 2010-12, 2010, https://webstore.iec.ch/preview/info_iec62305-1%7Bed2.0%7Den.pdf.
2. International Electrotechnical Commission (IEC), "Protection against lightning — Part 2: Risk management," 2010, https://webstore.iec.ch/preview/info_iec62305-2%7Bed2.0%7Den.pdf.
3. International Electrotecnical Commission, "Protection against lightning — Part 3: Physical damage to structures and life hazard, IEC 62305-3," 2010, https://webstore.iec.ch/publication/6795.
4. International Electrotecnical Commission, "Protection against lightning — Part 4: Electrical and electronic systems within structures, IEC 62305-4," 2010, https://webstore.iec.ch/searchform&q=IEC 62305-4.
5. "ITC-BT-18," Ministerio de Ciencia y Tecnologia, 2018.
6. Ueng, T. T.-S., Y.-C. Lin, J.-C. Chang, and C.-K. Kuan, "The ground testing of tps ground system," 2011, https://accelconf.web.cern.ch/ipac2011/papers/tups062.pdf (accessed: Jun. 06, 2020).
7. British Standards Institution, "Code of practice for protective earthing of electrical installations BS 7430:2011," No. 1, 1–96, 2011, https://global.ihs.com/doc_detail.cfm?document_name=BS 7430&item_s_key=00131083&csf=TIA (accessed: Jun. 06, 2020).
8. "Military handbook grounding, bonding and shielding for electronic equipments and facilities Volume I of II Volumes basic Theory," 1982, https://www.wbdg.org/FFC/NAVFAC/DMMHNAV/hdbk419a_vol1.pdf (accessed: Jun. 06, 2020).
9. Electric Engineer Portal, "Measurements and calculations of Earth electrode systems," https://electrical-engineering-portal.com/earth-electrode-systems#types-earth-electrodes (accessed: Jun. 06, 2020).
10. IEEE Std 80, *Guide for Safety In AC Substation Grounding*, Vol. 2000, Feb. 2000.
11. Okyere, P. Y. and G. Eduful, "Reducing Earth electrode resistance by replacing soil in critical resistance area," *J. Mod. Eng.*, 2006, doi: 10.4314/just.v29i2.46230.

12. "IEC 62561-7:2018 Lightning protection system components (LPSC) — Part 7: Requirements for earthing enhancing compound," *International Standard*, 2018, https://webstore.iec.ch/publication/33885 (accessed: Jun. 06, 2020).
13. Lindsay, T., "National electrical grounding research project, technical report," 2007, https://www.nfpa.org/-/media/Files/News-and-Research/Archived-reports/negrpfinalreport.ashx?la=en.
14. "LST — Cherenkov telescope array," https://www.cta-observatory.org/project/technology/lst/ (accessed: Jun. 15, 2020).
15. Cortina, J. and M. Teshima, "Status of the Cherenkov telescope array's large size telescopes," 2015, http://cta-observatory.org (accessed: Jun. 15, 2020).
16. Sabiha, N. A. and N. I. Elkalashy, "Evaluation of grounding system design for wind farm using COMSOL," 2018, http://www.ripublication.com (accessed: Jun. 26, 2020).
17. Malanda, S. C., I. E. Davidson, E. Singh, and E. Buraimoh, "Analysis of soil resistivity and its impact on grounding systems design," *2018 IEEE PES/IAS PowerAfrica, PowerAfrica 2018*, 324–329, Nov. 2018, doi: 10.1109/PowerAfrica.2018.8520960.
18. Wenner, F., "A Method of measuring Earth resistivity," *Bull. Bur. Stand.*, Vol. 12, 469–478, 1916, doi: https://doi.org/10.6028/bulletin.282.
19. Ronda, S., O. Martinez, C. Oliver, P. Marquez, and J. M. Miranda, "Finite element analysis and experimental characterization of soil electrical resistivity at El roque de los muchachos observatory," *Journal of Electromagnetic Analysis and Applications*, Vol. 12, No. 7, 89–102, 2020.
20. De A. de Canarias, I., "LIC-15-034: Construction of foundation of Telescope LST1," 10, Plataforma de Contratación del Estado (Spain), 2015, https://contrataciondelestado.es/wps/wcm/connect/8e64f971-f3eb-41d1-a206-edca7ec9b590/DOC_CD2015-229760.pdf?MOD=AJPERES (accessed: Jun. 15, 2020).
21. Ma, J., T. Del Pino, and S. P. Martí, "NTP-1.084: Prevención de riesgos laborales originados por la caída de rayos," 2017.
22. "UNE 21186:2011 Protección contra el rayo: Pararrayos con dispo," 2011, https://www.aenor.com/normas-y-libros/buscador-de-normas/une/?Tipo=N&c=N0048559 (accessed: Jun. 25, 2020).
23. El-Sayed Gouda, O., *Design Parameters of Electrical Network Grounding Systems*, IGI Global, 2018.
24. Zeng, R., J. He, Z. Wang, Y. Gao, W. Sun, and Q. Su, "Analysis on influence of long vertical grounding electrodes on grounding system for substation," *PowerCon 2000 — 2000 International Conference on Power System Technology, Proceedings*, Vol. 3, 1475–1480, 2000, doi: 10.1109/ICPST.2000.898188.
25. El-Sayed Gouda, O., *Design Parameters of Electrical Network Grounding Systems*, IGI Global, 2018.
26. Lim, S. C., C. Gomes, and M. Z. A. Ab Kadir, "Electrical earthing in troubled environment," *Int. J. Electr. Power Energy Syst.*, Vol. 47, No. 1, 117–128, May 2013, doi: 10.1016/j.ijepes.2012.10.058.
27. Zeng, R., J. He, Z. Wang, Y. Gao, W. Sun, and Q. Su, "Analysis on influence of long vertical grounding electrodes on grounding system for substation," *PowerCon 2000 — 2000 International Conference on Power System Technology, Proceedings*, Vol. 3, 1475–1480, 2000, doi: 10.1109/ICPST.2000.898188.
28. Malanda, S. C., I. E. Davidson, E. Singh, and E. Buraimoh, "Analysis of soil resistivity and its impact on grounding systems design," *2018 IEEE PES/IAS PowerAfrica, PowerAfrica 2018*, 324–329, Nov. 2018, doi: 10.1109/PowerAfrica.2018.8520960.
29. Mitolo, M., *Analysis of Grounding and Bounding Systems*, CRC Press, 2020.

Journal of Electromagnetic Analysis and Applications, 2020, 12, 89-102
https://www.scirp.org/journal/jemaa
ISSN Online: 1942-0749
ISSN Print: 1942-0730

Finite Element Analysis and Experimental Characterization of Soil Electrical Resistivity at El Roque de Los Muchachos Observatory

Ronda Silvia, Martinez Oibar, Oliver Clara, Marquez Patricia, Miranda Jose Miguel

Department of Matter Structure, Thermal and Electronics Physics, Faculty of Physics, University Complutense of Madrid, Madrid, Spain

Email: miranda@ucm.es

How to cite this paper: Silvia, R., Oibar, M., Clara, O., Patricia, M. and Miguel, M.J. (2020) Finite Element Analysis and Experimental Characterization of Soil Electrical Resistivity at El Roque de Los Muchachos Observatory. *Journal of Electromagnetic Analysis and Applications*, **12**, 89-102.
https://doi.org/10.4236/jemaa.2020.127008

Received: June 1, 2020
Accepted: July 13, 2020
Published: July 16, 2020

Abstract

This paper presents a study of the soil electrical resistivity of El Roque de los Muchachos Observatory, located in La Palma Island (Spain). This work is mainly motivated by the current plans of building an array of Cherenkov Telescopes (CTA) as well as other scientific installations, which demand low earth resistances for the operation of sensitive instruments, prevention of damage due to electrostatic discharges and protection against lightning strikes. Despite the top quality of the sky, the terrain is mostly filled of hard rocks and materials with high resistivity and hardness. No reliable data of resistivities could be found in available literature, therefore a dedicated resistivity survey onsite like the one presented here is essential to optimize the earth resistance of future installations. In this work, we present measurements done in six different locations of an area covering around 250 m × 275 m and centered on coordinates 28˚45'42.9"N, 17˚53'28.5"W. Low resistivity (<2 kΩ·m) layers have been found at specific places and depths. The resistivity at the sites has been simulated with COMSOL Multiphysics software using two different models: a simple single layer model and a three-layer model. Agreement with measurements within 10% discrepancies was obtained in all cases. The main contributions of this work are the presentation of reliable values of soil resistivity at ORM, together with the accurate simulation of the soil profiles.

Keywords

Resistivity, Wenner Method, FEM, COMSOL

1. Introduction

El Roque de los Muchachos Observatory (ORM) is located at the rim of Tabu-

riente National Park, at heights ranging from 2340 to 2396 meters above sea level, in the municipality of Garafía (La Palma, Spain). It hosts one of the largest fleets of telescopes in the world, including infrared, visible, microwave and gamma-ray instruments. ORM sky quality continuously attracts projects aimed at building large scale instruments. The Cherenkov Telescope Array (CTA) project is currently the most ambitious one, with plans for building four Cherenkov Large Size Telescopes with a 23 m dish diameter and a subarray of Medium Size Telescopes with 12 m dish diameter [1] [2]. The construction requirements approved for these instruments include tough specifications on the quality of the earth resistance, for which the terrain resistivity is a crucial factor. These specifications are mainly motivated by the need to comply with safety regulations as well as to mitigate the risks of damaging sensitive instrumentation due to static discharges and lightning strikes. However, no information about the electrical resistivity of the soil at ORM was found.

The four-point Wenner method [3] is currently the most popular procedure for electrical resistivity measurements, due to its simplicity and the low cost of the required equipment. Wenner's original work provides a simple equation to derive the soil resistivity ρ from the measured current I and voltage V, and the interelectrode distance a in a four-point configuration,

$$\rho = 2\pi a \frac{V}{I}. \tag{1}$$

This expression holds provided that several conditions are fulfilled, namely:

1) The resistivity is homogeneous;

2) The electrodes are point-shaped and placed on the surface, being interelectrode distance much larger than interelectrode depth;

3) The conductive volume is semi-infinite;

These measurements can only give what is usually called apparent resistivity, since in most cases the result is obtained from the contribution of different local resistivities within the volume through which the current flows. Despite these limitations it has been shown that Wenner method still provides accurate results even if some of the requirements for the model validity are not fully satisfied [4].

On the other hand, Schlumberger method provides a convenient alternative to speed up the measurements when detailed profiling is needed, since the resistivity can be obtained in several points by moving only the two electrodes of the voltage channel [5]. It is also convenient when using instrumentation lacking accurate voltage measurements and large interelectrode distances are needed. This is due to the fact that the Schlumberger method allows you to place the voltage electrodes closer to the current ones than in Wenner method [6]. This way the voltage to be measured is higher. Special procedures have also been proposed to determine soil resistivities in thin layers [7].

Other Geological surveys regularly use techniques like Electrical Resistivity Tomography (ERT) for hydrogeological, mining and geotechnical investigations [8] [9]. These techniques use electrodes arrays with the same basic operating

principles as the Wenner and Schlumberger methods. The patterns are built by means of numerical, inverse problem algorithms. 3D tomography techniques are especially powerful to characterize low resistivity (typically below 10 kΩ·m) soils when the terrain allows the proper insertion of a large number of electrodes in specific locations.

Mathematical expressions for the apparent resistivity in earth structures with an arbitrary number of layers (single, double or multilayered) have been derived for Wenner method [10] [11] [12]. Finite Element Modeling (FEM) software has been used in previous works to study the influence on electrical resistivity measurements in materials. However, most of these studies are focused on the role of concrete presence on soil resistivity [4] [13] [14]. FEM has been demonstrated to be an alternative method to realistically model the boundary conditions and the electrode geometry versus analytic methods, which rely on unnecessary approximations.

The original Wenner method was found to be the most convenient procedure to characterize experimentally the electrical resistivity of the ORM soil due to the optimum balance it offers between the degree of detail obtained and the required cost and time efforts. **Figure 1** shows two images of the measured areas.

The ORM is in a protected area where the soil is largely covered by adenocarpus viscosus plants, an endemic species which can reach heights of up to 1.5 m with deep and hard roots. In addition, the soil of this site is mostly filled of hard rocks and materials with resistivities exceeding 10 kΩ·m in some locations. Other measurement methods, such as 3D tomography, were ruled out due to the difficulty in carrying them out.

In this work, we present measurements done in six different locations of an area at ORM covering around 250 m × 275 m and centered at coordinates 28˚45'42.9"N, 17˚53'28.5"W. These locations correspond to the sites where the telescopes MAGIC I, MAGIC II and LST1 are built, as well as the future locations of LST2, LST3 and LST4. The resistivities at the sites have been simulated with COMSOL Multiphysics software using two different models: a simple single layer model and a three-layer model. Practical limitations of the measurements and the consistency of the mathematical model with the true terrain structure are discussed with the support of previous geotechnical studies and available literature of electrical properties of the materials of which the soil is composed.

Figure 1. Views of the LST area landscape showing the dominant vegetation.

2. Experimental Procedure

2.1. Resistivity Measurements

The resistivity meter used for the measurements is the Chauvin Arnaux's C.A 6470N Terca 3 [15], with its corresponding 150 m earth and resistivity kit's pikes and wires. This equipment, among other applications, calculates the apparent resistivity using Wenner method.

Wenner method provides a value of the average apparent resistivity at a point located around the middle of the pike line and at a depth of the order of the pike distance [16]. The standard Wenner protocol with occasional support of special procedures to improve the contacts, like pouring small amounts of saltwater around the pikes, worked properly at all sites except at LST3 area. The measurements at this area were particularly difficult to obtain, and several trials were needed to find places for the pikes giving reliable results. However, the measurements became significantly easier when the pike separation was increased. In order to understand this behaviour, it is necessary to revise the instrument capabilities. Table 1 shows the relevant specifications of the equipment [15]. As it can be observed, the maximum resistivity the instrument can measure is around 1 MΩ·m, which is well above the maximum reliable values measured on-site at all distances. The test signal was 32 V and the AC frequency 128 Hz.

Table 2 provides the threshold values which trigger an error message in the instrument. The one which triggered the observed errors in the display during

Table 1. Characteristics and limitations of the equipment [15].

Resistance Range	0.01 Ω to 99.99 kΩ
Resolution	0.01 Ω to 100 Ω
Test voltage	16 or 32 V, selectable
Measurement frequency	41 Hz or 128 Hz, selectable
Short-circuit current	>200 mA AC
Rejection of spurious signals	>80 dB for frequencies above or below 20%
Maximum acceptable overload	250 V_{rms}
Maximum value of ρ	999 kΩ·m

Table 2. Error indications according to manufacturer. 3P and 4P refer to instrument functions that were not used for the results shown in this work. $I_{H\text{-}E}$ is the measured current applied to current path. U_i correspond to effective measured voltages between the electrodes.

Function	Threshold
3P, 4P, ρ	$I_{H\text{-}E} < 1$ mA
All	Unstable values of U, I, R that vary more than 5% from the average
All	$U_{S\text{-}ES}$, $U_{S\text{-}E}$, $U_{H\text{-}E} > 42$V
All	Parasitic voltage whose frequency or value can distort the measurement

the short-range measurements at LST3 is shown in the first row, which indicates that the current measured in the current channel $I_{H\text{-}E}$ was too low. The lack of other errors ensures us that stable contacts were achieved, and the measurements were free from parasitic interferences and stray signals.

We therefore associate these errors to the own irregularities of the terrain. We know that it is composed of different layers, but we believe that it is possible that within these layers there are also irregularities that cause the terrain to behave discontinuously, thus worsening the circulation of the current $I_{H\text{-}E}$. This would prevent the measurement from being taken correctly, as the current path inside the ground does not drive as it should. This behavior is illustrated in Figure 2, where we see the current represented as a dotted line, and a possible obstacle in the circulation of it and, therefore, in the closing of the circuit. Only the separation of the pikes could enable the generation of current paths below the obstacle and therefore the measurement of detectable currents. All unreliable measurements were disregarded for the modeling presented here.

For this study, two measurement campaigns have been carried out, in September 2018 and May 2019 respectively, from which the data extracted are displayed in Figure 3. MAGIC I, II and LST1 measurements were made around a terrain that was altered for the installation of the telescope foundations. The construction works required the removal of land for the foundation of each telescope

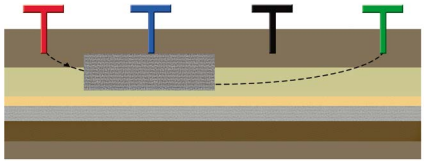

Figure 2. Schematic representation of a four-probe measurement with a current cut produced by a non-conductive obstacle. The obstacle is represented by the grey rectangle below blue pike, and current is represented by a dashed line.

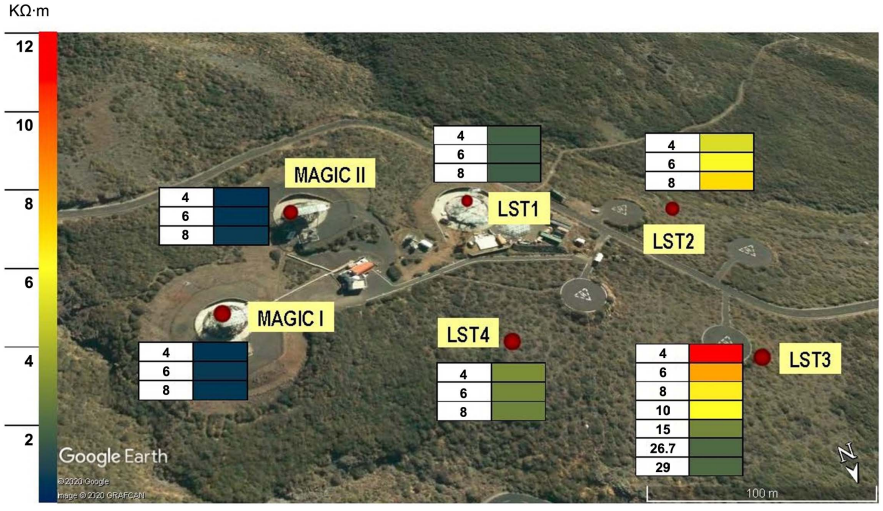

Figure 3. Soil resistivity measurements made in ORM. The numbers correspond to the interelectrode distance in m.

up to a depth around 2 m. The humidity values in the area were monitored during the measurements with the weather station facility of the MAGIC telescopes. Recorded relative humidity remained in the range [30% - 41%] for all measurements. At least three measurements with different pike distances were used at every site in order to check if the resistivity varies with depth.

Average resistivities were 1.44 kΩ·m, 5.14 kΩ·m, 2.45 kΩ·m, 0.57 kΩ·m and 0.53 kΩ·m for LST1, LST2, LST4, MAGIC I and MAGIC II, respectively. LST3 site exhibited resistivities ranging from 1.74 kΩ·m to 11.5 kΩ·m. The fact that resistivity decreases as interelectrode distances increase in this site indicates that there is a high resistance layer in the upper part of the soil whereas a layer of a lower resistivity was found at depths around 20 m.

2.2. Soil Composition

Additional information on the terrain can be obtained from Geotechnical Studies (GTS), where the physical evaluation of the soil is made, to identify its composition. So, these excavations give data about the subsurface material at different depths. The soil where the telescopes will be located in had to be analysed according to the "Guide for planning and carrying out Geotechnical Studies for building in the Comunidad Autonoma de Canarias" (GETCAN-011 [17]).

It is known that La Palma, part of Canary Islands, has a volcanic origin as almost the 100% of the geology of this archipelago. In particular, for the LST1-LST4 area we have altered basalt masses. The geotechnical unit is n˚ III, based on public geological and cartographic databases [18] [19], which explain that these types of soils correspond to basic castings of small thickness and moderate high alteration, which manifest as vertical alternation of basaltic compact levels.

Like resistivity measurements anticipate, the soil composition obtained in GTS where LST1 is placed, is almost a homogeneous layer of slag altered with clay (≈15%). However, the LST3 soil has layers of several materials. A reconstruction of the terrain based on the excavations made in different points around LST3 site is shown in **Figure 4**.

The excavation in point T2 is the closest to the resistivity measurements site in LST3 locations. According to this, composition of the soil in LST1 and LST3 is shown in **Table 3**. The deepest layer of slag altered with silts is not considered since it was found only in T2 survey. We also neglected the deepest layer of fractured basalt for the same reason.

We can conclude that, in general, the rocks of LSTs area are a mixture of igneous and volcanic types [17]. According to the composition of the rocks, they are MAFIC with other materials (clay, gravel and silts) [20].

Knowing the composition of the soil, one would expect that the representative resistivity values can be approximated based on the electrical properties of each rock type. Therefore, the resistivity of the rock types found in the GST of LST1 and LST3 areas have been checked from several references and collected in **Table 4**.

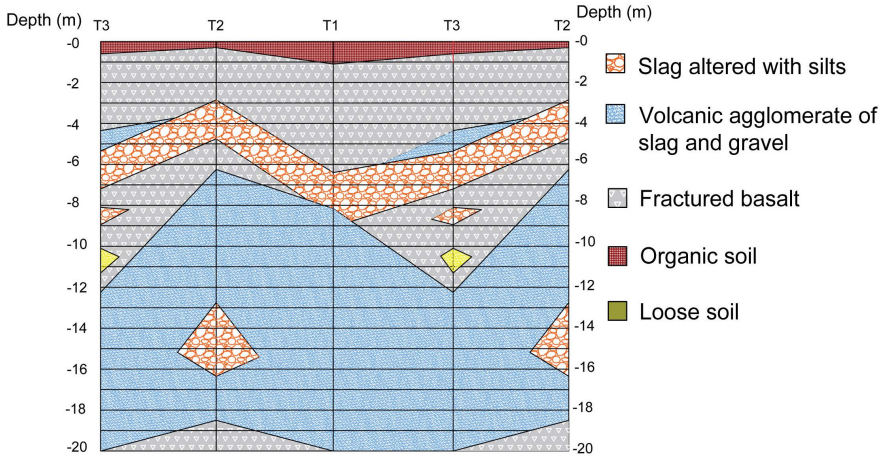

Figure 4. Draft of LST3 study based on the excavations made in different points (T1, T2 and T3) around the telescope.

Table 3. Composition of the soil based on the GTS closest to the measurement sites (T2 location).

SOIL	COMPOSITION OF THE SOIL (GTS)	Depth (m)	TYPE OF ROCK [20]
LST1	Slag altered with clay (clay < 15%)	0.00 - 7.00	MAFIC + CLAYS
LST3	Fractured basalt	0.30 - 2.85	MAFIC
	Slag altered with silts	2.85 - 4.75	MAFIC + SILT
	Fractured basalt	4.75 - 6.25	MAFIC
	Volcanic agglomerate of slag and gravel	6.25 - 18.5	MAFIC + GRAVEL

Table 4. Representative resistivity values of the rock types found in GTS.

SITE	COMPOSITION	REFERENCES ρ (Ω·m)					
		[21]	[22]	[23]	[24]	[25]	[26]
LST1	Slag altered with clay (clay < 15%)	4 - 100	50 - $15{\cdot}10^3$	0.8 - 10^6	1 - 10^5	1.5 - 35	1 - 10^5
LST3	Fractured basalt	4 - 70	$5{\cdot}10^3$ - $15{\cdot}10^3$	100 - 10^6	10^3 - 10^5	7 - 25	40 - 10^5
	Slag altered with silts	4 - 100	20 - $15{\cdot}10^3$	100 - 10^6	50 - 10^5	3 - 30	10 - 10^5
	Fractured basalt	4 - 70	$5{\cdot}10^3$ - $15{\cdot}10^3$	100 - 10^6	10^3 - 10^5	7 - 25	40 - 10^5
	Volcanic agglomerate of slag and gravel	4 - 10^4	50 - $15{\cdot}10^3$	100 - 10^6	100 - 10^5	3 - 28	40 - 10^5

It can be observed that there is a considerable difference among the resistivities reported by references [21]-[26] for the materials found in the ORM GTS. References [21] and [25] provide a narrower margin of resistivities for each material than the others because they use a more detailed classification. Data shown in Table 4 from these references correspond to those types which are closer in nature to the ORM soil. On the other hand, resistivities reported in reference [25] offer the advantage that they distinguish between basalt and slag or scoria. There is a wider clasification of the sedimentary rocks too. Reference [23] con-

siders all possible igneous rocks as a single group.

It can be concluded that no reliable data on resistivities could be found in available literature. Furthermore, the composition of each soil layer is not necessarily homogeneous, and other factors like the humidity or cracks have a deep impact on the resistivity. Therefore a dedicated resistivity survey onsite is essential.

3. Finite Element Model

FEM has been used to calculate the apparent resistivity equipment using Wenner method should measure in two representative locations, which were selected based on the ORM measurements. According to the results shown in Figure 3, five sites (MAGIC I, MAGIC II, LST1, LST2 and LST4) exhibit a homogenous resistivity. LST3 exhibited a different behaviour, with a strong dependence of measured resistivity with pike separation. Therefore, two different simulation models have been implemented. We define a "Soil 1" type as a homogeneous soil. "Soil 2" type corresponds to a multi-layered soil, as the one found in LST3. The aim is to find by simulation of the electric field and current density the true terrain resistivities which would reproduce the measurements displayed by the equipment when the interelectrode separation distance changes in the range of interest, from 2 m to 30 m.

The model uses COMSOL Multiphysics v5.3a software. For this case, Electric Currents Module and a parametric sweep for *a* parameter in the frequency domain have been used for the study. The computational domain is a 3D parallelepiped containing the complete geometry modeled.

The electrodes are considered as "copper material" defined in COMSOL. Material parameters needed for each soil layer are displayed in Table 5. These data are based on the GTS made in LST1 (Soil 1) and LST3 (Soil 2). Several COMSOL studies have been made to estimate the resistivity values for each layer which lead to the best agreement with the measurements.

To avoid contour artifacts due to the finiteness of the model volume, the dimensions of the parallelepiped have been chosen large enough: its length is seven times the maximum electrode separation, 30 m, and its width is 3.5 times this distance. The parallelepiped has 65 m depth. An *Infinite Element Domain* condition has been imposed to an external layer of 2 m thickness in

Table 5. Soil resistivity parameters for the multi-layered soil designed in the COMSOL models.

	Depth (*m*)	*Material* (*GTS*)	ρ (kΩ·m)
***Soil* 1**	**0 - 65**	Slag altered with clay	**1.44**
***Soil* 2**	**0 - 2.85**	Fractured basalt	**18.4**
	2.85 - 4.75	Slag altered with silts	**3.5**
	4.75 - 6.25	Fractured basalt	**15.4**
	6.25 - 65	Volcanic agglomerate of slag and gravel	**1.5**

order to improve the simulation of an infinite volume.

The electrodes were simulated as square patches of 10 cm side. Although they could be simulated as point sources as well, the details of their geometry are irrelevant due to their negligible size as compared to interelectrode spacing [4]. For boundary conditions, current path electrodes are considered as voltage sources of ±16 V, respectively, which correspond to the 32 V source applied during the measurements, as indicated in Table 1. Ground is located at the limits of the parallelepiped. The simulation provides the voltage difference V between the inner electrodes and the current flowing thru the outer ones I. Then, we calculate the apparent resistivity applying Equation (1).

In our models, the mesh consisted of tetrahedral elements with a nonhomogeneous density. The *extra fine* default condition set by COMSOL was chosen for all the volume except a local region around the electrodes. A cube of 2 m side around each electrode was set to *extremely fine* mesh density condition. Figure 5 shows the details of the implemented model geometry.

4. Results and Discussion

The results of the simulation are shown in Figure 6 for a soil type 1, represented by the LST1 site, and Figure 7 for a soil type 2, corresponding to LST3. Each figure displays an image with an aerial view showing the place of the GTS survey as well as the line along which resistivity measurements with stable readings could be made. Also shown are the volume geometry simulated, a plot with both equipotential surfaces and current lines and the comparison between simulated and measured values of the apparent resistivity.

In the resistivity plots we include three simulations for each case, in order to provide an insight of the influence of the first layer characteristics on the final result. In soil 1 case (LST1 site) it is found that the best fit is obtained for a resistivity of 1.44 kΩ·m. Simulations agree with measurements within an error of

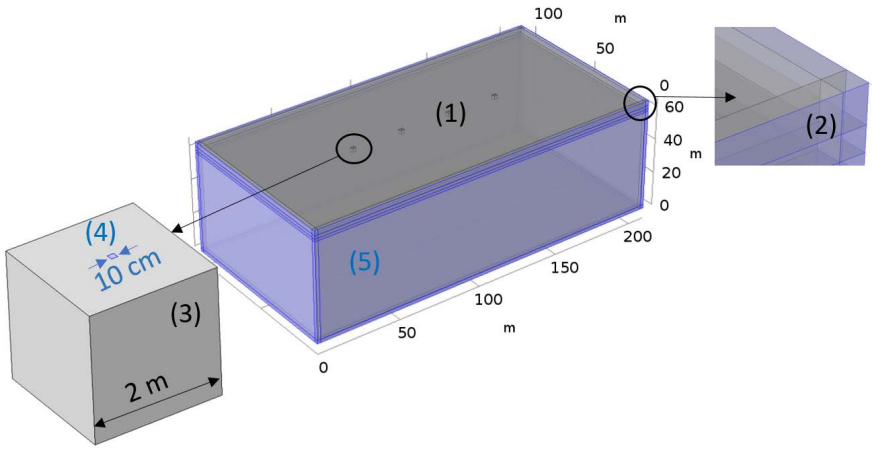

Figure 5. Implemented model geometry. Soil (multilayered case) (1). Infinite Element Domain Layer (2). Extremely fine mesh zone surrounding electrode (3). Electrodes patches (4). Ground (5).

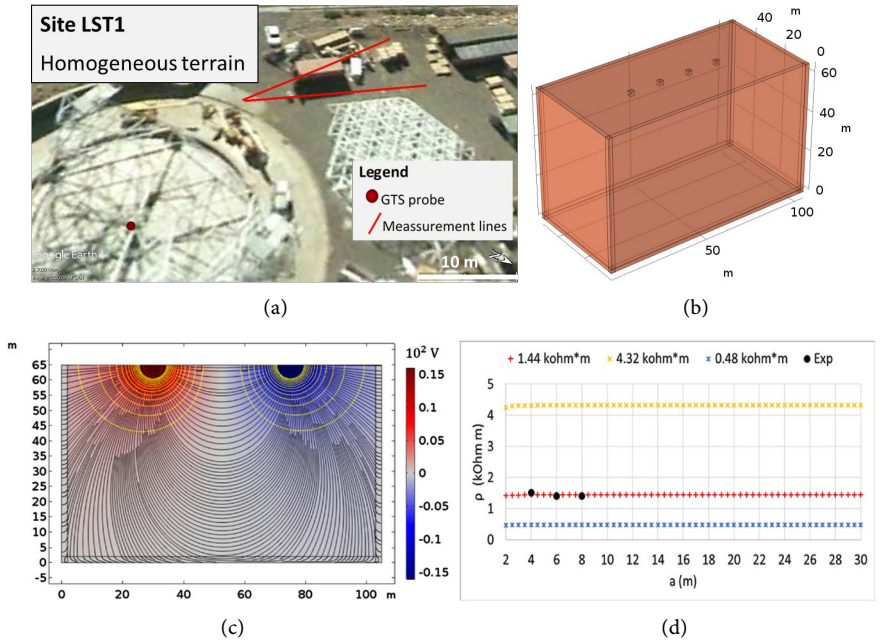

Figure 6. Aerial view of the Geotechnical Study and the measurements for Soil 1 (a). COMSOL model geometry (b). Voltage distribution in the longitudinal plane where electrodes are located. Equipotential surfaces (yellow) and current density lines (black) (c). Soil 1 apparent resistivity (ρ) obtained vs. distance between electrodes, a. Dashed lines: Finite element method calculations for different resistivity of the terrain. Solid circles: Measurements (d).

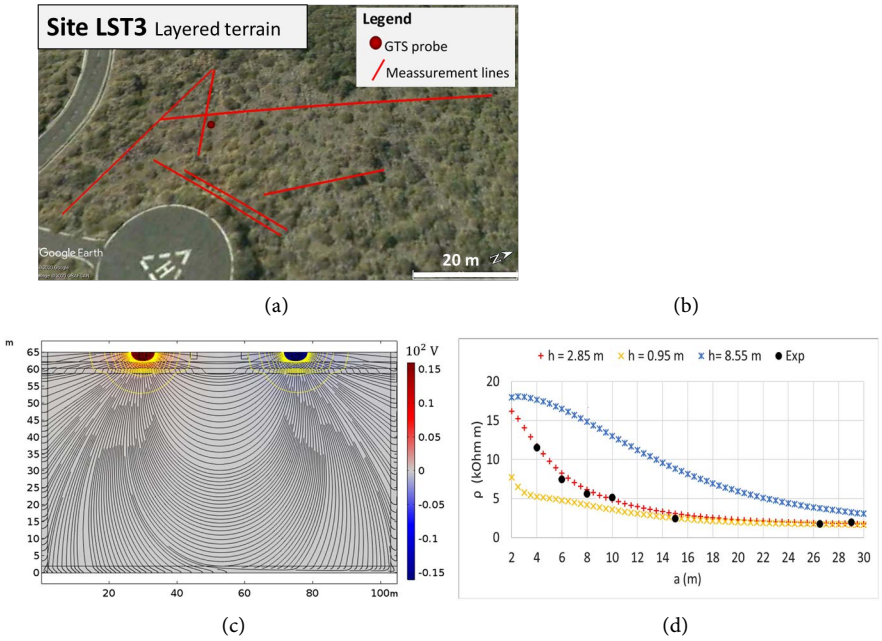

Figure 7. Aerial view of the Geotechnical Study and the measurements for Soil 2 (a). COMSOL model geometry (b). Voltage distribution in the longitudinal plane where electrodes are located. Equipotential surfaces (yellow) and current density lines (black) (c). Soil 2 apparent resistivity (ρ) obtained vs. distance between electrodes, a. Dashed lines: Finite element method calculations depending the thickness, h, of the first layer. Solid circles: Measurements (d).

4.1%. In soil type 2 the thickness of the first layer h makes a strong influence on the final result. For the adequate thickness (h = 2.85 m), discrepancies with measurements are close to 10%.

It can be observed how the current density curves between electrodes bend if the terrain is not homogeneous, as also happens with the equipotential surfaces, which lose their shape of perfect hemispheres. Therefore, the ideal behavior that is often assumed in theory does not work for these cases.

The measurements made at LST3 for the closest distances provided values around 12 kΩ·m, which were well below the maximum resistivity limit of the instrument. Nevertheless, there were several cases in which the measurement could not be done. This led us to the conclusion that the terrain at LST3 exhibits shallow obstacles providing current cuts that make short range readings difficult or impossible to obtain. The nature of these obstacles could not be clarified with the available GTS surveys, but despite the difficulties a layer of low resistivity, around 1.5 kΩ·m, was found when measurements with large interelectrode distances were made. So, if electrode separation is increased and the measurement corresponds to depths where the conductivity is greater, current lines flow through this area and the reading becomes feasible.

According to the simulations, we can also confirm that the main responsible for the low resistivity found at high depths could be the layer of volcanic agglomerates of slag and gravel located at depths around 8 m and below. The value of soil resistivity is determined by the properties of the terrain components: rock type or nature, the amount of salts dissolved, the water content, the compactness… Moreover, available literature on electrical resistivities of similar materials exhibited large discrepancies among the authors and could not provide us reliable data. Nevertheless, the orders of magnitude of resistivities found in this work are compatible with the wide margins reported in references [22] [23] [24] and [26], although they are not in agreement with the data provided in [21] and [25].

5. Conclusions

This work has presented a study of the electrical behavior of the terrain at El Roque de los Muchachos Observatory, which covers six different places located within an area centered at coordinates 28˚45'42.9"N, 17˚53'28.5"W and with an extension around 250 m × 275 m. This study has revealed a significant variability of the terrain not only in terms of the average apparent resistivity but also in the own layer structures.

While five of the studied places showed a behavior compatible with a single layer structure up to depths of around 10 m, the sixth one, the LST3 site, exhibited a dramatically different behavior. The soil at LST3 contained materials in the shallow layers with significantly higher resistivities, and it was considerably difficult to find places for the pikes that provided stable readings.

FEM simulations could provide an insight on the correlation between mate-

rials found in the GTS surveys and the measured resistivities. The four-layer model used for LST3 was found to accurately predict the measured resistivities while keeping a reasonable compatibility with the available surveys. The simulations confirm resistivity values ranging between 15 and 20 kΩ·m for the fractured basalt layers found at El Roque, with lower values for deeper layers (<2 kΩ·m).

We believe that this information might help to efficiently optimize the future ground structures for the telescopes under construction at ORM or other similar sites with soils of volcanic nature.

Acknowledgements

This work has been funded by the Spanish Ministry of Science and Innovation, thru the research project FPA2017-82729-C6-4-R.

Conflicts of Interest

The authors declare no conflicts of interest regarding the publication of this paper.

References

[1] Acharya, B.S., *et al.* (2013) Introducing the CTA Concept. *Astroparticle Physics*, **43**, 3-18. https://doi.org/10.1016/j.astropartphys.2013.01.007

[2] Actis, M., *et al.* (2011) Design Concepts for the Cherenkov Telescope Array CTA: An Advanced Facility for Ground-Based High-Energy Gamma-Ray Astronomy. *Experimental Astronomy*, **32**, 193-316. https://doi.org/10.1007/s10686-011-9247-0

[3] Wenner, F. (1916) A Method of Measuring Earth Resistivity. *Bulletin of the Bureau of Standards*, **12**, 469-478. https://doi.org/10.6028/bulletin.282

[4] Angst, U.M. and Elsener, B. (2014) On the Applicability of the Wenner Method for Resistivity Measurements of Concrete. *ACI Materials Journal*, **111**, 661-672. https://doi.org/10.14359/51686831

[5] Ruan, W., Southey, R.D., Fortin, S. and Dawalibi, F.P. (2005) Effective Sounding Depths for HVDC Grounding Electrode Design: Wenner versus Schlumberger Methods. 2005 *IEEE/PES Transmission Distribution Conference Exposition: Asia and Pacific*, Dalian, 1-7.

[6] Measurement Subcommittee Working Group of the RLC (2012) IEEE Guide for Measuring Earth Resistivity, Ground Impedance, and Earth Surface Potentials of a Grounding System. https://doi.org/10.1109/IEEESTD.2012.6392181

[7] Monarque, A., Gastonguay, L., Gagnon, J. and Champagne, G.Y. (1994) New Method for Measuring the Electrical Resistivity of a Thin Layer of Earth. *Sixteenth International Telecommunications Energy Conference*, Vancouver, 30 October-3 November 1994, 381-384. https://doi.org/10.1109/INTLEC.1994.396640

[8] Samouelian, A., Cousin, I., Tabbagh, A., Bruand, A. and Richard, G. (2005) Electrical Resistivity Survey in Soil Science: A Review. *Soil & Tillage Research*, **83**, 173-193. https://doi.org/10.1016/j.still.2004.10.004

[9] Osinowo, O.O. and Falufosi, M.O. (2018) 3D Electrical Resistivity Imaging (ERI) for Subsurface Evaluation in Pre-Engineering Construction Site Investigation. *NRIAG*

Journal of Astronomy and Geophysics, **7**, 309-317.
https://doi.org/10.1016/j.nrjag.2018.07.001

[10] Takahashi, T. and Kawase, T. (1990) Analysis of Apparent Resistivity in a Multi-Layer Earth Structure. *IEEE Transactions on Power Delivery*, **5**, 604-612.
https://doi.org/10.1109/61.53062

[11] Zhang, B., Cui, X., Member, S., Li, L., He, J. and Member, S. (2005) Parameter Estimation of Horizontal Multilayer Earth by Complex Image Method. *IEEE Transactions on Power Delivery*, **20**, 1394-1401.
https://doi.org/10.1109/TPWRD.2004.834673

[12] Mooney, H.M., Orellana, E., Pickett, H. and Tornheim, L. (1966) A Resistivity Computation Method for Layered Earth Models. *Geophysics*, **31**, 192-203.
https://doi.org/10.1190/1.1439733

[13] Salehi, M., Ghods, P. and Burkan Isgor, O. (2016) Numerical Investigation of the Role of Embedded Reinforcement Mesh on Electrical Resistivity Measurements of Concrete Using the Wenner Probe Technique. *Materials and Structures*, **49**, 301-316.
https://doi.org/10.1617/s11527-014-0498-x

[14] Millard, S.G. and Gowers, K.R. (1992) Resistivity Assessment of *In-Situ* Concrete: The Influence of Conductive and Resistive Surface Layers. *Proceedings of the Institution of Civil Engineers*: *Structures and Buildings*, **94**, 389-396.
https://doi.org/10.1680/istbu.1992.21502

[15] Chavin Arnaux (2018) C.A 6470n terca 3 Manual.

[16] Power System Instrumentation and Measurements Committee of the IEEE Power Engineering Society (2012) IEEE Guide for Measuring Earth Resistivity, Ground Impedance, and Earth Surface Potentials of a Grounding System—Redline.
https://doi.org/10.1109/IEEESTD.2012.6392181

[17] Gobierno de Canarias (2010) GETCAN-011. Guía para la planificación y realización de estudios geotécnicos para la edificación en la Comunidad Autónoma de Canarias.
https://www.gobiernodecanarias.org/optv/doc/labobras/descargas/getcan011.pdf

[18] Carracedo, J.C., de la Nuez, J., Pérez Torrado, F.J., Rodríguez Badiola, E. and Guillou, H. (2001) Mapas geológicos de Canarias.
http://digital.csic.es/handle/10261/4431

[19] Gobierno de Canarias (2020) GRAFCAN-Mapas de Canarias.
https://www.grafcan.es

[20] C. University (2017) Igneous Rocks. http://www.columbia.edu/~vjd1/igneous.htm

[21] American Society Testing & Materials (2005) ASTM D6431-99 Standard Guide for Using the Direct Current Resistivity Method for Subsurface Investigation. ASTM D6431-99.

[22] Sanz, J.H.A., Duque, E.C. and Gomez Estrada, S. (2010) Soil Resistivity as a Function of Frequency. Sci. Tech. Año XVI, 44.

[23] Meju, M.A. (2002) Geoelectromagnetic Exploration for Natural Resources: Models, Case Studies and Challenges. https://doi.org/10.1023/A:1015052419222

[24] Andrés López Hidalgo (2004) La Tomografía geoeléctrica como herramienta de diagnostico ambiental del subsuelo. Estrucplan.
https://estrucplan.com.ar/la-tomografia-geoelectrica-como-herramienta-de-diagnostico-ambiental-del-subsuelo

[25] Pollack, A., Cladouhos, T.T., Swyer, M., Horne, R. and Mukerji, T. (2020) Stochastic Structural Modeling of a Geothermal Field: Patua Geothermal Field Case Study.

[26] Hearst, R. (2018) Applications of DC Resistivity and Magnetotelluric Methods in Exploration.
https://csegrecorder.com/articles/view/applications-of-dc-resistivity-and-magnetotelluric-methods-in-exploration